The Massachusetts and Cape Cod Bays Hydrodynamic Model: 2002-2004 Simulation

Massachusetts Water Resources Authority
Environmental Quality Department
Report ENQUAD 2006-12

Jiang, M, and M. Zhou. 2006. The Massachusetts and Cape Cod Bays Hydrodynamic Model: 2002-2004 Simulation. Boston: Massachusetts Water Resources Authority. Report ENQUAD 2006-12. 128 p.

EXECUTIVE SUMMARY

Under the cooperative agreement between the University of Massachusetts Boston (UMB) and Massachusetts Water Resources Authority (MWRA) in 2001, the UMB modeling team has been maintaining, enhancing and applying the existing hydrodynamic and water quality models for Boston Harbor, Massachusetts Bay and Cape Cod Bay system. Five years (2000-2004) simulations have been conducted since 2001. This report presents the validation of the Massachusetts Bay (MB) hydrodynamic model for years 2002-2004, the new improvements and new findings.

The results from the hydrodynamic model, such as temperature, salinity and currents, are well compared with observed ones from moorings and surveys. The modeled temperature, salinity and currents show seasonal changes in stratification and circulation patterns responding to seasonal meteorological forcing, short term changes in upwelling, mixing and mesoscale eddies and jets responding to storms and freshwater runoff events. The correlations between modeled and observed currents can reach to R^2 equal to 0.6 and 0.32 in the N-S and E-W directions, respectively. The validation of modeled results indicates that the MB hydrodynamic model is robust, and has provided significant understandings to various environmental processes.

The discrepancies between model results and observations in temperature, salinity and currents in MB provide an index that helps to guide the design of monitoring work and the method of incorporating observed data to improve model performance and scientific understanding. The paucity of observations at the open boundary leads to an over-smoothed open boundary condition, which caused under-estimation of water exchanges between MB and the GOM, and the overestimation of salinity in western MB during spring. The interactions between the topography, coastline, coastal currents and freshwater plume determine the current bifurcation near Cape Ann and the intruding current of the GOM waters. A lack of understanding of this process has caused great uncertainty in determining the volume transport of the GOM waters into MB that drives the circulation in MB.

The model consistently performed well in simulating upwelling events along the Scituate to Plymouth section, though it performed with certain bias in phase and amplitude within the Boston Harbor vicinity. The existing model grids are too coarse in Boston Harbor to represent realistic coastal lines and topography, and grid resolution does not resolve the horizontal temperature, salinity and current gradients in Boston Harbor vicinity. Currently, the UMB modeling team is testing a high resolution nested model in Boston Harbor for improving the model performance.

The hydrodynamic model performance has been enhanced by assimilating measurements at GoMOOS buoy B, which significantly improves the upstream boundary conditions, especially short-term variability between two Outfall Monitoring surveys. A simple nudging scheme has been developed for assimilating temperature, salinity, and currents. This method has significantly improved modeled salinity and currents in spring and early summer.

The validation of this hydrodynamic model in MB from past many years has once more demonstrated the consistently robust performance of the model, especially its

reliability, which has led us to develop a Massachusetts Bay Forecast System at UMB funded by the UMass President fund for developing marine sciences and technologies. This system has been operational (http://www.harbor1.umb.edu/forecast/) since January 1 2006 under support by the UMB. This forecast system is a successful product produced from the collaboration between the UMB and MWRA.

TABLE OF CONTENTS

LIST OF FIGURES

LIST OF TABLES

1. INTRODUCTION

1.1 Project overview

The Boston Harbor (BH), Massachusetts Bay (MB) and Cape Cod Bay (CCB) system (MBS) is important to the regional economy by serving a busy commercial harbor, a productive fishing ground, a critical habitat of endangered North Atlantic Right whales and a prosperous tourism industry. A healthy marine environment is important to the more than three million people living in the surrounding area. Significant efforts have been made to clean up Boston Harbor in last decades. The construction of the Deer Island wastewater treatment plant and the relocation of the effluent outfall from Deer Island to 15 km offshore were among the biggest human efforts in the nation to restore an urbanized harbor.

To evaluate environmental and ecological impacts of the new treatment and outfall relocation on the MBS, the Massachusetts Bay Program, US Geological Survey and Massachusetts Water Resources Authority (MWRA) have funded a number of projects to study the physical-biological-chemical processes and monitor the marine environment changes in the MBS (Geyer et al., 1992; Werme and Hunt, 2002). Under these projects, numerical models have been developed to simulate and predict the physical and biological environment in the MBS (HydroQual, 2000; HydroQual, 2003; HydroQual and Signell, 2001; Jiang and Zhou, 2004a, 2004b, 2004c).

A long-term Cooperative Research Agreement made in 2001 between the University of Massachusetts Boston (UMB) and MWRA stated that the UMB and MWRA will maintain, enhance and apply the existing MB Hydrodynamic and Water Quality Models (MB model), and provide model run results to the MWRA for its obligations under its National Pollutant Discharge Elimination System (NDPES) permit. The hydrodynamic model for the MBS was constructed by the U.S. Geological Survey (USGS) in Woods Hole based on the ECOM-si developed by HydroQual Inc. (HydroQual) (Signell et al., 1996). The Water Quality Model was developed by HydroQual (HydroQual, 2000). HydroQual had maintained and conducted model runs up to 1999. Under the agreement between the MWRA and HydroQual, the MB Model was transferred to the UMB in 2001. To ensure successful model transfer and consistency between model results produced by different computer systems, a comparison task between the UMB and

HydroQual model runs has been completed at the UMB (Zhou, 2002; Jiang and Zhou, 2003). The UMB modeling team had successfully simulated and validated hydrodynamic and water quality simulations for 2000-2001. The results were presented in two MWRA reports (Jiang and Zhou, 2004b, 2004c), and several regional and national conferences. The performance of the MB model was reviewed at the Model Evaluation Group (MEG) meeting held on September 12, 2005.

1.2 Physical setting

The MBS is a semi-enclosed embayment located in the western Gulf of Maine (GOM) and surrounded by the Boston metropolitan region in the north and west, and Cape Cod in the south (Figure 1.1). The MBS is about 100 km long and 50 km wide, and has an average depth of 35 m. Stellwagen Basin is the only deep basin in the MBS with a maximum depth up to 90 m. It is bounded in the east by Stellwagen Bank with the shallowest depth of about 20 m. Thus the MBS is connected to the GOM mostly through the North Passage off Cape Ann and the South Passage off Race Point.

Previous studies have indicated that the circulation in the MBS varies in response to short- and long-term local and remote forcing including 1) wind stresses and heat fluxes at the sea surface, 2) tides and mean surface slopes at the open boundary, and 3) freshwater runoff including outfall effluent (Geyer et al., 1992; Signell et al., 1996; Jiang and Zhou, 2004b). The yearly-mean current in the MBS is characterized by a counterclockwise circulation, which is primarily driven by the GOM intruding current through the North Passage, surface winds, local freshwater runoff, and surface heating. Tides are dominated by the semi-diurnal M_2 constituent. Tidal currents vary from 10 cm s^{-1} in the Stellwagen Basin, to 50 cm s^{-1} in the South Passage. The water column stratification varies seasonally. Stratification occurs in spring due to both freshwater runoff and surface heating, which is intensified and reaches a maximum strength during summer. The water column is destratified during fall due to surface cooling and increasing wind mixing, and is well mixed in winter.

The seasonal surface slope off Cape Ann represents the southward flow of the Western Maine Coastal Current (WMCC). As early as 1927, Bigelow suggested that this current breaks into two branches at Cape Ann: one intrudes deeply into MB, and another follows the outer edge of the Stellwagen Bank (Bigelow, 1927; Lynch et al., 1996). This bifurcation is determined by

the interactions between topography, coastal lines and freshwater plume of the Merrimack River though the specific mechanisms remain unclear. The volume transport of this intruding current primarily determines the general circulation in the MBS. It circulates counterclockwise along western Massachusetts Bay and frequently penetrates into CCB, especially in winter and spring seasons (Geyer et al., 1992; Jiang and Zhou, 2004b).

Our modeling study indicates pronounced seasonal variation in the circulation pattern (Jiang and Zhou, 2004b). In western MB, surface currents are strongly driven by winds. In winter and spring seasons, northerly winds drive a southward coastal current creating a counterclockwise circulation (Geyer et al., 1992). In summer and early fall, predominantly southwesterly winds produce offshore Ekman transport and coastal upwelling, which induce a northward coastal current along the upwelling front along the western coast. The coastal upwelling and downwelling have also been discussed in previous studies (e.g., Geyer et al., 1992; HydroQual and Signell, 2001; Signell et al., 1996; Butman, et al., 2002).

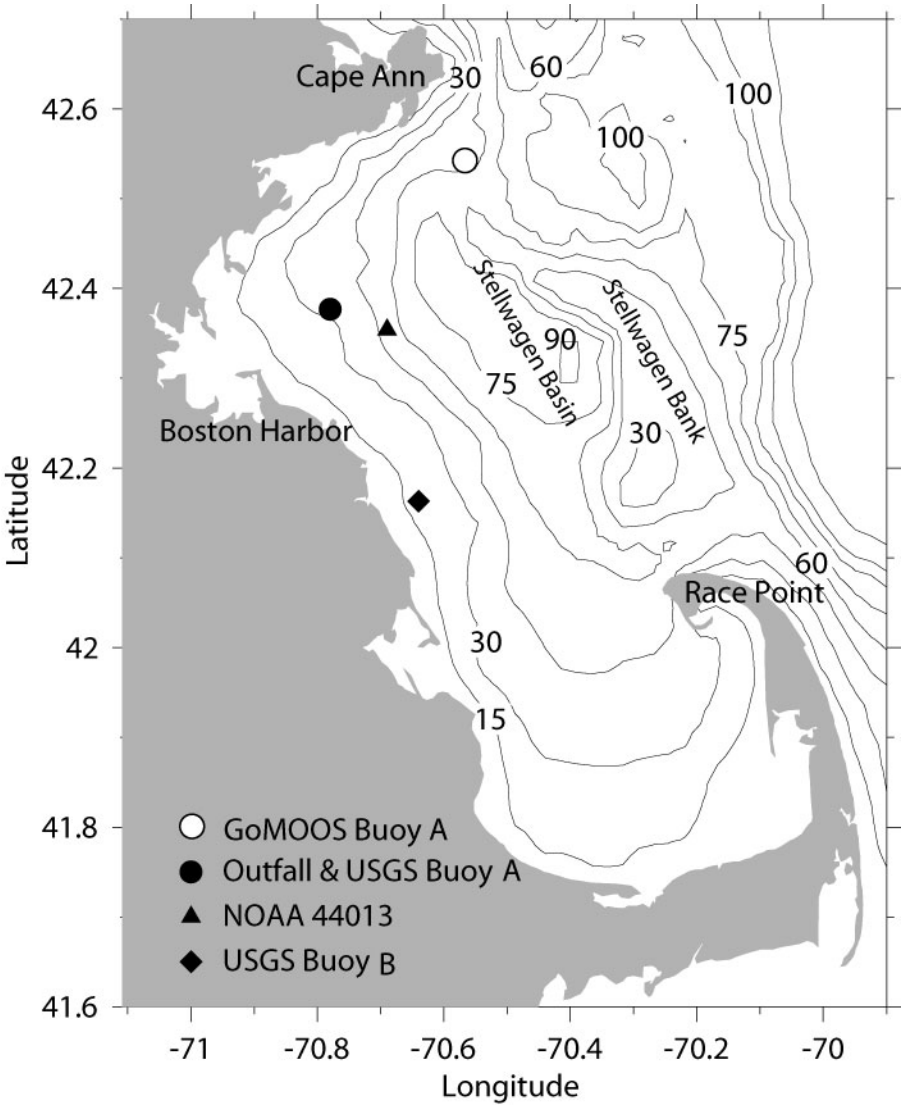

Figure 1.1. Bathymetry and existing buoy stations in the Boston Harbor, Massachusetts Bay and Cape Cod Bay system (MBS).

2. MODEL DESCRIPTION

A brief model description is presented in this section. Table 2.1 and Table 2.2 list the model prognostic variables and values of key parameters, and Table 2.3 lists the frequencies and filters of forcing data, validation data, and model output. More details of this model, such as the basic model equations and treatment of solar radiation, can be found in earlier reports (Signell et al., 1996, HydroQual and Signell, 2001). In 2002-2004 simulations, we used the same model implementation (parameters, forcing data frequencies, boundary conditions, etc.) as in 2000-2001 simulations except (1) the additional data assimilation for GoMOOS buoy B (Figure 2.1) measurements and (2) hot restart (i.e., initial conditions used the model results at the end of previous simulation years).

2.1 Numerical schemes

The Massachusetts Bay and Cape Cod Bay hydrodynamic model is based on the semi-implicit Estuarine, Coastal and Ocean Model (ECOM-si), which is a derivative of the Princeton Ocean Model (POM) (Blumberg and Mellor, 1987; Signell et al., 1996). The model solves the three-dimensional primitive equations using a terrain-following coordinate (sigma coordinate) and a semi-implicit scheme developed by Casulli et al. (1990) in the calculation of the free sea surface elevation to avoid the splitting of barotropic and baroclinic modes. The integration of passive tracer equations is further enhanced by using an anti-diffusion algorithm (Smolarkiewicz et al., 1984).

The vertical turbulent closure is the Mellor-Yamada 2 ½ scheme (Mellor and Yamada, 1982) with modifications by Galperin et al. (1988), while the horizontal mixing is parameterized as formulated by Smagorinsky (1963). In addition to turbulent mixing, a background vertical mixing is chosen to be 5×10^{-6} m^2 s^{-1}. Moreover, a Shapiro filter is applied to velocity field every 2 hours to remove the 2 grid-length variability (Shapiro, 1975).

2.2 Model domain and grids

The model domain extends into the GOM with an open boundary from Portsmouth, NH to offshore off Cape Cod, MA. The domain includes the Merrimack River, the largest source of fresh water in the region (Figure 2.1). This configuration minimizes the influences of inaccurate boundary conditions due to insufficient data in the construction of open boundary conditions.

The bottom topography is smoothed with the maximum depth of 140 m near the eastern boundary and the minimum depth of 3 m near coastal areas to avoid treating flooding and drying grids.

The model has 68×68 grids with the grid spacing approximately from 600 m in Boston Harbor to about 6 km along the open boundary. Vertically, the model has 12 sigma levels with upper three levels located at 0.01, 0.04 and 0.1 sigma depths, and the remaining 9 layers at a 0.1 sigma depth interval evenly distributed over the rest of water column.

2.3 Time step

A time step of 207 seconds is used throughout the entire simulation between years 2002 and 2004. Though the semi-implicit scheme used for the sea surface elevation avoids the instability of an explicit scheme produced by the gravity waves, the model time step is limited by the advective Courant-Levis-Frederick (CFL) condition, which requires the modeled time step less than or equal to grid spacing divided by current speed ($\Delta t \leq \Delta x/U$). A time step of 207 seconds is a very conservative choice. The model was executed stably. The model was run for all days of the years (e.g., 365 days in 2002), although the time-series figures shown below only plot up to 360 day (for graphing convenience).

2.4 Forcing

2.4.1 Surface forcing

The surface forcing includes wind stresses, incoming short wave radiation, net outgoing long wave radiation, sensible heat fluxes and latent heat fluxes. The freshwater input at the surface was set to zero because there were no measurements of precipitation and evaporation at offshore stations, and the precipitation was measured at Logan Airport but not evaporation. Thus a wet or dry year was reflected in river discharges. Wind stresses and heat fluxes were calculated based on meteorological measurements made at NOAA buoy 44013 and solar radiation measurements at Woods Hole Oceanographic Institution (Figure 2.2-2.4). Because there was no humidity measurement at these stations, relative humidity measurements from Logan Airport were used in the calculation of sensible and latent heat fluxes. The wind stresses were calculated using the Large and Pond formulation (Large and Pond, 1981), and long wave radiation, sensible and latent heat fluxes were calculated using the formulation developed by Weller et al. (1995).

The meteorological forcing is typical of mid-latitude regions: in fall and winter, northerly

wind is dominant with a wind speed frequently exceeding 10 m s^{-1}; and in spring and summer, southerly wind is dominant with an overall wind speed less than 5 m s^{-1}. The air temperature is lowest (well below -10ºC) in January and highest in July and August reaching 25ºC. The seasonal meteorological conditions were similar in all three-years except winter 2002, which was exceptionally warm with frequent south winds. Such a condition was extended into March, 2002.

Solar radiation penetrates into the water column. The absorption of short wave radiation is computed as a function of water depth, i.e.,

$$I(z) = I_0 \exp(-k_e z) \tag{2.1}$$

where I_0 is the solar radiation at the sea surface, k_e is the light attenuation coefficient, z is the water depth, and $I(z)$ is the solar radiation at depth z. The value of k_e is calculated based on light transmissivity data collected during the outfall monitoring program and is spatially variable ranging from 0.6 m^{-1} in Boston Harbor to 0.16 m^{-1} offshore (HydroQual and Signell, 2001). Same values of k_e were used in 2002-2004 simulation because no significant change in the Boston Harbor water clarity was observed during the three-year surveys (2001-2003) after the outfall relocation (Taylor, 2005).

2.4.2 Freshwater inputs

There are four major land sources of freshwater, the Merrimack River, Charles River, Neponset River, and MWRA sewage effluent (Figures 2.5-2.7). Among them, the Merrimack River is the largest with an averaged flux of 200 m^3 s^{-1} and the other sources are much smaller with an averaged flux of ~20 m^3 s^{-1}. All river discharges have strong seasonality with the maximum runoff between late March and early May. The effluent from the MWRA Deer Island facility has been completely diverted to the new outfall site in Massachusetts Bay since September 2000. The effluent flow from the MWRA Deer Island facility has been nearly constant throughout these years with episodic events of relatively high flows. The runoff from the Mystic River is included in the model freshwater source though it is small. The sewage flux from South Essex plant flow is not included because it is less than 1.3 m^3 s^{-1}. Daily mean flows of these rivers were used for model inputs.

2.4.3 Open boundary conditions

Open boundary conditions required by the model include surface elevation, temperature and salinity. Surface elevation consists of tidal and low frequency components. The low frequency

surface slope determines the geostrophic currents normal to the boundary. The tidal elevation is a combination of M_2, N_2, and S_2 elevations derived from the tidal model by Lynch and Naimie (1993) (for details, see HydroQual and Signell, 2001).

An objective interpolation procedure is used to derive the temperature and salinity along the open boundary, which is similar to the interpolation procedure in the previous simulations (HydroQual and Signell, 2001). The interpolation software, called OAX, is developed by Bedford Institute of Oceanography (http://www.mar.dfo-mpo.gc.ca/science/ocean/coastal_hydrodynamics/oax.html). The interpolation is made by weighting available data onto the open boundary based on a specified statistical correlation function of horizontal distance, depth and time, so that the statistical interpolation error is known. The correlation function is as follows,

$$R(r) = \left(1 + r + \frac{r^3}{3}\right)\exp(-r) \tag{2.2}$$

where r is the pseudo-distance between the data point and the target point,

$$r = \sqrt{\left(\frac{x - x_0}{a}\right)^2 + \left(\frac{y - y_0}{a}\right)^2 + \left(\frac{z - z_0}{b}\right)^2 + \left(\frac{t - t_0}{T}\right)^2} \tag{2.3}$$

where a, b, and T are the horizontal (30 km), vertical (15 m) and temporal (20 day) correlation scales respectively. The pseudo-distance controls the selection of nearest points for interpolation. The RMS represents the relative estimation error, defined as the square-root of the error variance by interpolation, and is scaled from 0 to 1.

Temperature and salinity measurements from the National Marine Fisheries Service (NMFS), MWRA, University of New Hampshire (UNH), and Stellwagen Bank National Marine Sanctuary (SBNMS) were compiled based on latitude, longitude, depth, and time. For example, the monthly station maps in April and in August for 2002-2004 are shown in Figures 2.8-2.10. The monthly data coverage varies significantly in space and time, and is summarized in Table 2.1.

The same procedure for calculating the low frequency surface elevation along the open boundary as in the 2000-2001 simulation was used. Using the interpolated temperature and salinity along the open boundary, the low frequency surface elevation gradient was inferred from the density field based on the thermal wind relation, which is the relation between geosptrophic currents and horizontal density gradient (see e.g., Pedlosky, 1987), with a zero-velocity reference depth of 100 m or the ocean floor if it is shallower than 100m. The calculation of absolute sea

surface elevation along the open boundary requires a reference point where the absolute sea surface elevation is known. We use the outer coast of Cape Cod as the reference point.

The transects of interpolated temperature, salinity, density and RMS (for overall quality of interpolation of temperature, salinity and density) along the open boundary in April and August, 2002-2004 are shown in Figures 2.11-2.13. The RMS estimates in April on the open boundary are lower than that of August because the station coverage in April is better than that of August (Figures 2.6 and 2.7). In April, the water column was partially mixed except in areas near the northern coast where freshwater runoff creates strong horizontal and vertical salinity gradients. In August, both surface heating and freshwater runoff produce a warm and fresh surface layer. Overall, the interpolated temperature and salinity distributions on the open boundary well represent the seasonal cycles of the water column stratification in the GOM throughout the year. However, short-term (days-weeks) variations are not resolved in these boundary forcings due to inadequate spatial-temporal coverage of data. In addition, the cross-shelf density gradient near the northern coast, which represents the baroclinic component of the WMCC, may not be well characterized.

The estimated monthly surface elevations in 2002-2004 are shown in Figures 2.14-2.16. The horizontal gradients determine the long-term geostrophic currents into or out of the model domain. Note that the nearly flat elevation in January is caused by the absence of observations during that month. In the rest of the year, the results indicate an overall inflow in the northern portion of the open boundary and a nearly permanent outflow in the southern portion of the open boundary. The interpolated seasonal patterns of temperature, salinity and currents are consistent with other modeling results for the GOM region (Lynch et al., 1996; Xue et al., 2000).

As in previous simulations, the numerical schemes of boundary conditions for all scalars in the hydrodynamic model were radiation condition during out-going flow and relaxation to specified boundary values during in-coming flow, respectively (HydroQual and Signell, 2001; Jiang and Zhou, 2004). The tangential and vertical velocities along the open boundary were derived from values at the nearest interior grid-points (i.e., zero horizontal velocity gradients), whereas the normal velocities were allowed to change freely.

2.4.4 Assimilation of GoMOOS B measurements

Measurements at GoMOOS buoy B, which is close to the model northern open boundary,

started in August, 2001. Temperature, salinity and currents measured at this location all show strong short-term variability that are of course absent in the objectively interpolated open boundary conditions (Figure 2.17-2.22). The mooring station resides in the core of the WMCC and because the WMCC normally flows southwestward toward the MBS, the variability in these measurements represents the variability of upstream open boundary conditions. Incorporation of this information into the model should improve the model performance. The assimilation for 2002-2004 simulation is implemented on the first interior grid-line (I=67) of the model domain (Figure 2.1). Because the horizontal gradients of temperature, salinity and currents cannot be resolved by measurements at a single station, some subjective choices are used to extrapolate the single-station to a coastal band (see below). The data assimilation technique used is called nudging, which is essentially restoring model fields (temperature, salinity and currents in our case) to the values from observations (with processing) with a specified time-lag. In our case, we restore the model values to the final values of temperature, salinity, and currents in a coastal band (see below Eq. 2.4).

At GoMOOS buoy B, temperature and salinity were measured at three depths (1m, 20m, 50m) (Figures 2.17-2.19). Measured temperature and salinity were first smoothed using a 25-hr running mean filter to remove high frequency signals and then linearly interpolated between measured depths to derive vertical profiles (referred to as observed values hereafter). These profiles were projected onto the closest interior grid point BB (I=67, J=58). To maximize the assimilation effect, the observed values were further projected horizontally over the grid-line between the coast (point C) and an offshore location (point D) (Figure 2.1). The projection for the segment C-BB was based on the observed values at BB and the modeled temperature and salinity gradients at BB (from previous time-step), while for the segment D-BB, the projection was based on the linear interpolation between modeled values at D (from previous time-step) and observed values at BB. In the simulations, the temperature and salinity between C and D were restored to the final temperature and salinity values with a time-lag of t_{lag}=2 hour as follows (using temperature as an example),

$$\frac{dT}{dt} = \frac{T - T_{final}}{t_{lag}} \tag{2.4}$$

Similar assimilation was made for currents at GoMOOS buoy B, which were measured by an Aanderaa current meter (2m) and an Acoustic Doppler Current Profiler (ADCP) (10-54m).

Measured currents were first linearly interpolated into model sigma layers. Then all of the modeled currents at the grid-points between C and BB were restored to the interpolated current values with a time-lag of 1-hr, whereas currents at the grid-points between BB and D were restored to the interpolated current values with a time-lag increasing from 1-hr at BB to 8-hr at point D.

Numerical simulations were conducted by assimilating (1) temperature and salinity (TS) only and (2) both TS and currents. The results indicate that the assimilation of TS only significantly improves modeled temperature and salinity but biases the modeled bottom currents, while the assimilation of both TS and currents improves both modeled temperature and salinity, and currents. All results presented below were from simulations assimilating both TS and currents.

2.4.5 Initial conditions

The initial conditions for the hydrodynamic model are derived from the modeled results in the end of previous year without spin-up. For example, the initial conditions for 2002 were derived from the end of 2001 simulations.

2.5 Model enhancements in the last decade

This model has been developed over more than 10 years since the original work of Signell et al. (1996). Though the majority of the model features remain unchanged, several significant enhancements have been made over the years as listed below (as compared to Signell et al., 1996),

(1) The solar radiation was allowed to penetrate into deep water with a spatially variable light attenuation coefficient, as opposed to leaving all solar radiation at the surface layer (HydroQual and Signell, 2001);

(2) The sea surface slope along the boundary was calculated based on the objectively interpolated temperature and salinity along the boundary and the thermal wind relation, as opposed to a manual derivation (Jiang and Zhou, 2004b);

(3) A data assimilation method has been developed and used to incorporate GoMOOS buoy B measurements since 2002 (this report); and

(4) A forecasting system has been developed to provide real-time forecast for hydrographical conditions in Massachusetts Bay (this report).

Table 2.1 Prognostic model variables

Variables	Descriptions
el	surface elevation (m)
u & v	horizontal velocities (m/sec)
w	sigma coordinate vertical velocity (m/sec)
t	temperature (ºC)
s	salinity (psu)
rho	density (kg/m^3) (derived from t and s)
q2	twice the turbulent kinetic energy (m^2/sec^2)
q2l	q2 times turbulent length scale (m^3/sec^2)
l	turbulent length scale (m) (=q2l/q2)

Table 2.2 Key parameters of hydrodynamic model

Parameters	Values
Smagorinsky coefficient (horizontal mixing)	0.1
Bottom roughness	0.003 m
Vertical background mixing	$5x10^{-6}$ m^2/sec
Light attenuation coefficient	0.16~0.6 m^{-1}

Table 2.3 Frequencies and filtering of forcing data, validation data, and model output.

Parameters	Frequencies used in the model implementation or validation	Frequencies of original data	Filtering	Sources
Winds, air temperature, air pressure	hourly	hourly	no	NDBC 44013
Solar radiation	hourly	hourly	no	WHOI
Humidity	hourly	hourly	no	Logan Airport
Boundary temperature, salinity, elevation	monthly	various	Objective interpolation	NMFS, MWRA, UNH, SBNMS
River discharges	daily	daily	no	USGS
Outfall effluent flow	daily	daily	no	MWRA
GoMOOS buoy A&B (t, s, currents)	hourly	hourly	25-hour running mean for t&s Lanczos filter (25-hour cut-off frequency) for currents	University of Maine
USGS buoy A & B (t, s, currents)	hourly	hourly	Lanczos filters with 25-hour cut-off frequency	USGS
MWRA Outfall Monitoring (t and s)	17 cruises per year for nearfield 6 cruises per year for farfield	17 cruises per year for nearfield 6 cruises per year for farfield	no	MWRA
Model output: time series (t, s, currents)	hourly	207 sec	Lanczos filter with 25-hour cut-off frequency	UMB
Model output: snap shots	Averages over one tidal cycle	207 sec	no	UMB

Table 2.4 Quality of data coverage for objective interpolation in 2002-2004

Month	Rating*		
	2002	**2003**	**2004**
January	-	-	-
February	0	0	0
March	-	0	+
April	+	+	+
May	-	-	-
June	0	0	0
July	-	-	-
August	0	0	0
September	-	0	-
October	+	+	+
November	-	-	0
December	-	-	-

* Definitions of symbols: + (good), 0 (fair) and - (poor).

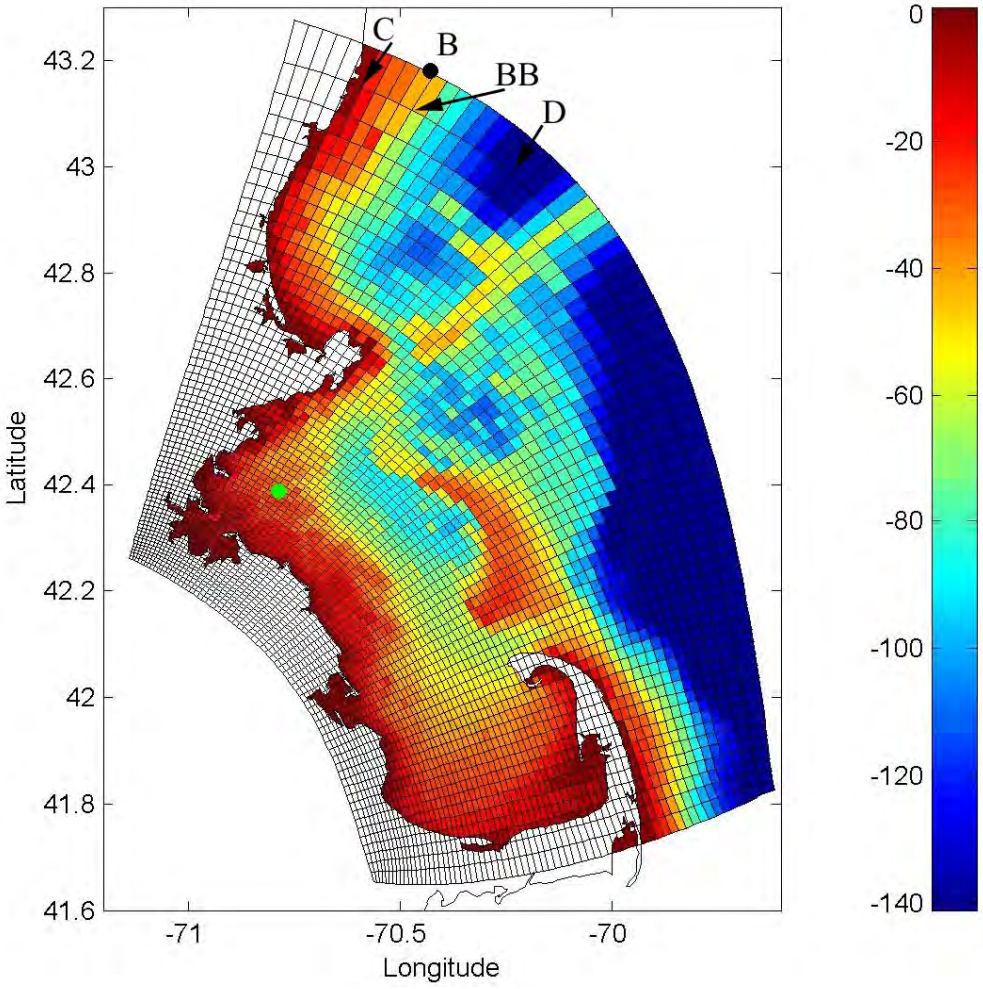

Figure 2.1. Model domain and grids in the MBS. Also shown are GoMOOS buoy B (black dot) and the MWRA outfall (green dot). Points C, BB, and D are reference points for data assimilation (see text).

(a)

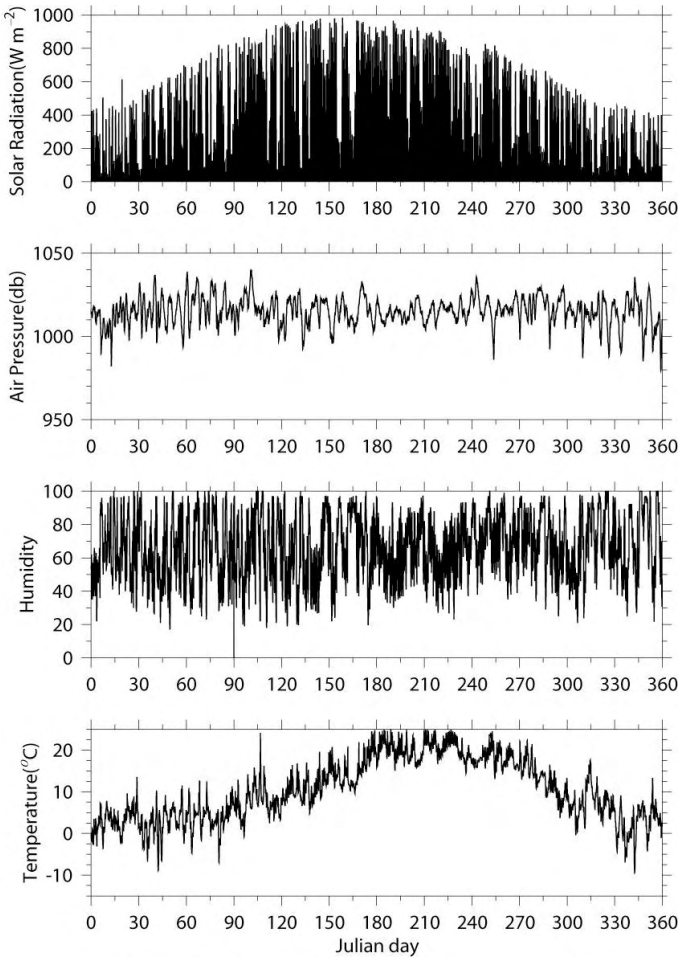

(b)

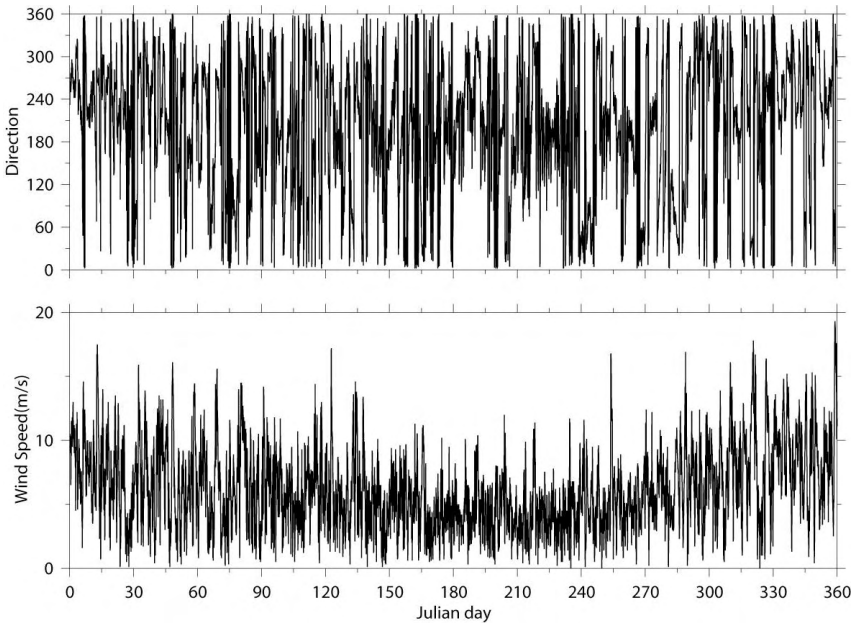

Figure 2.2. Meteorological forcing in 2002: (a) solar radiation, air pressure, humidity, and air temperature, and (b) wind speed and directions.

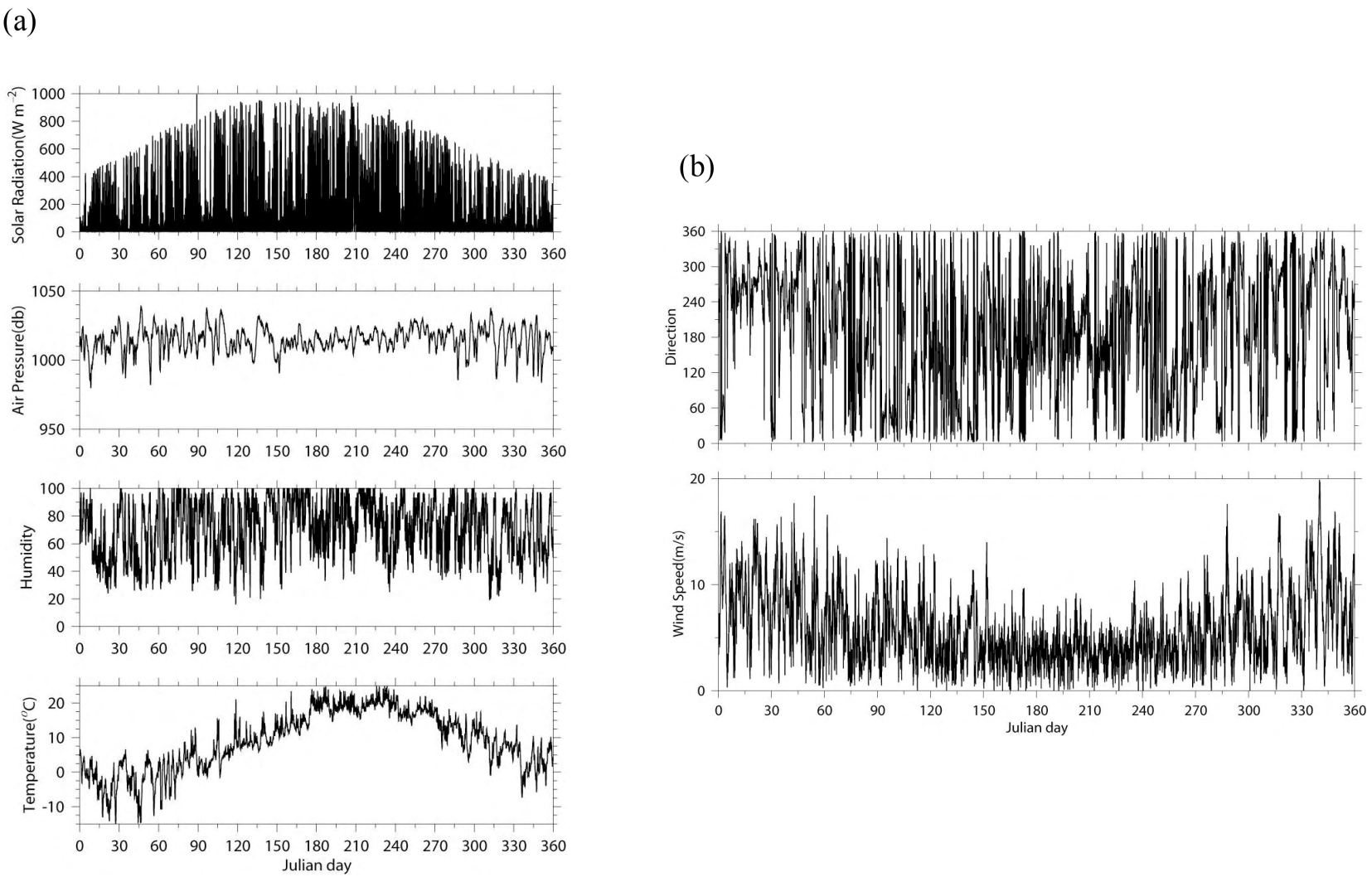

Figure 2.3. Meteorological forcing in 2003: (a) solar radiation, air pressure, humidity, and air temperature, and (b) wind speed and directions.

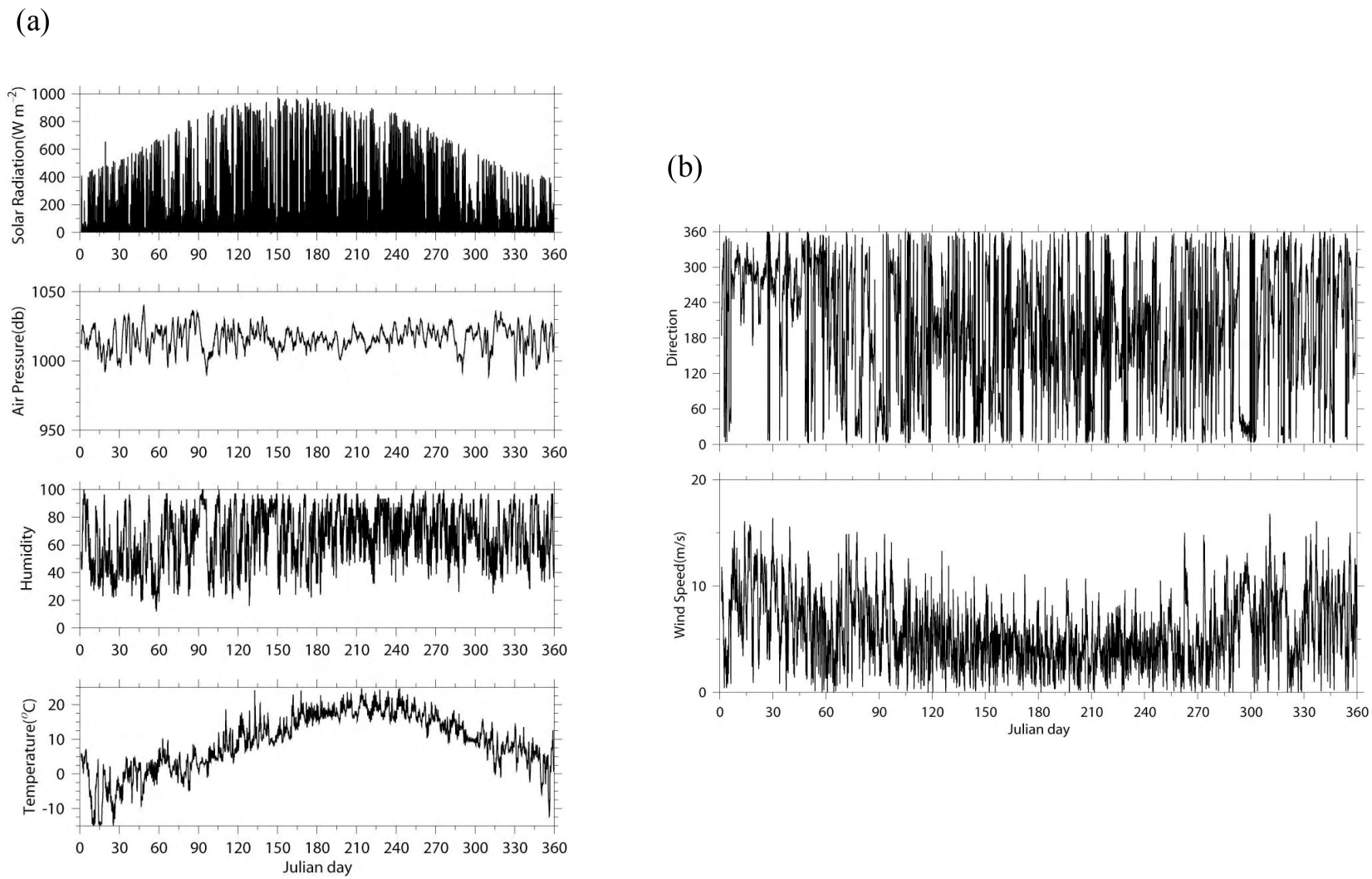

Figure 2.4. Meteorological forcing in 2004: (a) solar radiation, air pressure, humidity, and air temperature, and (b) wind speed and directions.

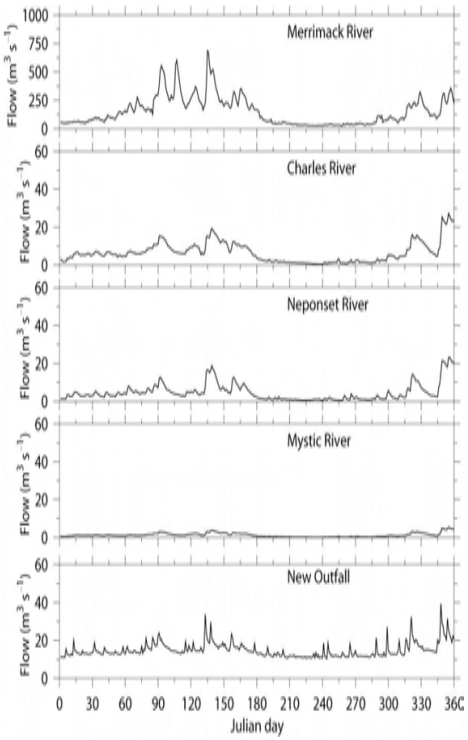

Figure 2.5. Daily discharges from the Merrimack River, Charles River, Neponset River, Mystic River, and MWRA outfall in 2002.

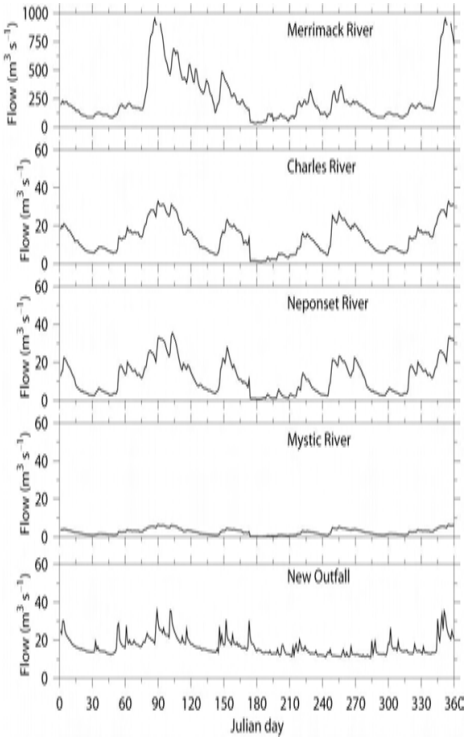

Figure 2.6. Daily discharges from the Merrimack River, Charles River, Neponset River, Mystic River, and MWRA outfall in 2003.

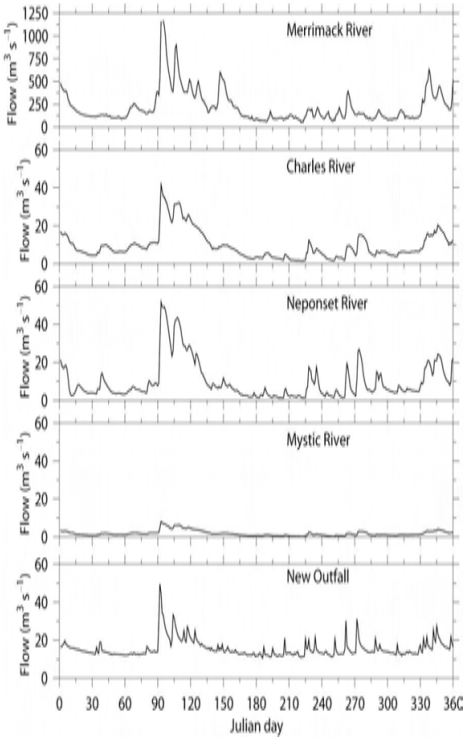

Figure 2.7. Daily discharges from the Merrimack River, Charles River, Neponset River, Mystic River, and MWRA outfall in 2004

.

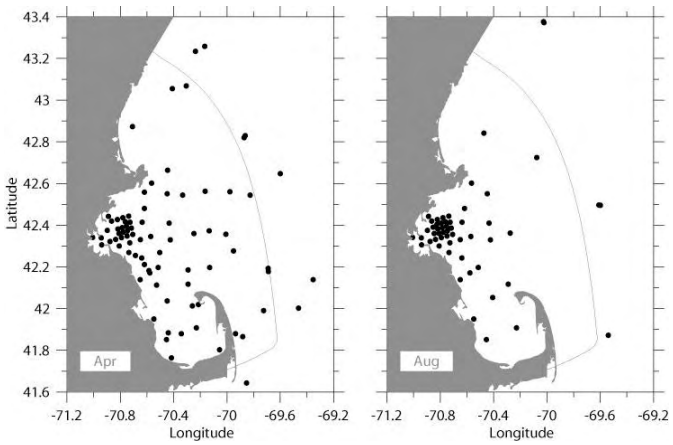

Figure 2.8. Station maps of available data in April and August, 2002.

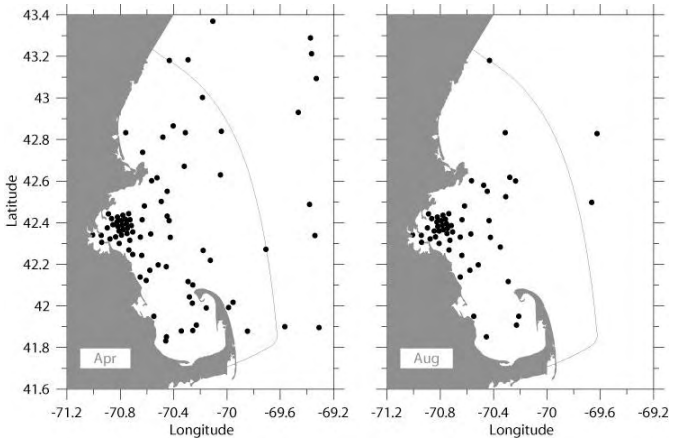

Figure 2.9. Station maps of available data in April and August, 2003.

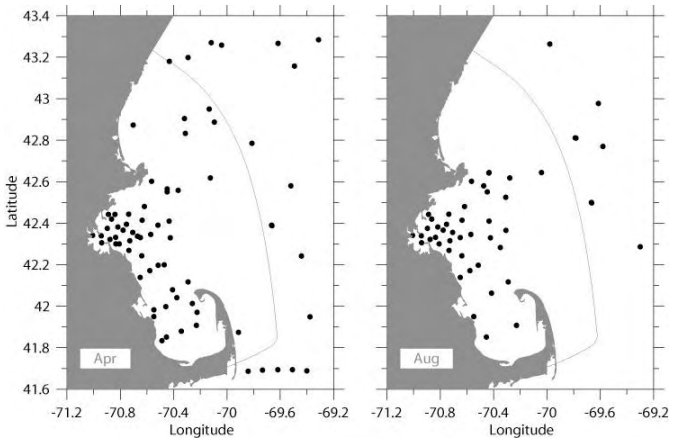

Figure 2.10. Station maps of available data in April and August, 2004.

(a)

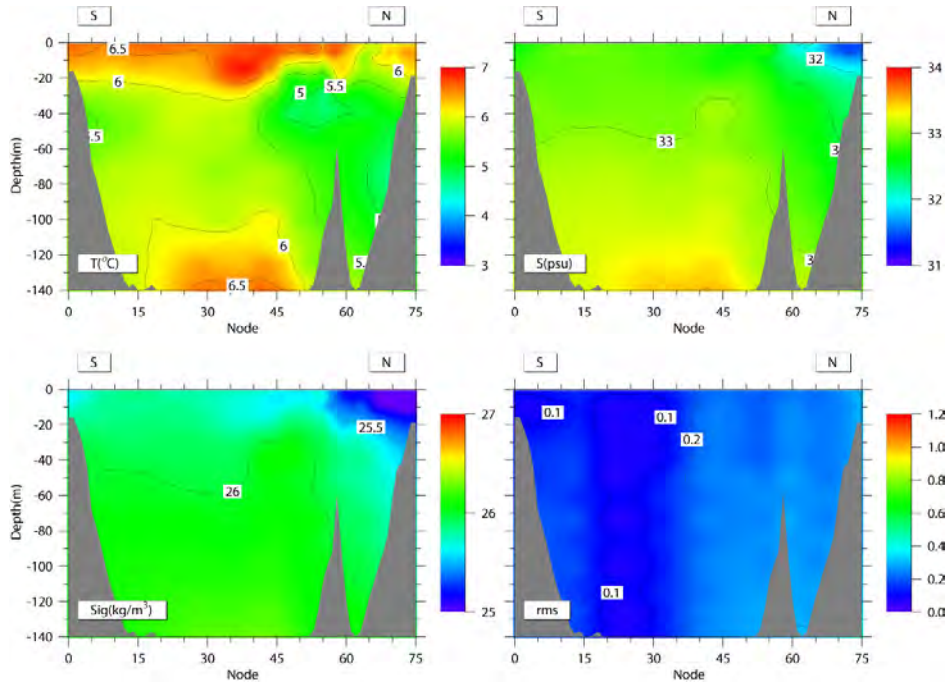

(b)

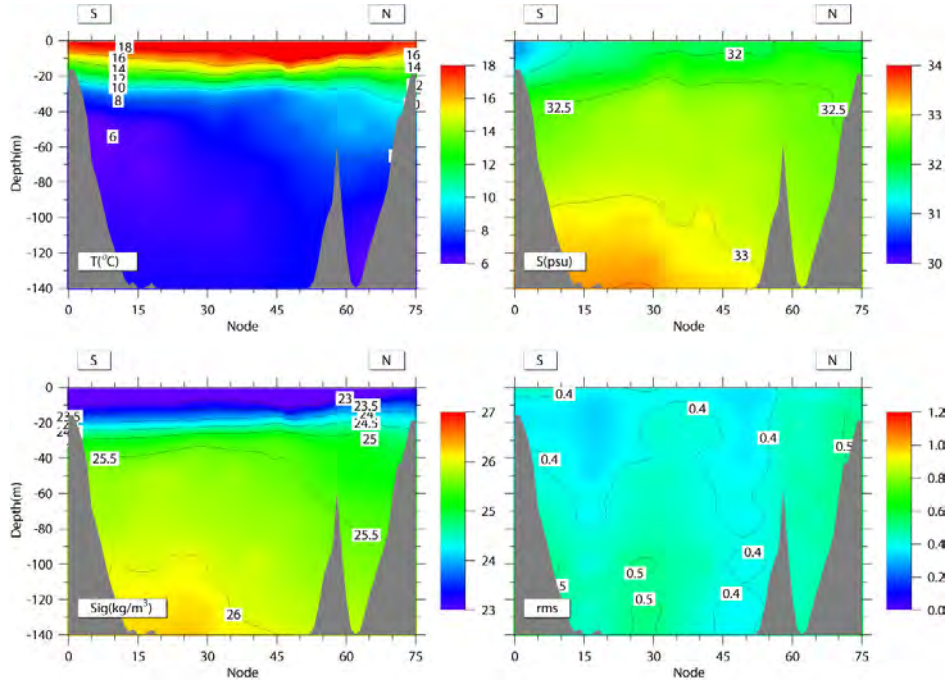

Figure 2.11. Open boundary conditions of temperature, salinity, σ_t and rms errors in (a) April and (b) August, 2002.

(a)

(b)

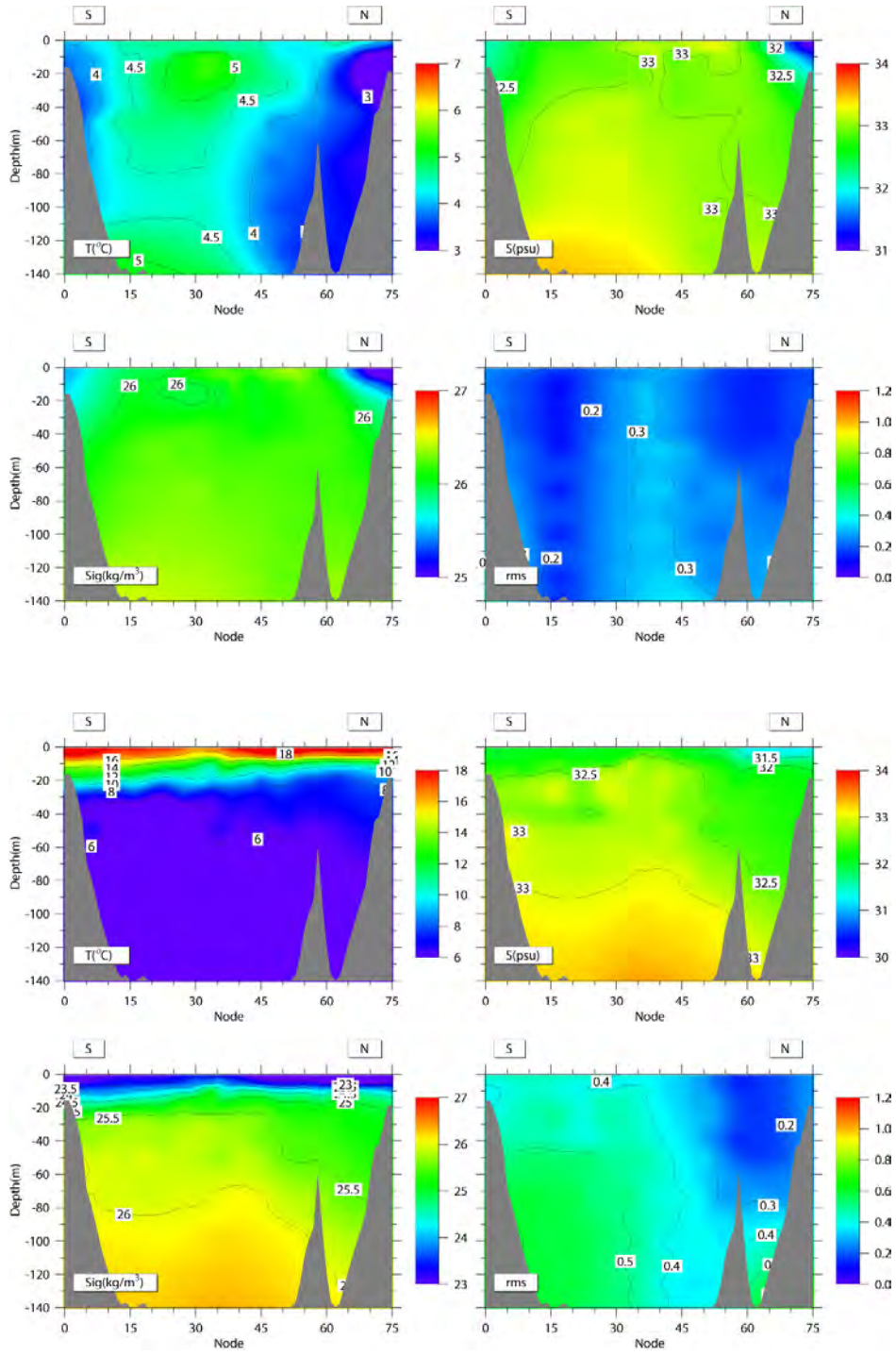

Figure 2.12. Open boundary conditions of temperature, salinity, σ_t and rms errors in (a) April and (b) August, 2003.

(a)

(b)

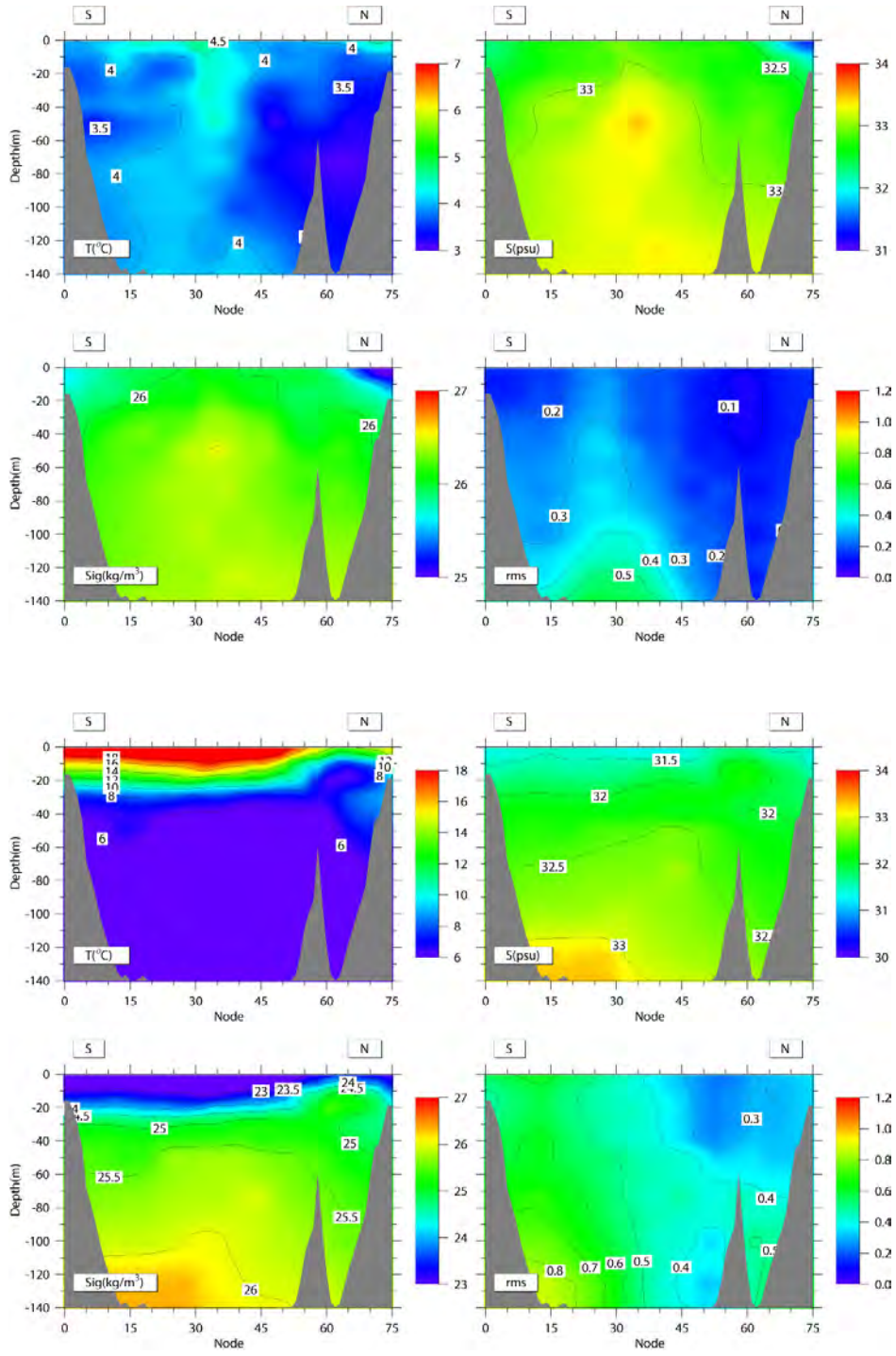

Figure 2.13. Open boundary conditions of temperature, salinity, σ_t and rms errors in (a) April and (b) August, 2004.

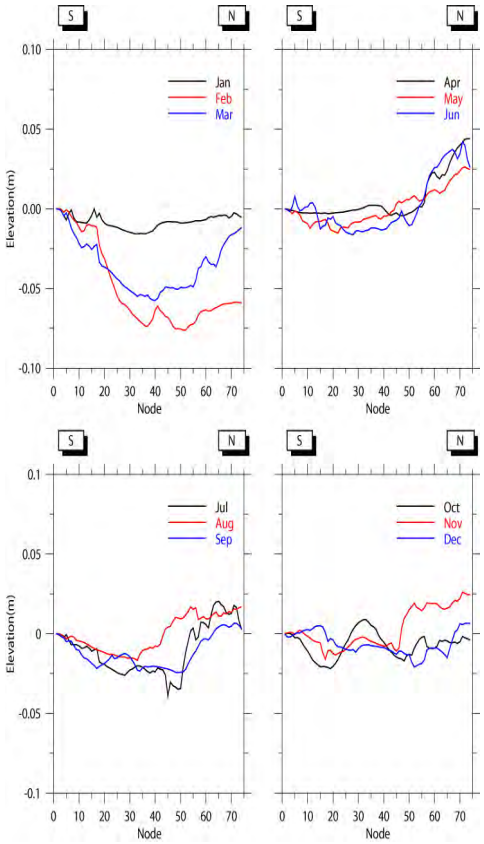

Figure 2.14. Monthly sea surface elevations at the open boundary in 2002.

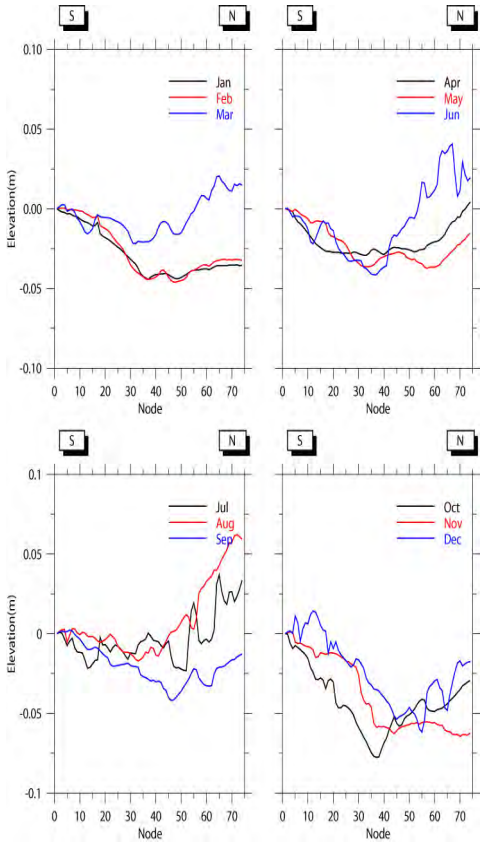

Figure 2.15. Monthly sea surface elevations at the open boundary in 2003.

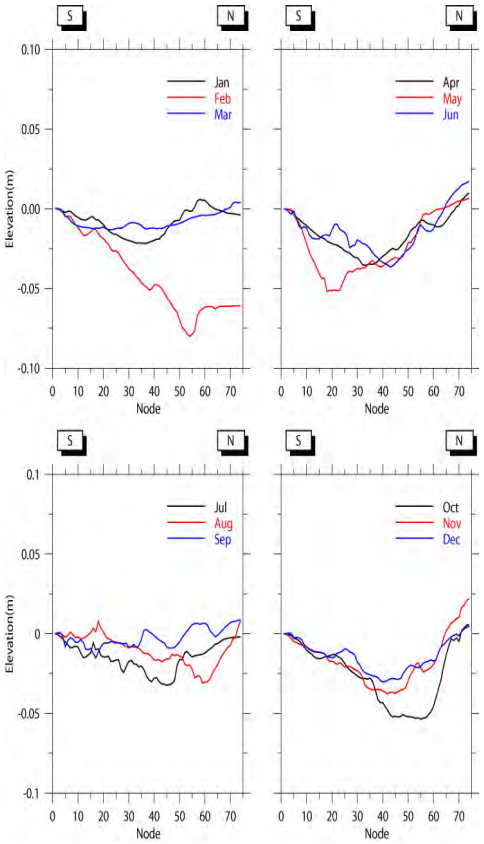

Figure 2.16. Monthly sea surface elevations at the open boundary in 2004.

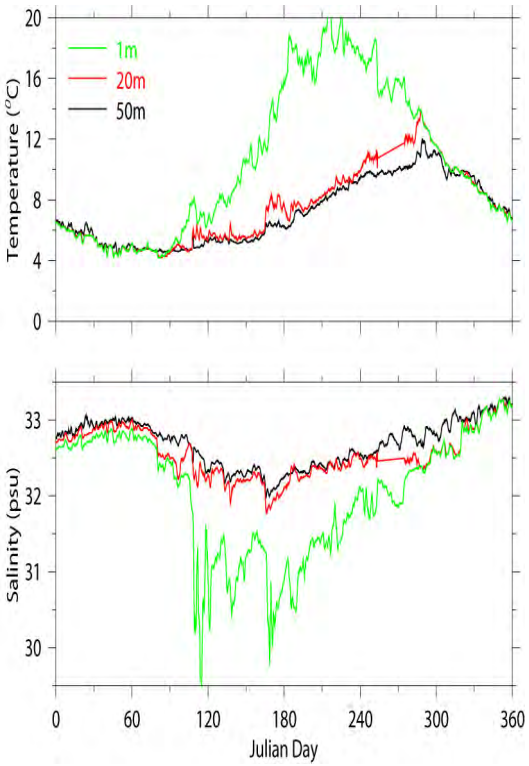

Figure 2.17. Temperature and salinity at GoMOOS Buoy B in 2002.

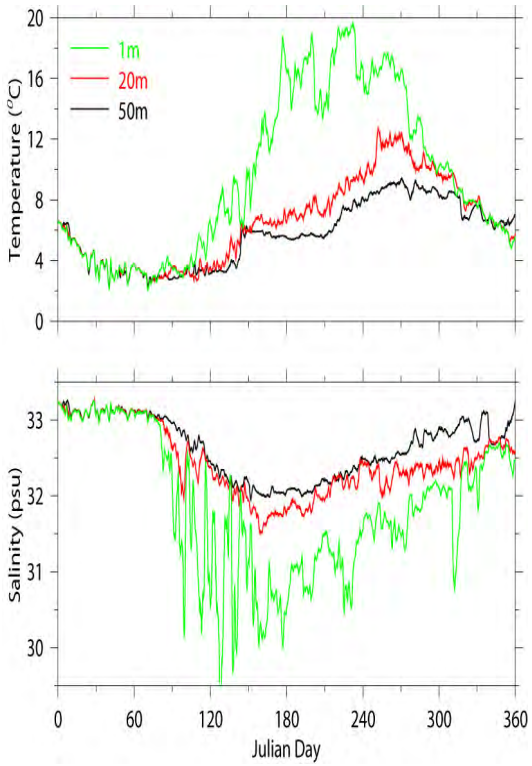

Figure 2.18. Temperature and salinity at GoMOOS Buoy B in 2003.

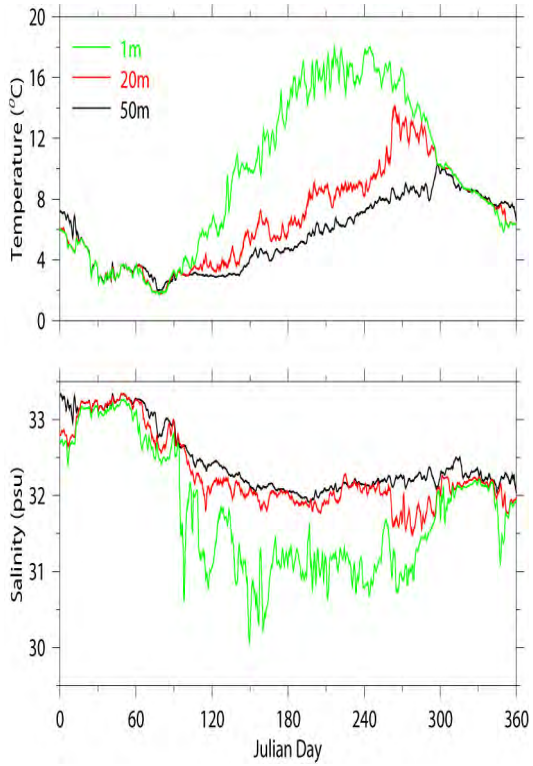

Figure 2.19. Temperature and salinity at GoMOOS Buoy B in 2004

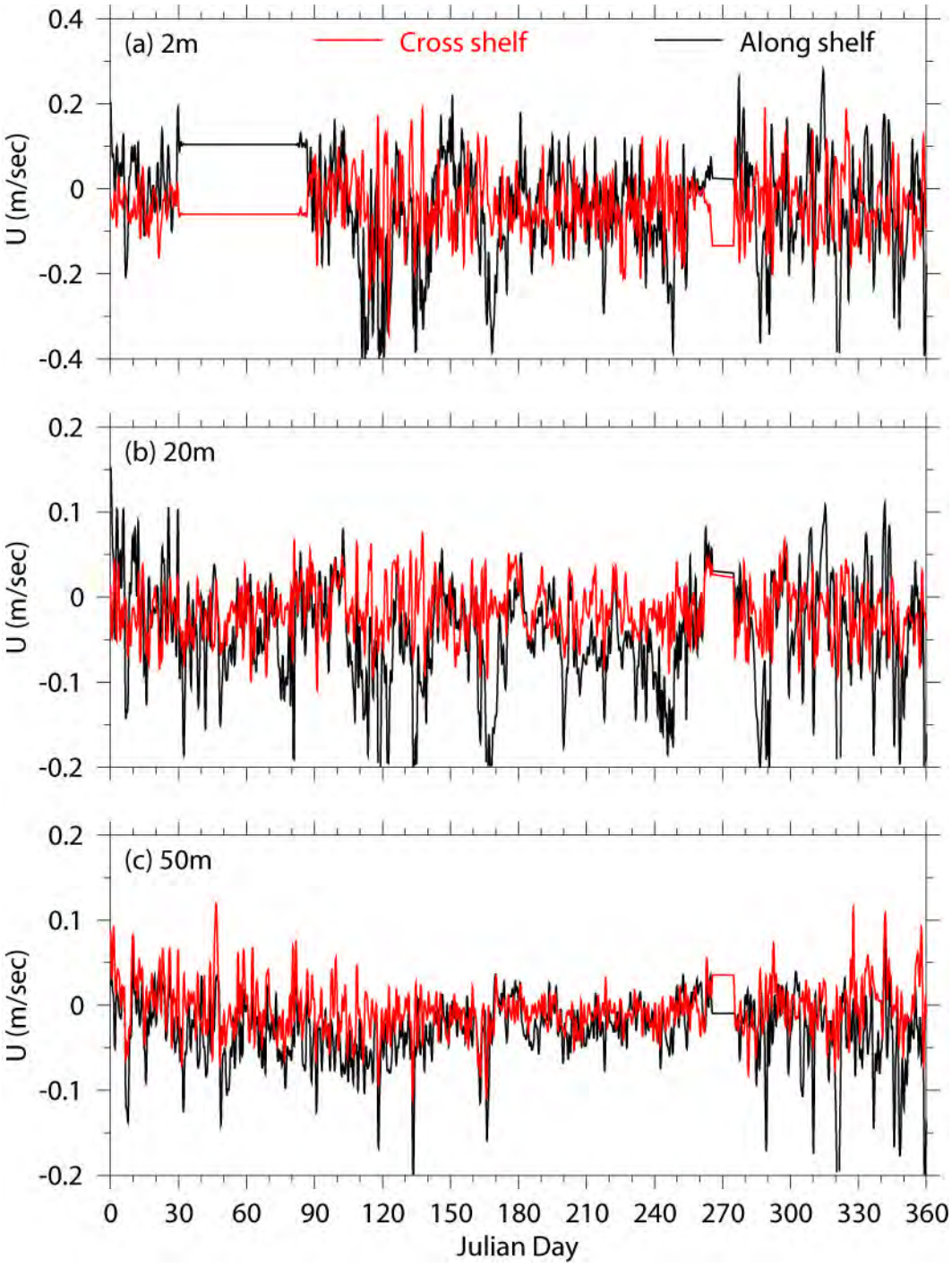

Figure 2.20. Along shelf and cross shelf currents at GoMOOS Buoy B in 2002. Measured currents were rotated counterclockwise approximately 60º.

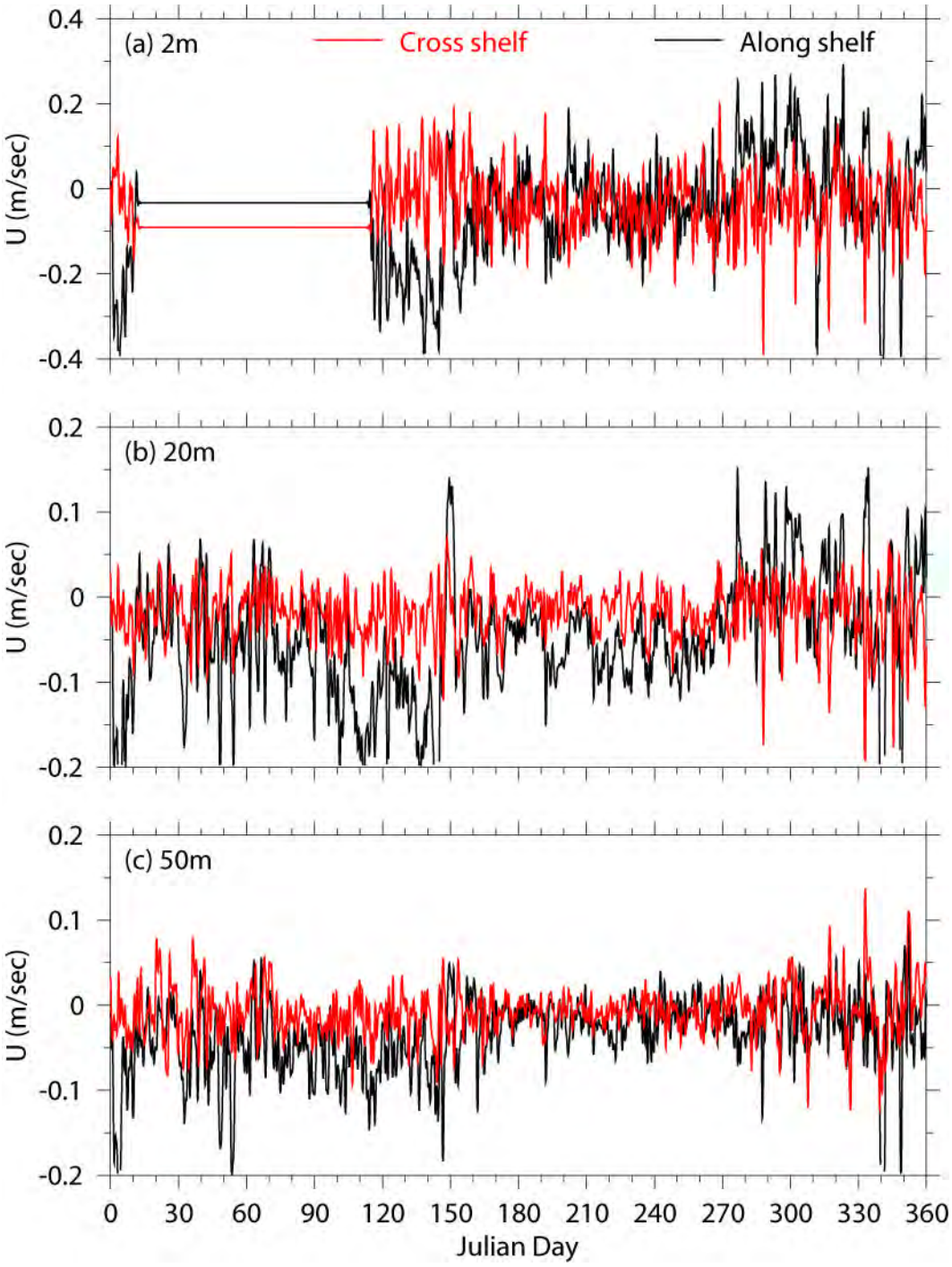

Figure 2.21. Along shelf and cross shelf currents at GoMOOS Buoy B in 2003. Measured currents were rotated counterclockwise approximately 60º.

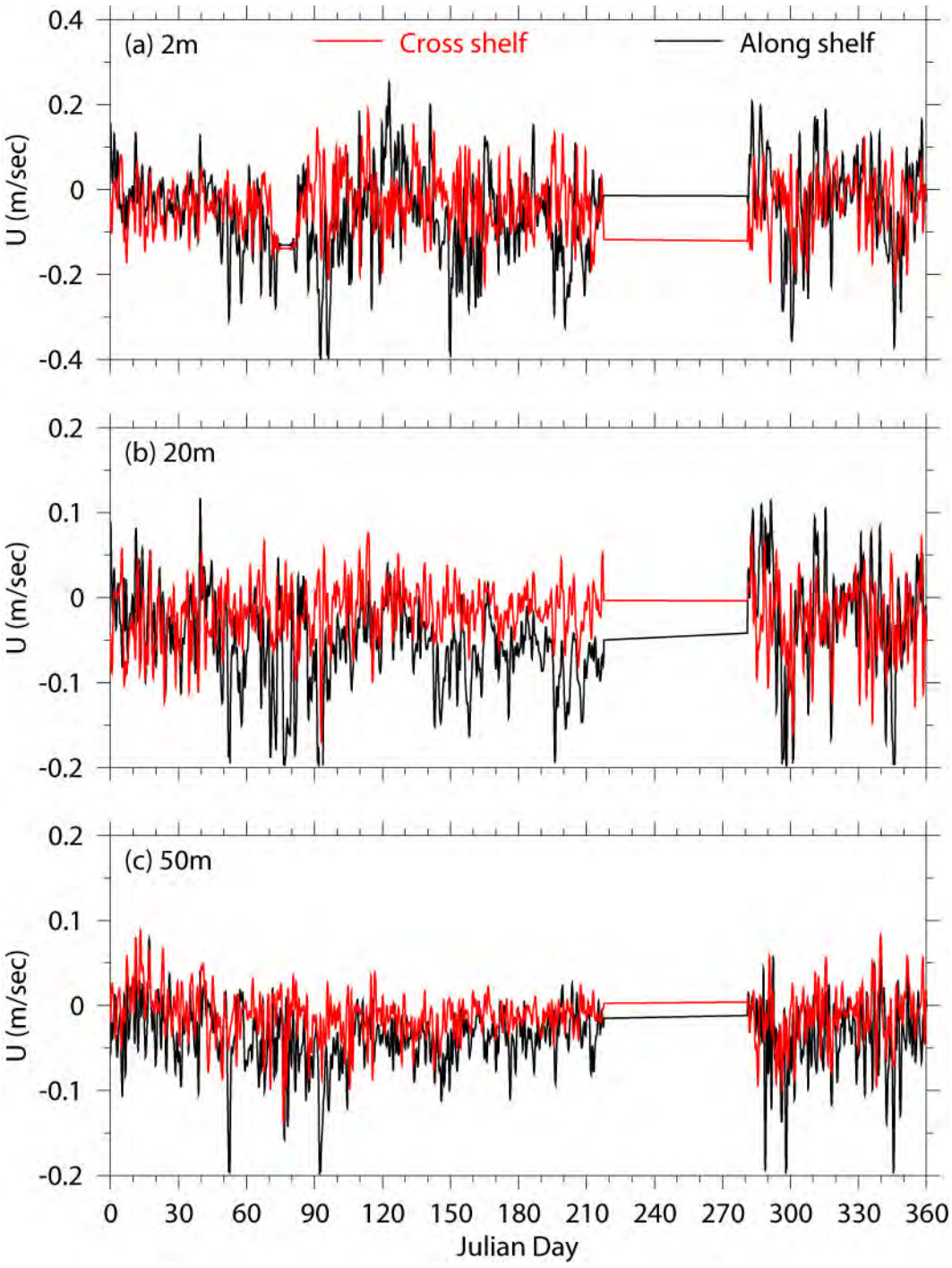

Figure 2.22. Along shelf and cross shelf currents at GoMOOS Buoy B in 2004. Measured currents were rotated counterclockwise approximately 60º.

3. MODEL VALIDATION

We will validate the model results by comparing them with time series and spatial distributions of temperature, salinity and currents measured at mooring stations and from monitoring surveys, and highlight and discuss major hydrodynamic events and year-to-year differences.

3.1 Time series

3.1.1 Temperature and salinity at the MWRA monitoring stations

Twelve stations are chosen for data comparison to represent the sampling network (Figure 3.1). These stations are organized into four groups: a) stations F26, F27 and F29 along the eastern boundary of MB, b) stations F31, N01 and N10 in the coastal area of northwestern MB, c) stations F07, F01 and F02 in southern MB and CCB, and d) stations N04, N07 and F17 in the offshore region of northern MB. In the following discussion, measurements at surface and bottom are compared with modeled results taken at the third and 12th sigma levels, respectively.

2002. Observed and modeled temperature and salinity in 2002 are shown in Figure 3.2. In this year, temperature and salinity values were normal except for a relatively warm winter and relatively high surface salinity in late spring, as compared to other years. Model results compared well with observations in terms of seasonal cycles and overall values. In particular, the model captured the strengths and timings of stratification in summer and de-stratification in fall. The model predicted strong variations in bottom temperature at coastal stations during late spring and summer period, associated with coastal upwelling/downwelling, which were observed at more-frequently sampled stations (N01 and N10), but were missed at less-frequently sampled far field coastal stations (F01 and F02). The discrepancies between model and observations are: 1) weak stratification existed during Jan.-Feb. at most offshore stations (e.g., N04, F07, F26) in the model results, while observations showed well-mixed waters; and 2) the model over-estimated the surface salinity in coastal areas (N01, N10, F01 and F02) during spring and summer.

2003. Observed and modeled temperature and salinity in 2003 are shown in Figure 3.3. This year had with very cold temperature in February and low surface salinity in springtime, e.g., reaching 30‰ at station N07. Similar to 2002, modeled temperature and salinity agreed with the observed fields in general but detailed differences existed. Noticeable differences between the

observations and modeled results are: 1) during May-July surface salinity was over-predicted at most stations except for N04 and F26; 2) the model predicted warmer bottom temperature in coastal areas (F31, N01, N10, F01, F02) during summer and fall.

2004. Observed and modeled temperature and salinity in 2004 are shown in Figure 3.4. This was a relatively normal year in terms of temperature and salinity except for low winter temperature. Similarly the model reproduced the seasonal cycles of observed temperature and salinity quite well but differed from the observations in some details: 1) the model over-estimated both surface and bottom salinity during spring and early summer at all stations including F26 and F27; 2) the model over-predicted bottom temperature in the western coast (N01, N10, F01 and F02) in summer.

3.1.2 Temperature and salinity at USGS buoys A and B

We used the model results at sigma levels k=5 and k=12 for buoy A, and k=9 and k=12 for buoy B, respectively. There is an overall good agreement between the observed and modeled temperature and salinity (Figures 3.5-3.10). Here, we will focus on major hydrodynamic features and discrepancies between the modeled and observed results.

2002. The comparison of modeled and observed temperature and salinity at USGS buoys A and B indicates the model reproduced both observed short-term and seasonal variability well except the strong upwelling/downwelling events in July-August (Figure 3.5). At site A, the water column was strongly stratified in summer. The upwelling and downwelling associated with wind-induced Ekman pumping led to variations of temperature and salinity at both surface and bottom.

The model reproduced the strong fluctuations in the near bottom temperature observed at station B, although modeled temperature is about 1-3ºC warmer than the observed temperature. Unfortunately, no surface temperature measurement at this station is available to verify if the warmer bottom water predicted is due to over-mixed water column.

2003. The comparison of modeled and observed results for buoy A in 2003 is shown in Figure 3.6a. The model well reproduced the freshening of surface water in March-May. In June, the modeled surface salinity was slightly (0.3~0.5‰) higher than the observed. The model reproduced the increase of salinity but failed to predict the decreasing of surface temperature

during the prolonged upwelling events in summer (days 180-230), suggesting that the model correctly simulated the cross-shelf gradient of salinity, but not temperature (see section 3.2).

At station B, the model results are consistent with the observed, although it under-predicted the salinity in Jan.-Feb. (Figure 3.6b). In summer, the buoy data is unavailable for comparison.

2004. Up to now only data at station A are available for comparison (Figure 3.7). The model reproduced the seasonal cycle and short-term variability, though the summer surface temperature was over-estimated with less variability.

3.1.3 Temperature and salinity at GoMOOS buoy A

The model results are extracted from sigma levels k=1 (surface) and k=12 (bottom), respectively. The comparison of modeled temperature and salinity with observations at GoMOOS buoy A during three year simulations (2002-2004) indicates that the modeled results tracked the observed values very well except the bottom salinity in the summer 2004 and surface temperature during July-August in all three years (Figures 3.8-3.10). The observed surface temperature during July-August showed weaker variability than that of USGS buoy A. It suggests that the decrease in surface water temperature in western MB during summer was a result of local coastal upwelling. This will be furthered discussed in section 3.2.

3.1.4 Currents at USGS buoys A and B

The comparisons at both buoy stations in 2002-2004 indicate that there is a good agreement between modeled and observed surface and bottom currents in both short-term variability (days-weeks) and seasonal cycles (Figures 3.11-3.30). Here, we discuss major features and differences between modeled and observed currents in these years.

2002. In the winter-spring period currents at Buoy A were generally strong and southward at surface and northward at depth, while during the summer time both the surface and bottom currents were weak without clear directions (Figures 3.11-3.14). Clearly, the bottom currents were much weaker than the surface currents throughout the year. The model produced similar values and directions of observed currents with the following discrepancies: (1) In January, the modeled bottom currents were oriented more toward to northward, and (2) The model under-estimated the strength of upwelling/downwelling event in Junes (days 150-180), which is also reflected in modeled and observed temperature (Figure 3.5a).

In January-March and November-December, the surface currents at Buoy B were generally westward, while the bottom currents were weak and northward (Figure 3.15). In the rest of the year, there were no general directions for both the surface and bottom currents (Figures 3.16-3.18). Both the surface and bottom currents were strongest in the late spring and early summer. The model generally reproduced the values and directions of the observed currents but did not reproduce the surface cross-shelf transport in days 110-150, even though the modeled near bottom temperature and salinity agreed with data (Figure 3.5b).

2003. At Buoy A the seasonal characteristics of both surface and bottom currents were very similar to that of 2002 (Figures 3.19-3.22). The model reproduced the overall observed features except the under-estimated upwelling in days 200-220 (Figure 3.21), which can be seen in the surface temperature and salinity (Figure 3.6a).

At Buoy B the seasonal characteristics of both surface and bottom currents were markedly different from those in 2002 due to stronger winds and freshwater discharges in 2003 (Figures 3.23-3.26). For example, both surface and bottom currents were strong and predominantly southwestward in the winter and spring seasons (Figures 3.23 and 3.26). In the summer and fall, surface currents were characterized by strong upwelling/downwelling events with a mean offshore flow (eastward), whereas bottom currents are generally in opposite directions (Figures 3.24-3.25). The model reproduced these features except that it over-estimated surface currents by about 30-40% in the winter.

2004. Only data at Buoy A are available for comparison. The general seasonal characteristics of surface and bottom currents were very similar to those in 2003. One exception is that a series of inertial oscillations occurring between days 110-145 were in the observed results, which are not reproduced by the model (Figures 3.27-30). Since no similar inertial motion was found in currents measurements at the GoMOOS buoy A, these oscillations could be generated by the spatial variability of local mesoscale meteorological processes, which was excluded in the uniform meteorological conditions used in these simulations. Similar to 2003, the model over-estimated surface currents in Jan.-Mar. (Figure 3.27) and under-estimated the surface currents during the strong upwelling period between days 190-230 (Figure 3.29).

3.1.5 Currents at the GoMOOS A

2002. The observed surface currents were predominantly southwestward throughout the year

with strongest currents in late spring and early summer (Figures 3.31-3.34). The bottom currents were mostly southwestward throughout the year. The model reproduced the overall surface and bottom currents reasonably well (Figure 3.31-3.34). In particular, the model reproduced the upwelling events during summers (days 120-240). The modeled bottom currents tracked the observations very well in E-W direction, but not the N-S direction. The model under-estimated surface currents in the freshwater plumes during days 110-125 and days 160-180, and westward surface intruding current in November and December. In winter, modeled currents had less variability than the observed currents.

2003. The seasonal characteristics of both surface and bottom currents in 2003 were similar to that of 2002 except that (1) the variability of currents during spring were stronger, consistent with the stronger freshwater discharges in the Merrimack River, and (2) summer bottom currents were lack of median-range oscillations seen in 2002. The model performance is similar to that of 2002: (1) the model simulated the E-W component of bottom currents better than it did the N-S component of bottom currents throughout the year, (2) modeled currents had less variability than the observed in spring and summer.

2004. The observed currents were very much similar to those in 2003 (Figures 3.39-3.42). The model did not reproduce the N-S component of observed bottom currents well most of the year, and model currents had less variability than the observed in spring and summer.

The discrepancies of short-term variability between modeled and observed currents, especially bottom currents, at GoMOOS buoy A reflects the complexity of the circulation around Cape Ann, which results from interactions of local surface winds, topography, freshwater plume and the WMCC. The smoothed open boundary conditions and bottom topography may also contribute to the less variability of model currents.

3.2 Spatial distributions in August

In the following comparisons, the observations represent the mean hydrographical conditions during survey periods of 3-4 days while the modeled results are one tidal cycle averages centered on each survey periods.

3.2.1 Surface patterns in August 2002

This event occurred in a period of rapid transition from upwelling to normal condition

(Figures 3.43a and 3.13). The temperature at 5m recorded at the USGS buoy A was about 14ºC on August 21, and increased to 16.8ºC by end of the next day.

The modeled surface temperature, salinity and currents on August 21, 2002 (day 233) are shown in Figure 3.43a and observed surface temperature and salinity in August 19-22, 2002 are shown in Figure 3.43b. Both modeled and observed surface temperature showed significant temperature gradients from the cooler water at Cape Ann to warmer water at Plymouth, and from cooler water in the Boston Harbor vicinity to the warmer water in offshore areas. The model also reproduced much more detailed mesoscale patterns in both temperature and salinity distributions than observations whose spatial resolution were too crude to resolve these features. This difference may also be biased by the time differences of measurements at different stations because the MWRA nearfield survey took place on August 22, 2002, while farfield survey at other coastal stations in western MB took place 2-3 days earlier (August 19-20).

3.2.2 Surface patterns in August 2003

The temperature and salinity from modeled results on August 20, and observations during August 18-21 are shown in Figures 3.44a and 3.44b, respectively. Also shown in Figure 3.44a are modeled surface currents, which are overall southward. We note that measurements were conducted when hydrographic conditions had restored completely from a strong upwelling event. The spatial variation of temperature at 5m was less than 1ºC and that of salinity was less than 0.2 ‰ during the 4-day survey period.

The model reproduced the spatial pattern of surface salinity well, but the predicted temperature pattern differed from the observed. It is unclear why surface water in the Boston Harbor vicinity remained cold during the 5-6 days restoring period. This upwelling was observed in the surface currents measurements at USGS buoy B, until August 20 (day 232). Because coastal upwelling is directly associated with winds, the spatial variability of winds might contribute to the spatial variability of upwelling, which was missing in the model forcing. The low surface salinity in western MB represents the extension of the Merrimack River freshwater plume.

3.2.3 Surface patterns in August 2004

The survey was conducted during the peak of an upwelling event (August 18, 2004) (see

Figures 3.7 and 3.29). The modeled currents and surface temperature indicate clearly an upwelling situation, consistent with the observed surface temperature (Figure 3.45). The observed cold water was found in a much narrower band and with much lower temperature than the modeled. Again, the modeled water temperature in Boston Harbor was warmer than the observed. Both modeled and observed salinities show small horizontal gradients.

Similar discrepancies between modeled and observed summer upwelling events in western MB have been noted in previous simulations (HydroQual and Signell, 2001; Jiang and Zhou, 2004a). The reasons for such discrepancies have not been understood. We can speculate that the current model resolution in coastal areas is unable to resolve the narrow upwelling band in western MB or the model over-estimates the horizontal mixing and hence under-estimates horizontal temperature and salinity gradients. The spatial variability of surface winds, which was missing in the model, may have contributed to the cold water found in the BH vicinity during these upwelling events.

3.3. Inter-annual variability of springtime circulation

The inter-annual variability of circulation in spring can be illustrated by the variability in the strength of both modeled and observed coastal currents, especially the N-S component (Table 3.1). Modeled coastal current has good correlation with the observed in the N-S direction (R^2=0.6) but less correlation in the E-W direction (R^2=0.32).

Changes of the coastal current were normally associated with the changes of the circulation pattern in MB. For example, typically the MBS circulation in spring has a counter-clockwise pattern formed by an intruding current from the GOM, a southward coastal current that penetrates into CCB and a counter-clockwise circulation in CCB (Figure 3.46a). The circulation in spring 2002 was significantly different: both the intruding current and the coastal current were significantly reduced and the intruding current flowed directly toward the South Passage, bypassing Cape Cod Bay (Figure 3.46b).

The anomalies might be caused by several mechanisms: (1) inter-annual variability of the WMCC (Pettigrew et al., 2005), (2) variability of the Merrimack River discharge, and (3) variability of the local wind forcing. For example, the freshwater input from the Merrimack River was low in spring 2002 (Figure 2.5) and southerly winds occurred frequently during spring 2002 (Figure 2.2), both of which contributed to the weak coastal currents and abnormal

circulation pattern in the MBS.

3.4 Summary of model validation

Significant inter-annual variability exists in the MBS hydrographic environment. For example, the temperature in January-February 2002 was warmest among three years, while the surface salinity in spring was highest in 2002 and lowest in 2003. During spring, the coastal currents at Scituate were weakest in 2002, while the currents at the GoMOOS buoy A were strongest in 2004.

The model was able to capture major dynamics features including (1) the seasonal cycle of temperature, salinity and currents, (2) the spring-time freshening of surface waters, (3) both short-term variability and long-term means of currents, and (4) major inter-annual variability noted above. For example, the model and observed springtime coastal current has a R^2=0.6 ($p<0.05$) (Table 3.1).

There are significant differences between model and data: (1) the model underestimated the coastal upwelling in late spring and summer, which caused overestimated surface and bottom temperature in western MB, and underestimated horizontal currents at both USGS buoy A and B; (2) in spring and early summer the model tended to over-estimate surface salinity along the western coast, which could be due to the underestimation of Merrimack plume and the zero precipitation in the model; (3) the model tended to over-estimate surface currents in winter; (4) the model over-estimated the bottom salinity at GoMOOS buoy A in summer 2003 and 2004, which is likely due to a lack of observations at the open boundary; and (5) the modeled currents at GoMOOS buoy A show less variability than the observed in late spring and summer, which is likely due to smooth model topography, coarse model grid and a lack of observations at the open boundary resolving short-term variability in the boundary forcing.

Table 3.1 Modeled and observed mean currents (unit: cm/sec) in March-April at USGS buoy B.

Year	Model		Observations	
	N-S	E-W	N-S	E-W
1998	-7.0	3.5	-6.6	2.8
1999	-7.4	3.9	-5.9	1.9
2000	-5.8	2.3	-3.2	0.8
2001	-7.2	2.6	-4.3	2.3
2002	-1.2	0.6	-1.6	1.0
2003	-4.3	1.4	-5.0	2.0
2004	-3.5	1.1	N.A.	N.A.

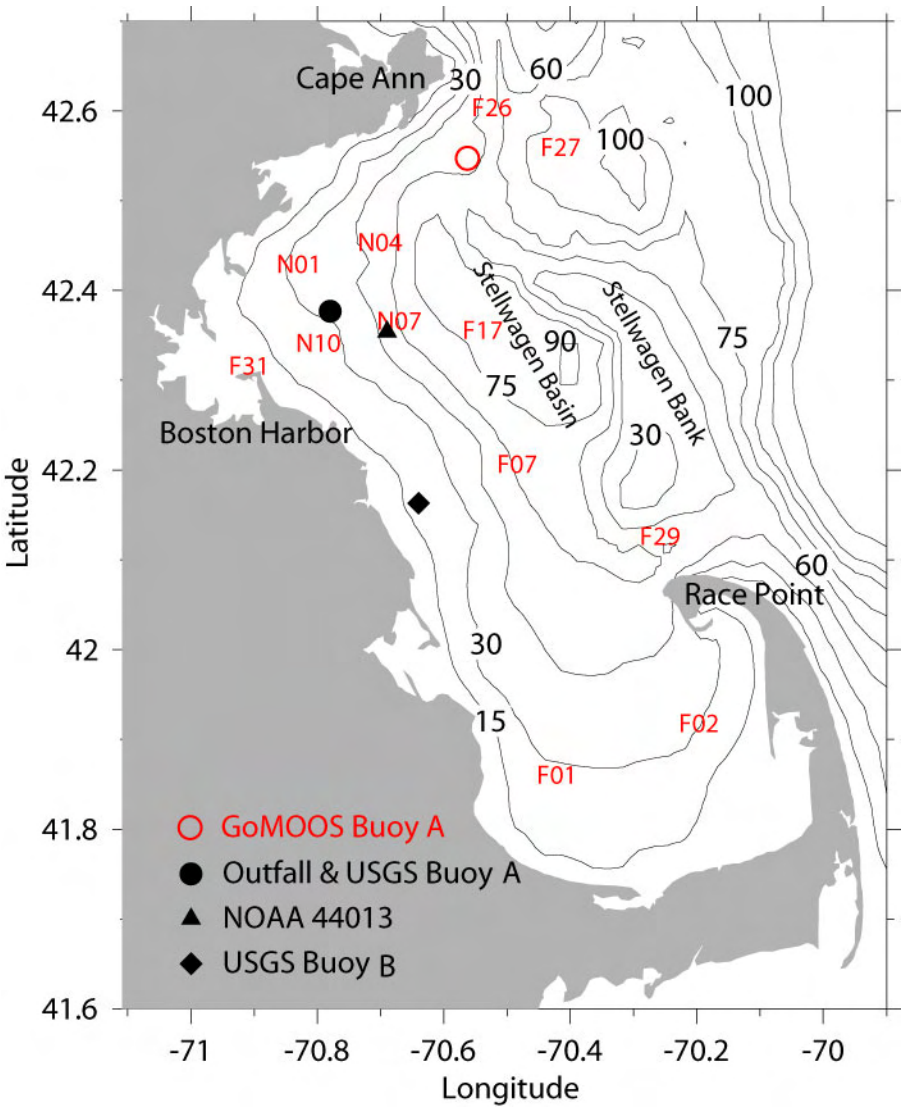

Figure 3.1. Stations used for the model validation.

(a)

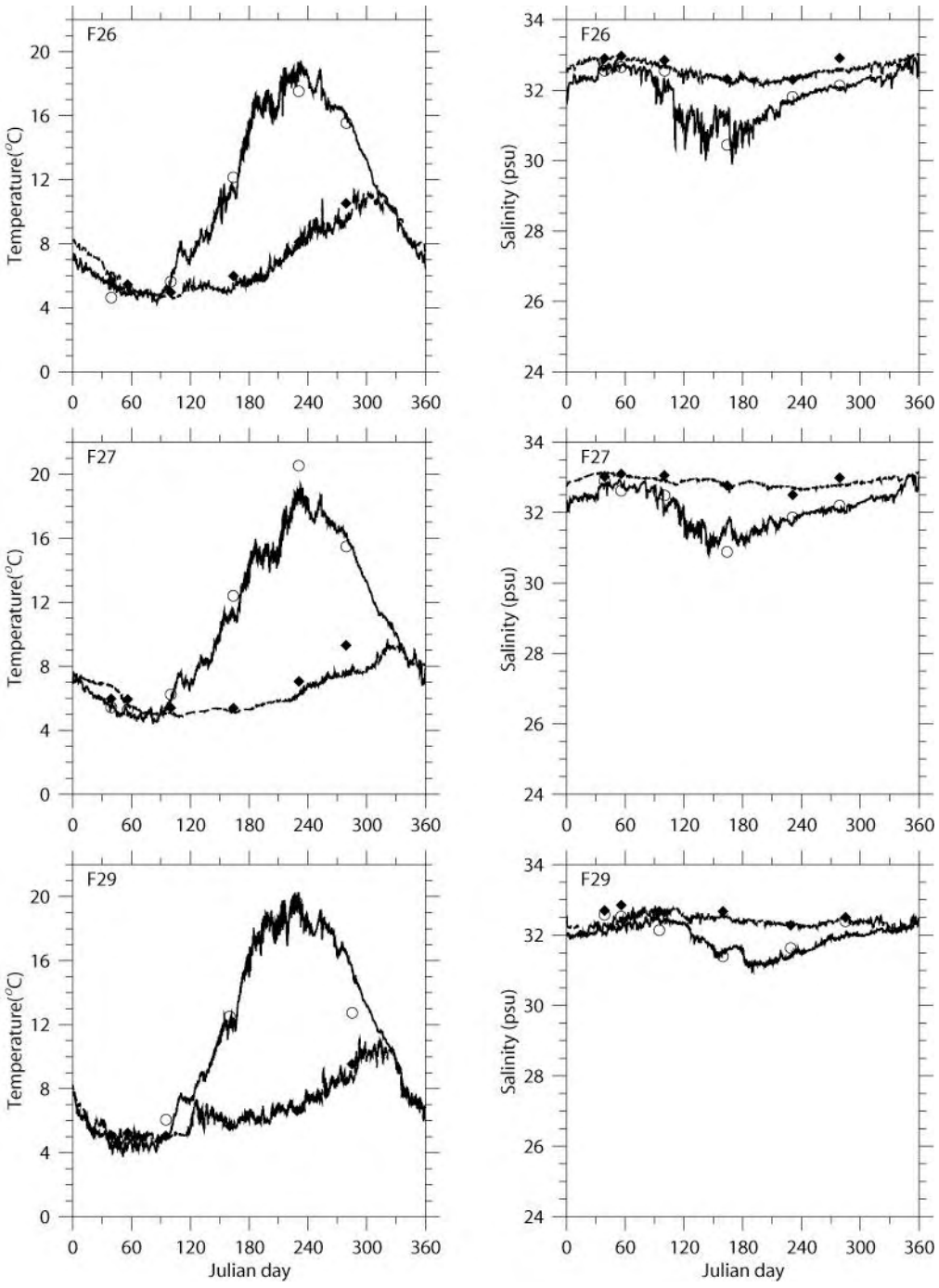

Figure 3.2. Modeled and observed temperature and salinity at selected stations in 2002.

(b)

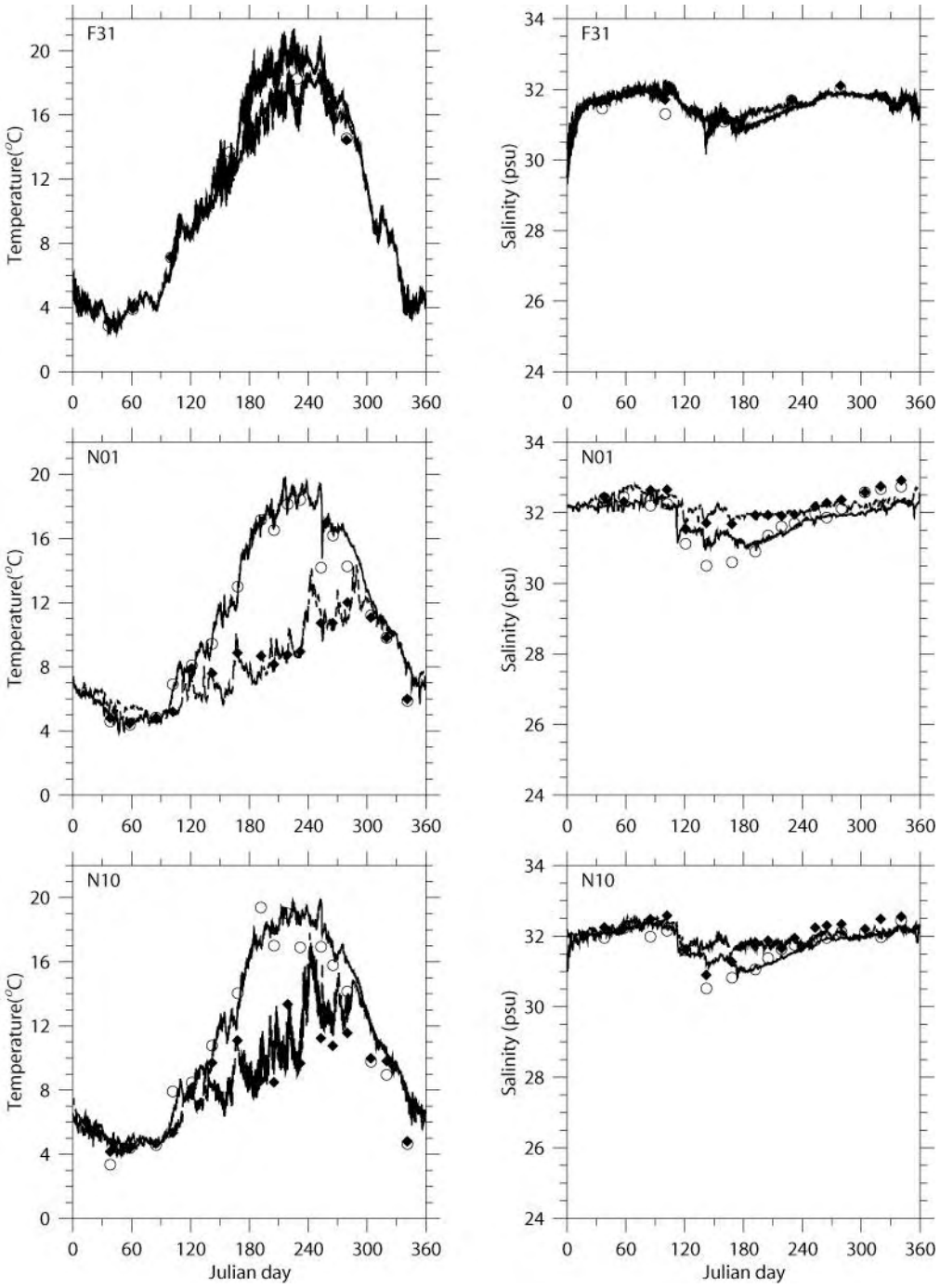

Figure 3.2. Continued.

(c)

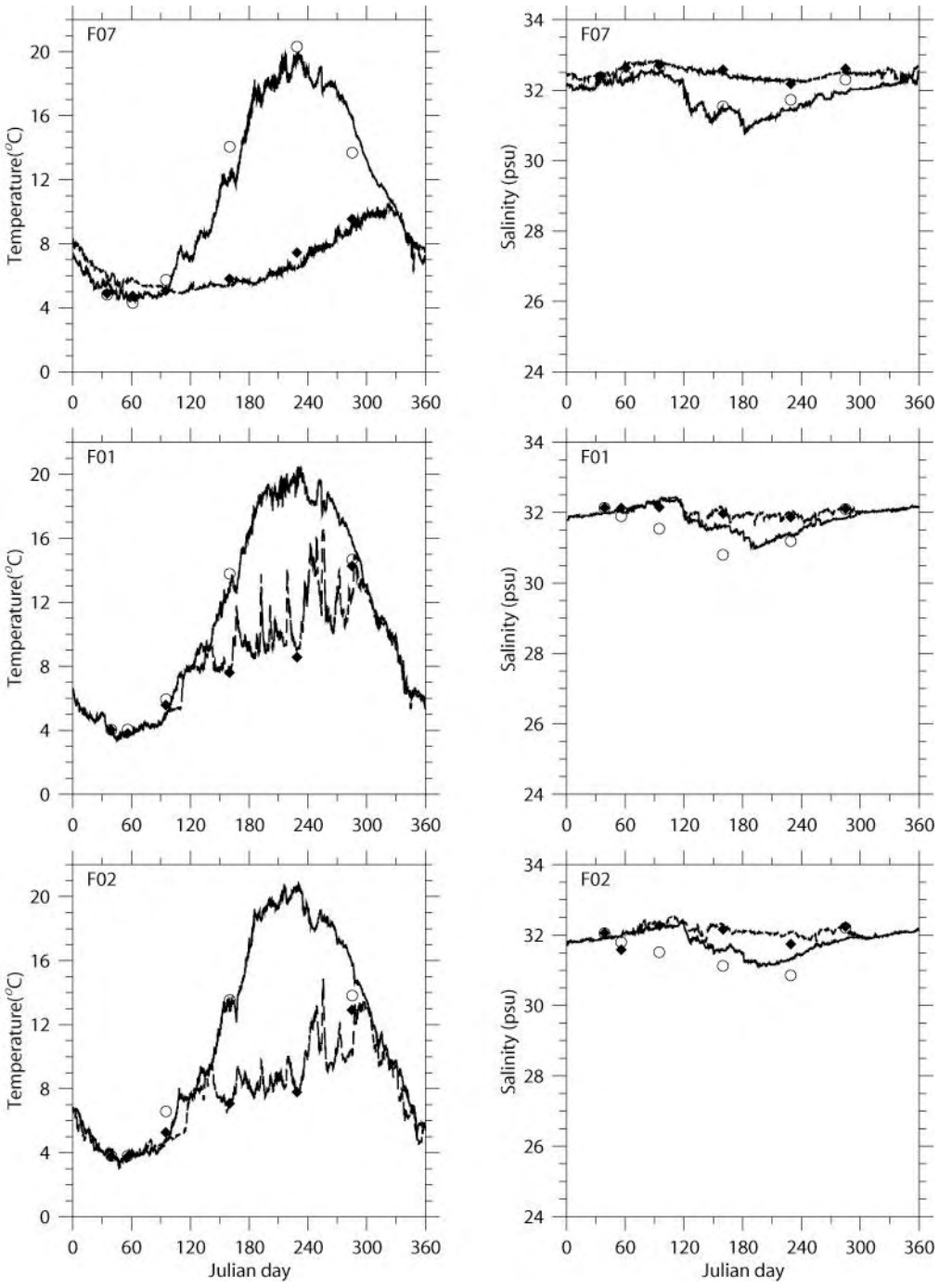

Figure 3.2. Continued.

(d)

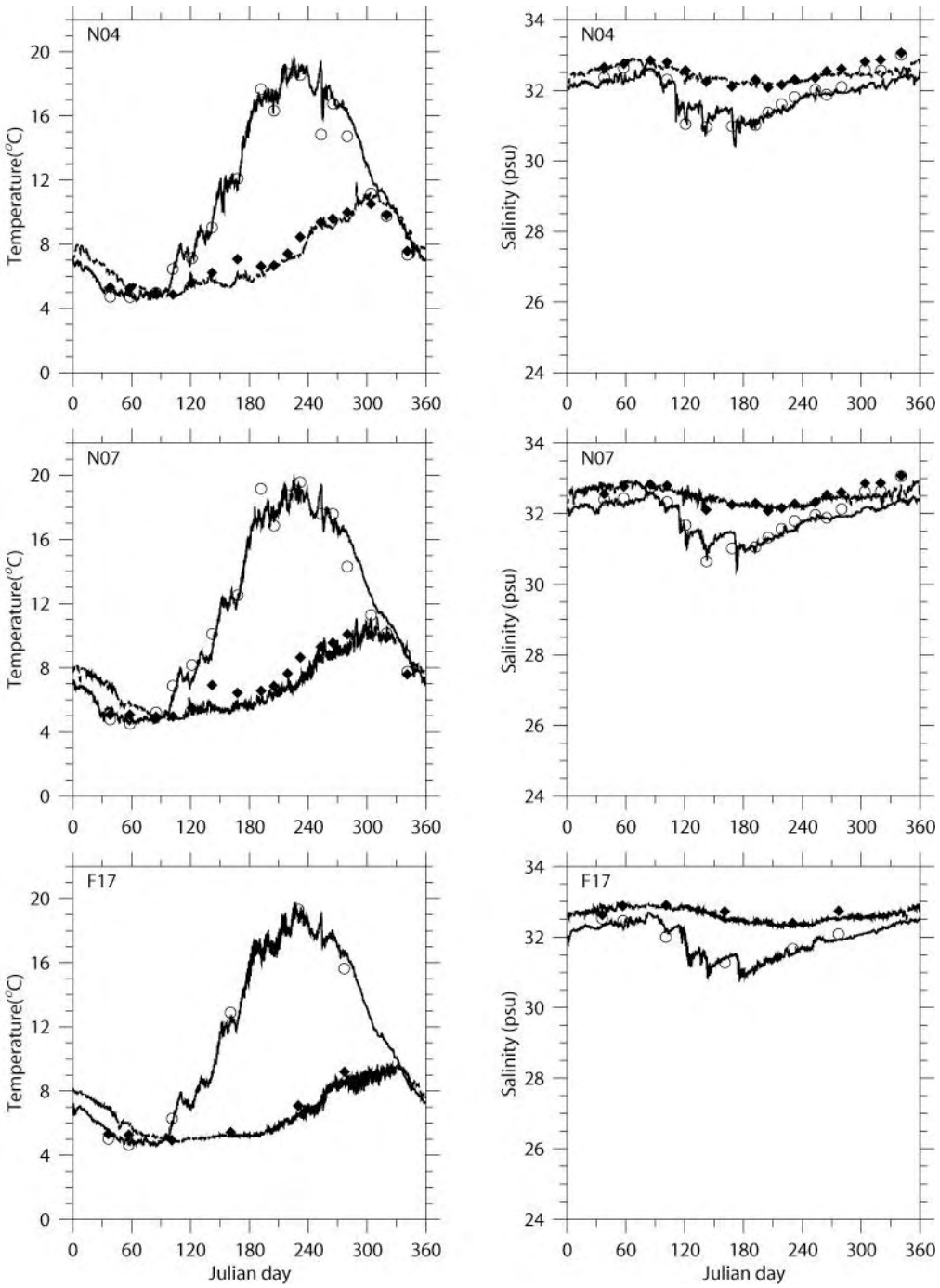

Figure 3.2. Continued.

(a)

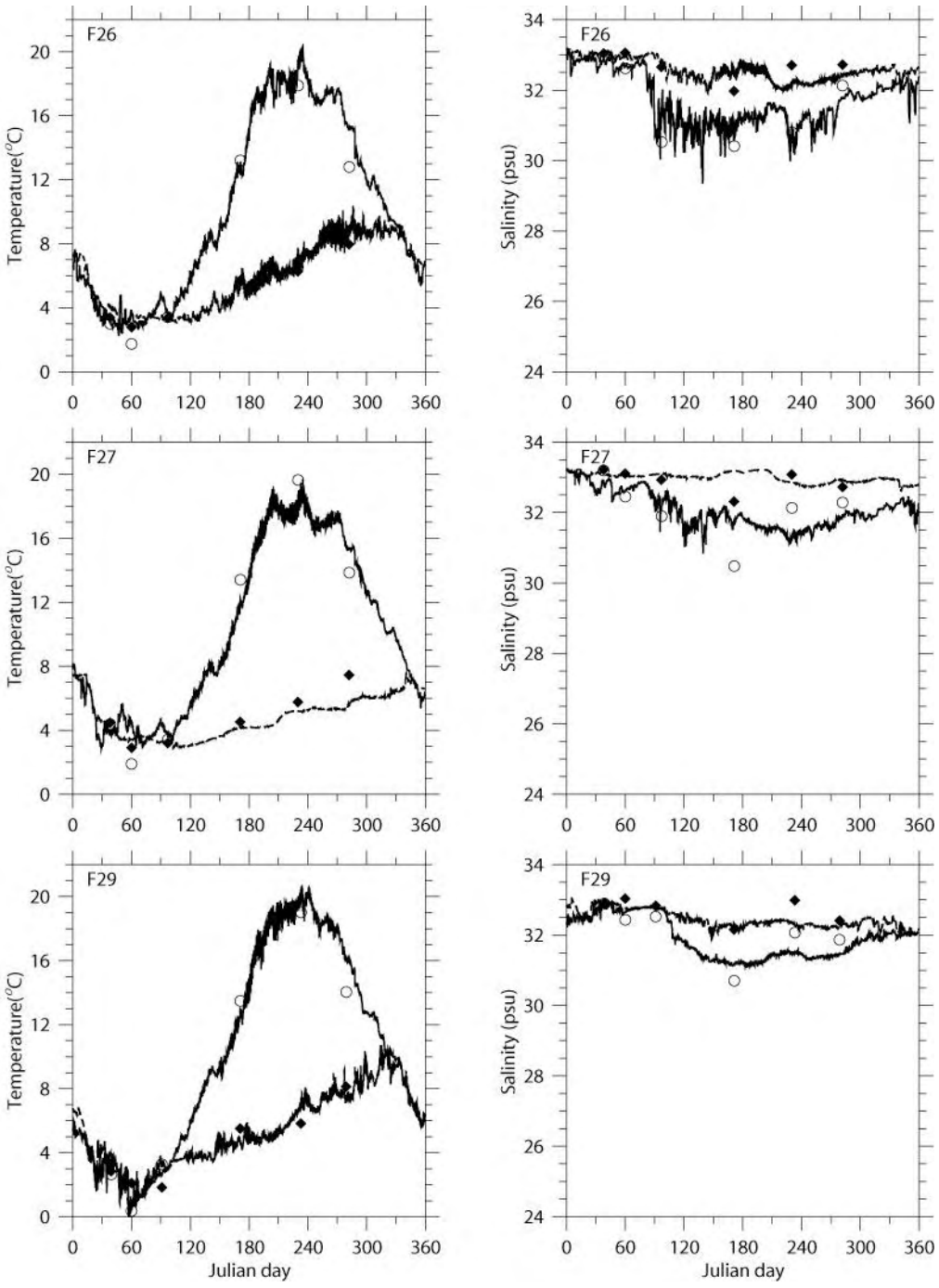

Figure 3.3. Modeled and observed temperature and salinity at selected stations in 2003.

(b)

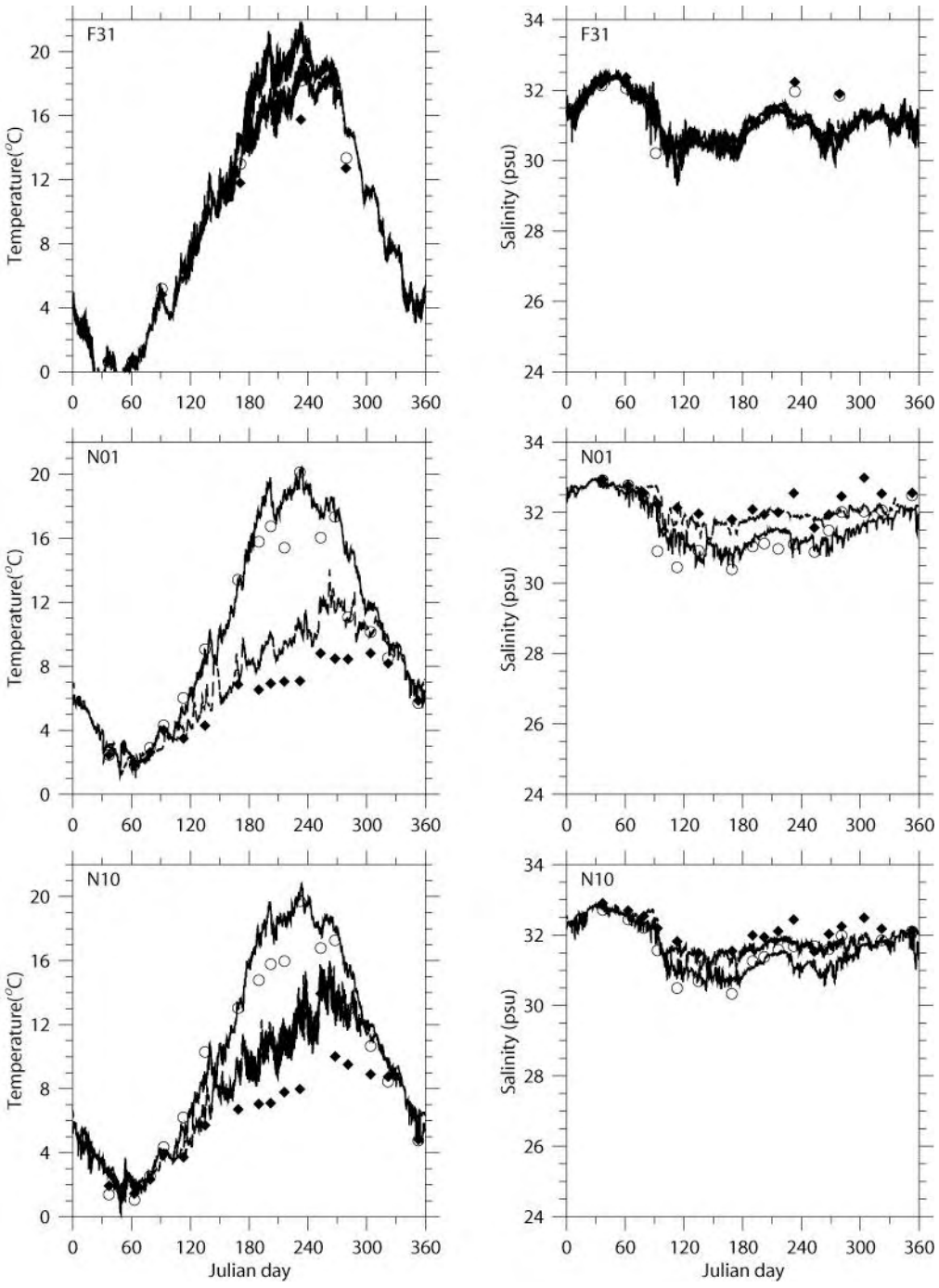

Figure 3.3. Continued.

(c)

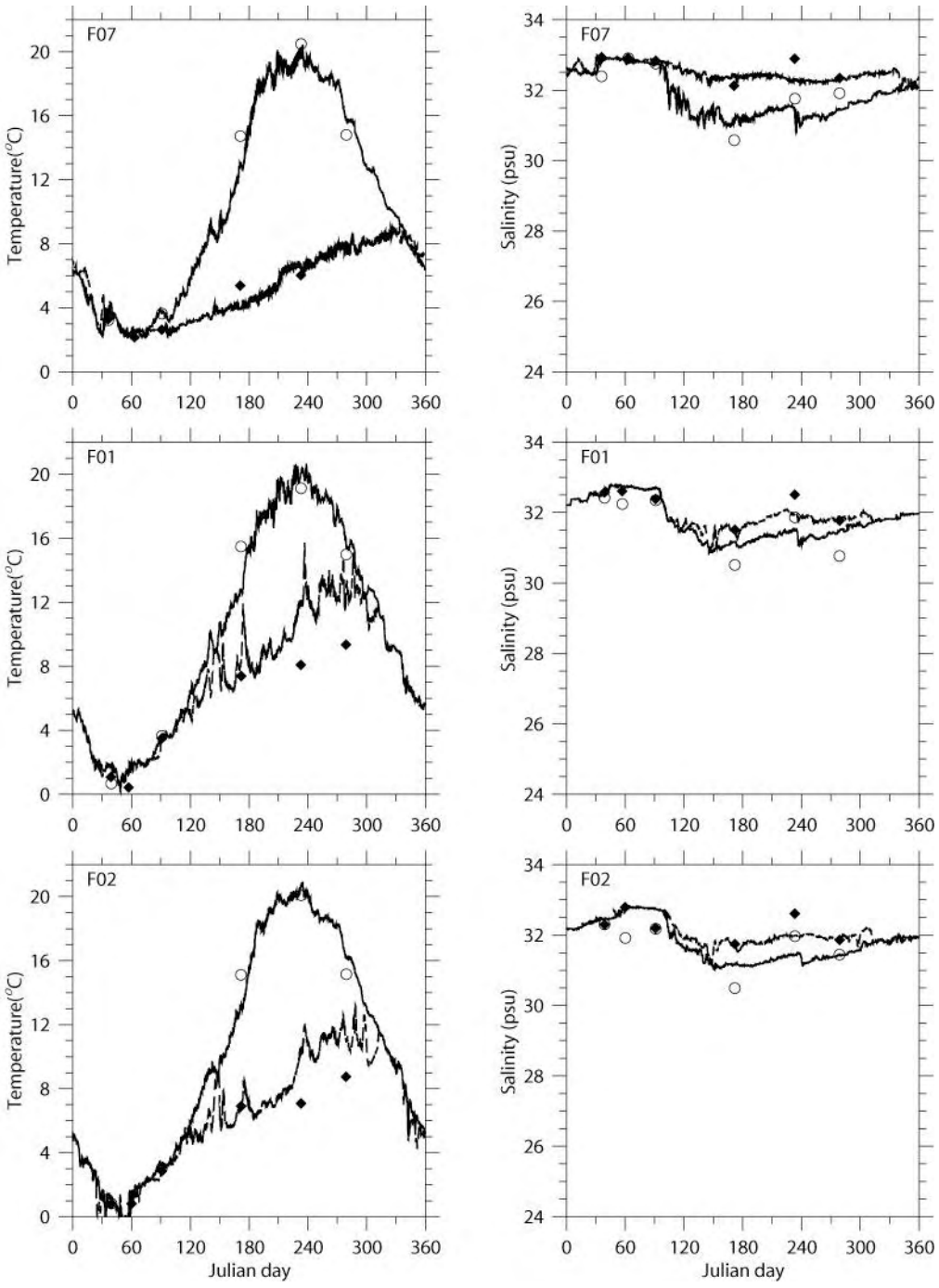

Figure 3.3. Continued.

(d)

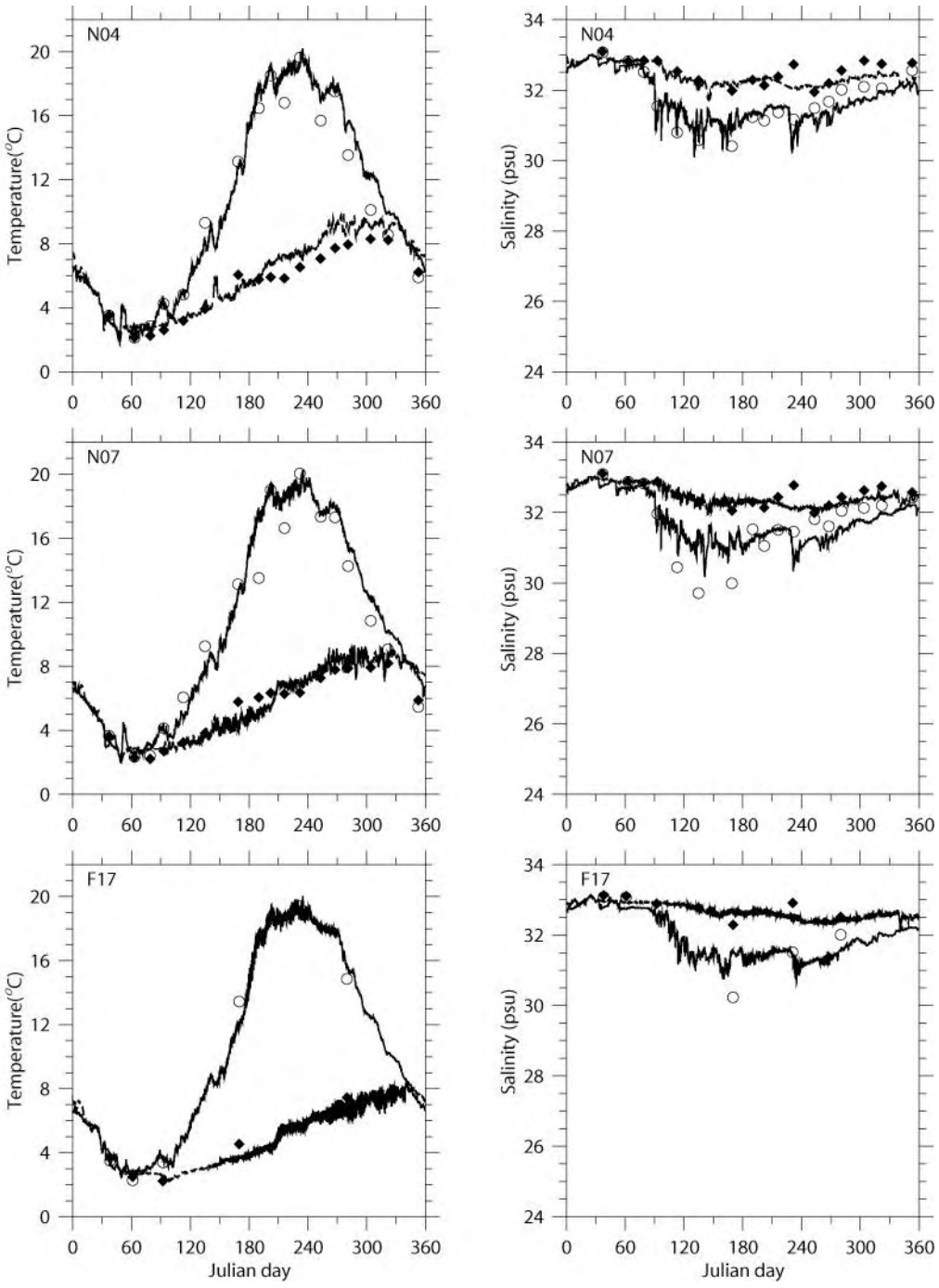

Figure 3.3. Continued.

(a)

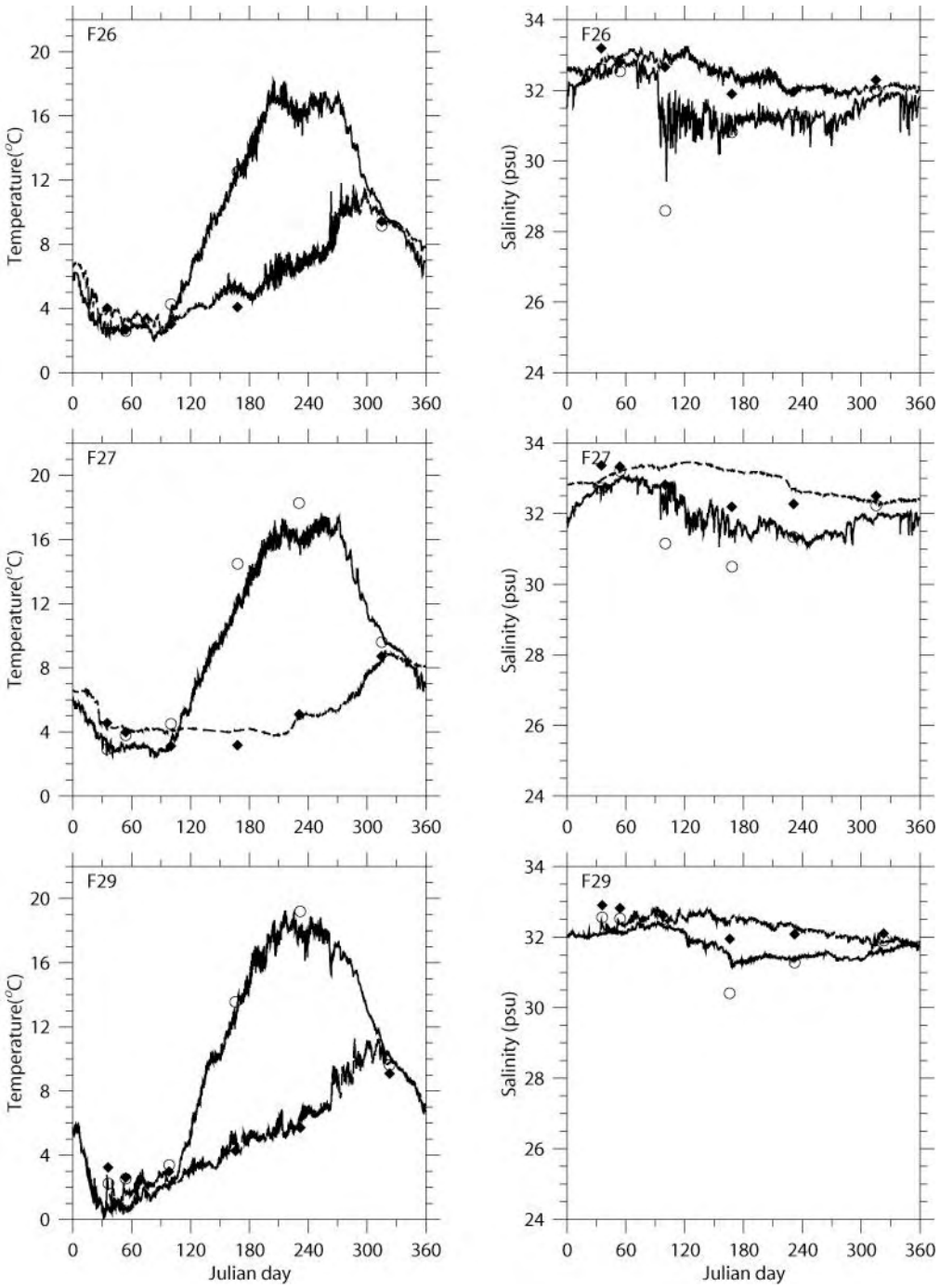

Figure 3.4. Modeled and observed temperature and salinity at selected stations in 2004.

(b)

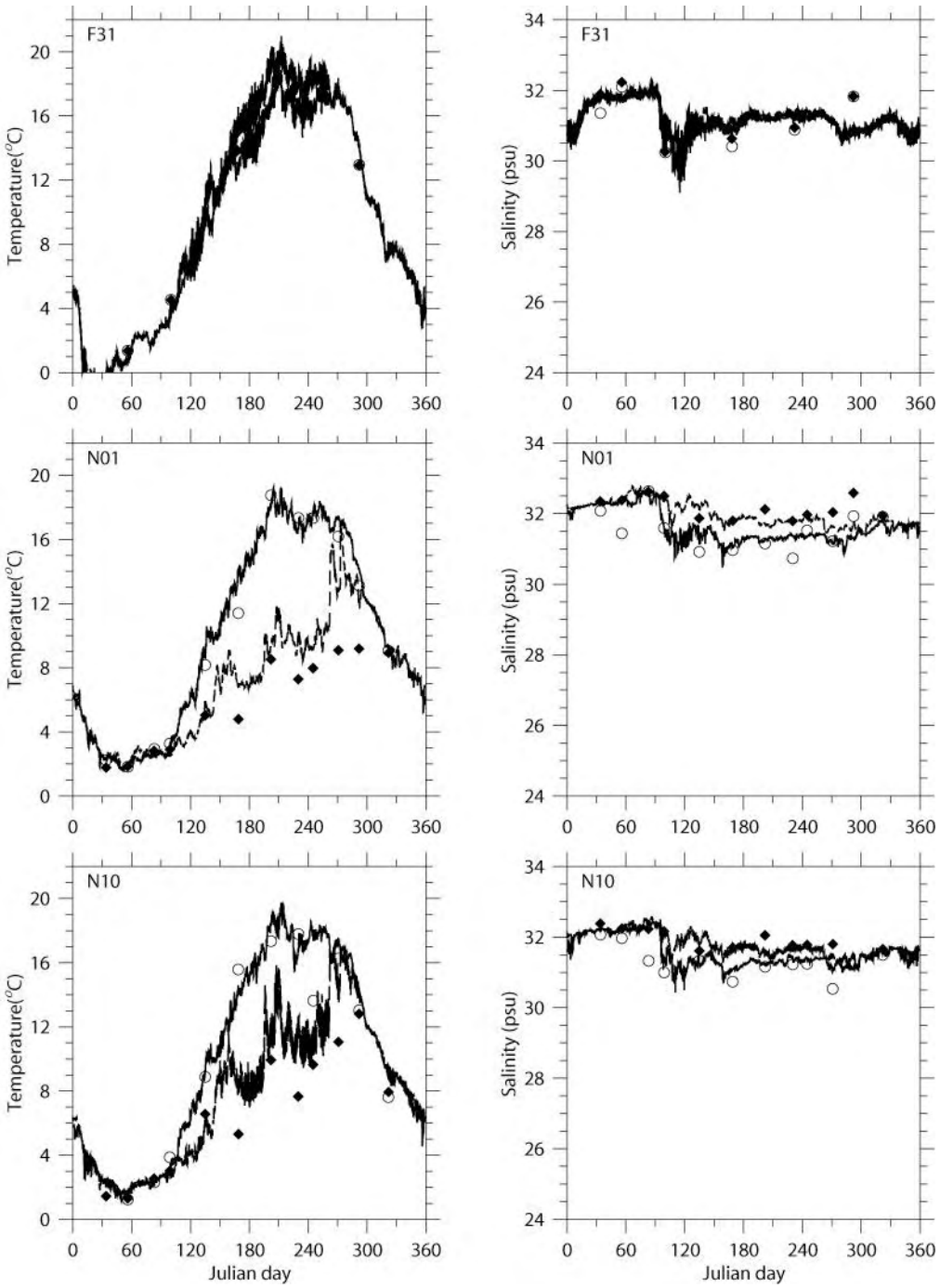

Figure 3.4. Continued.

(c)

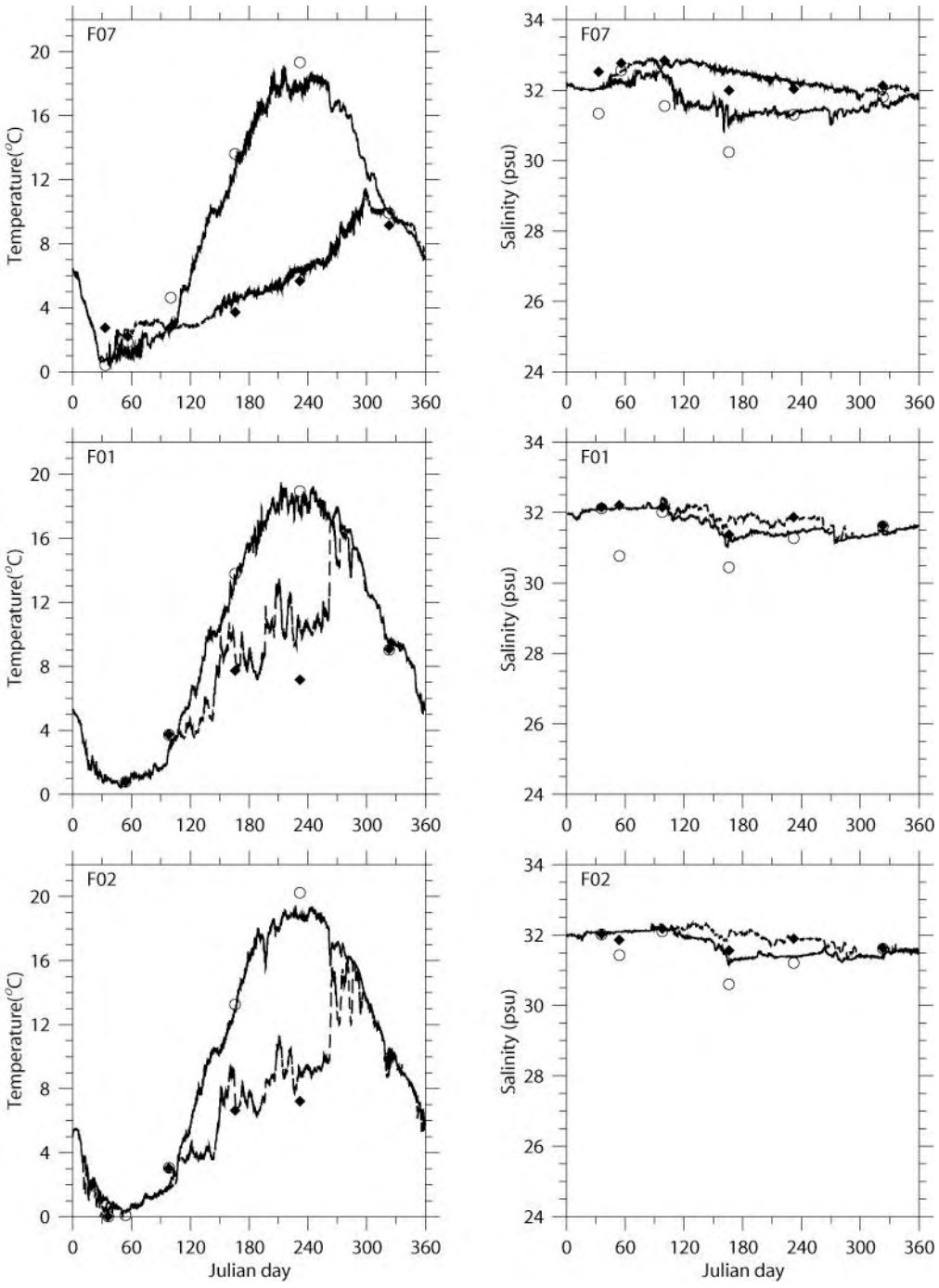

Figure 3.4. Continued.

(d)

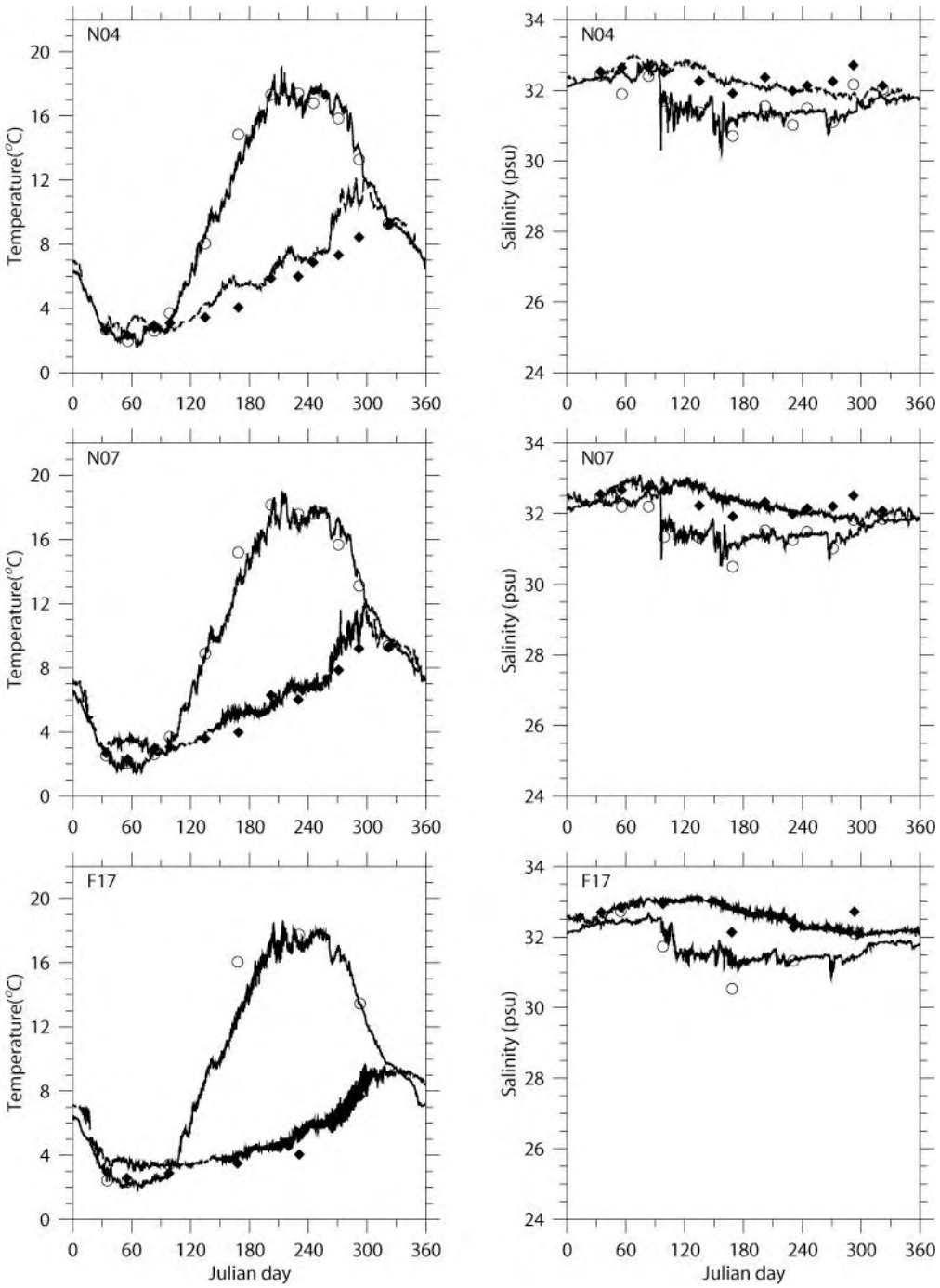

Figure 3.4. Continued.

(a)

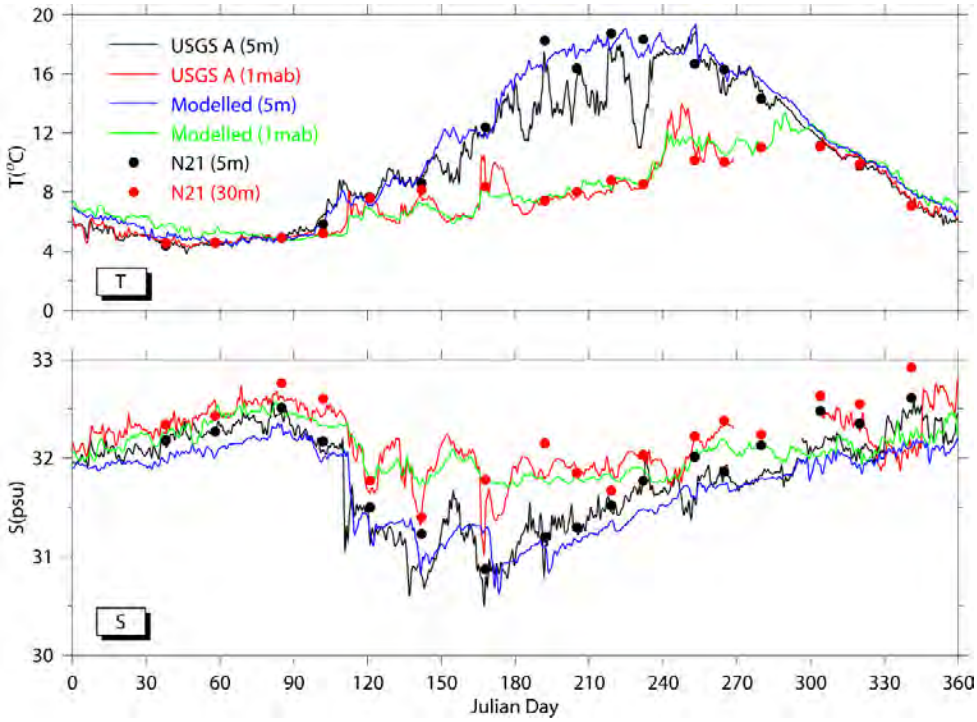

(b)

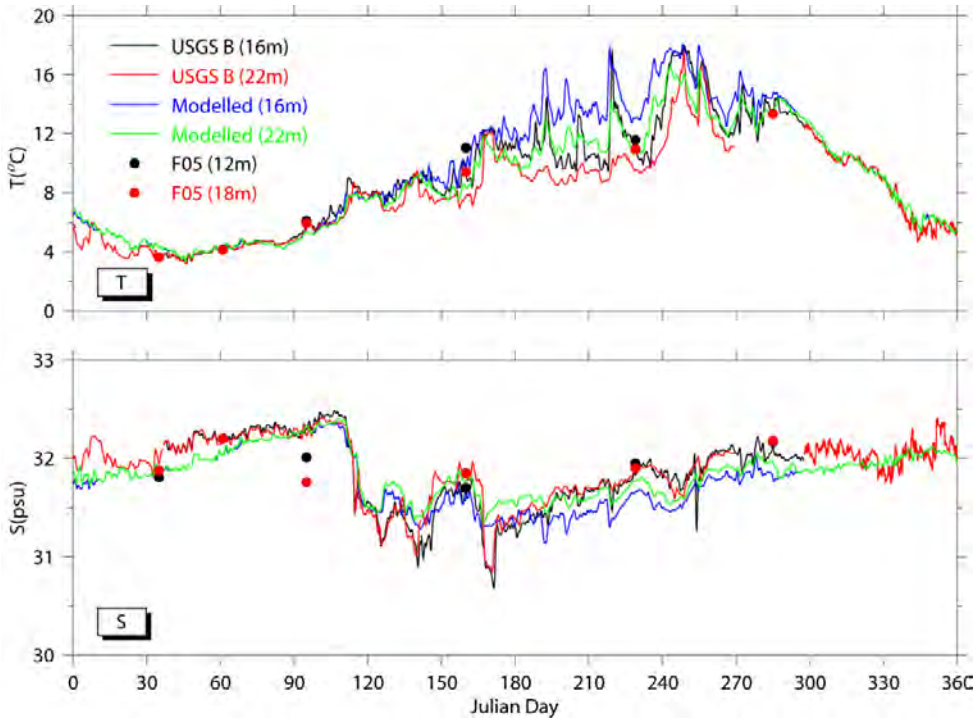

Figure 3.5. Modeled and observed temperature and salinity at (a) USGS Buoy A and (b) USGS Buoy B in 2002.

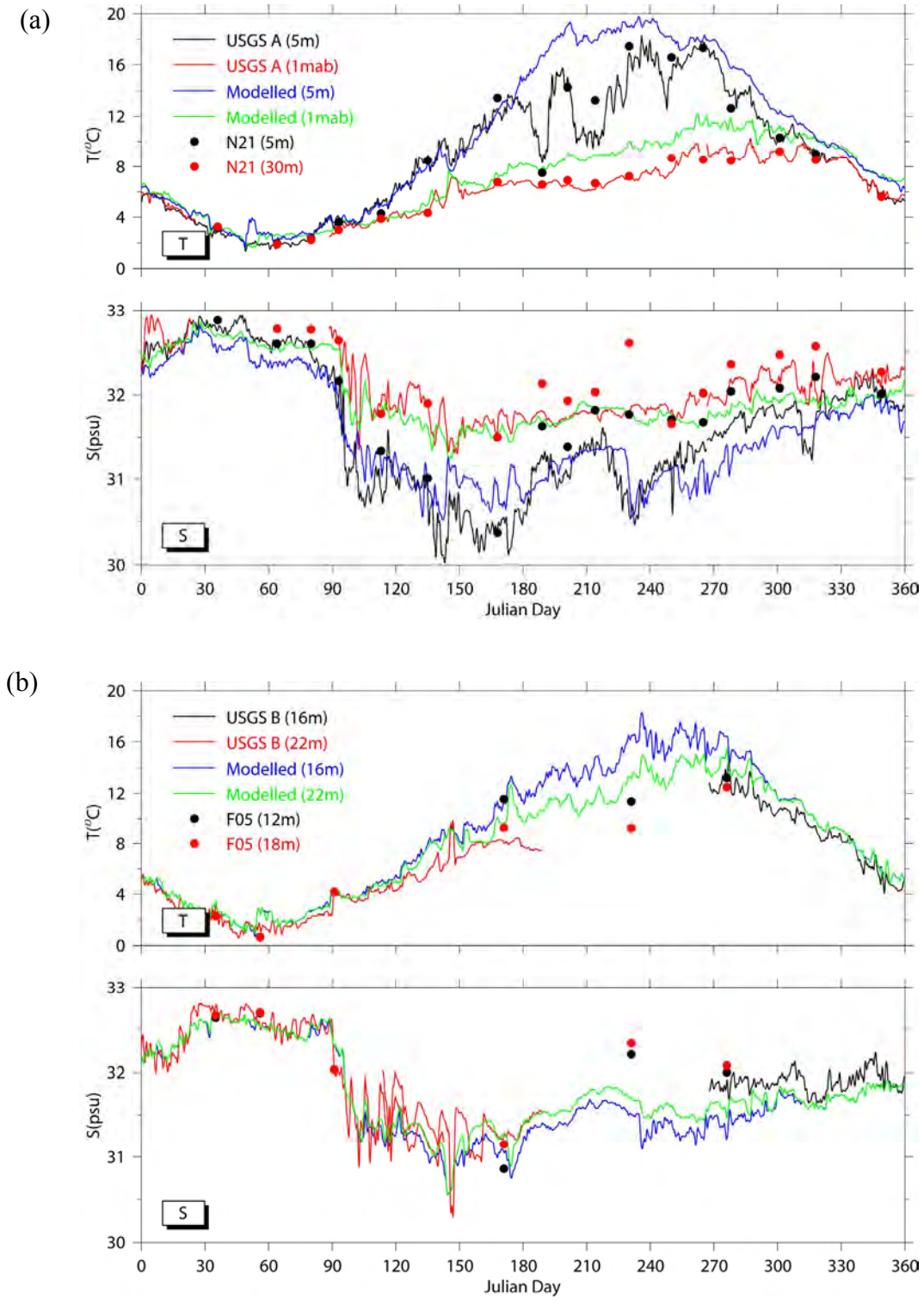

Figure 3.6. Modeled and observed temperature and salinity at (a) USGS Buoy A and (b) USGS Buoy B in 2003.

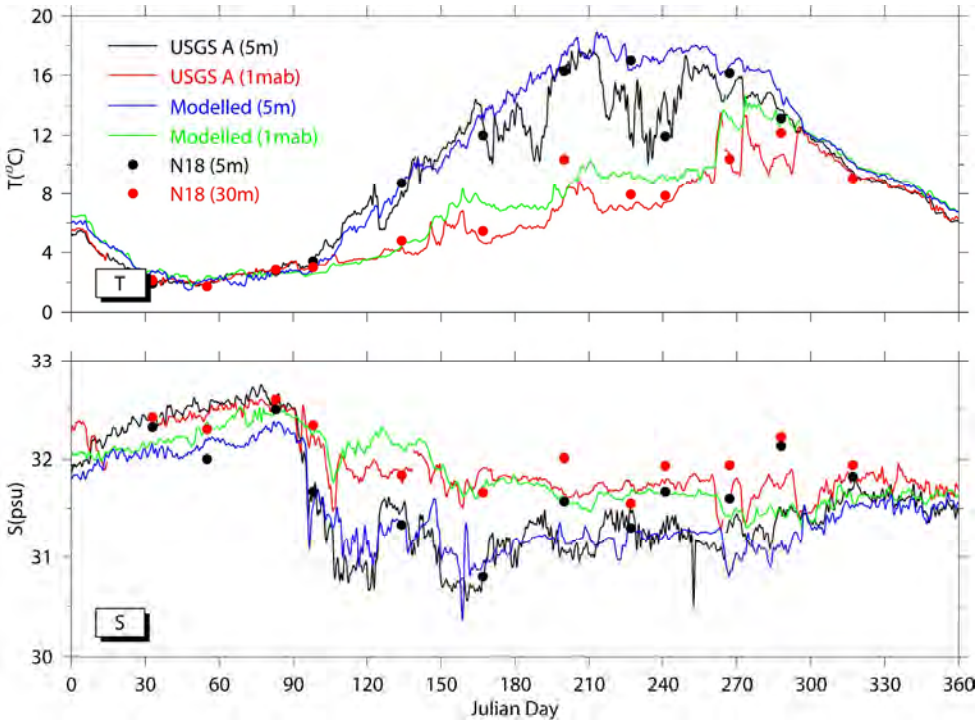

Figure 3.7. Modeled and observed temperature and salinity at USGS Buoy A in 2004.

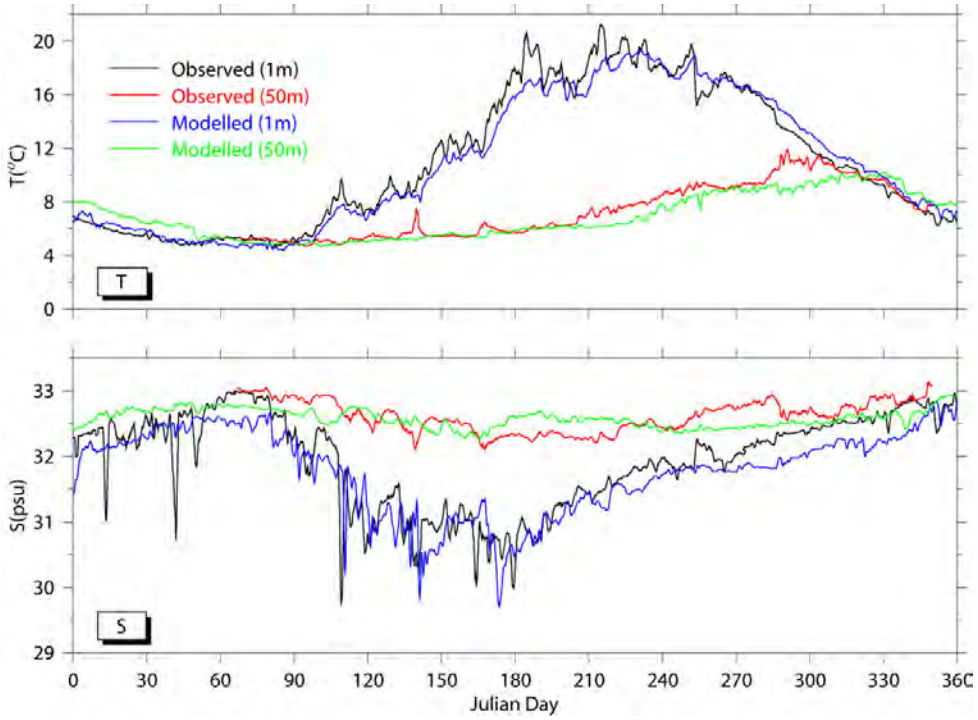

Figure 3.8. Modeled and observed temperature and salinity at GoMOOS Buoy A in 2002.

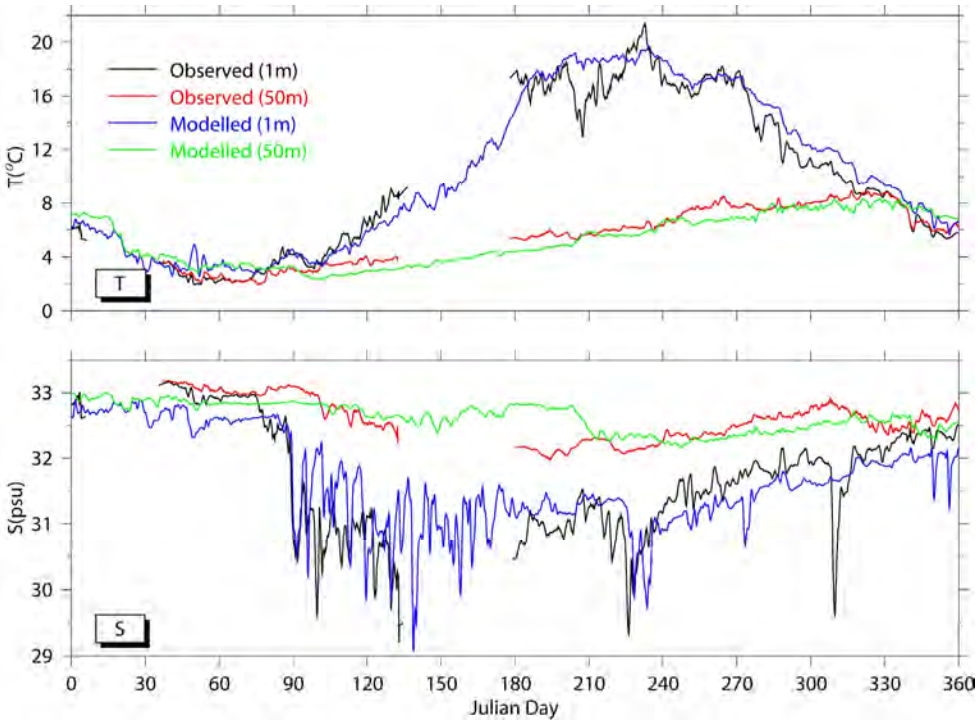

Figure 3.9. Modeled and observed temperature and salinity at GoMOOS Buoy A in 2003.

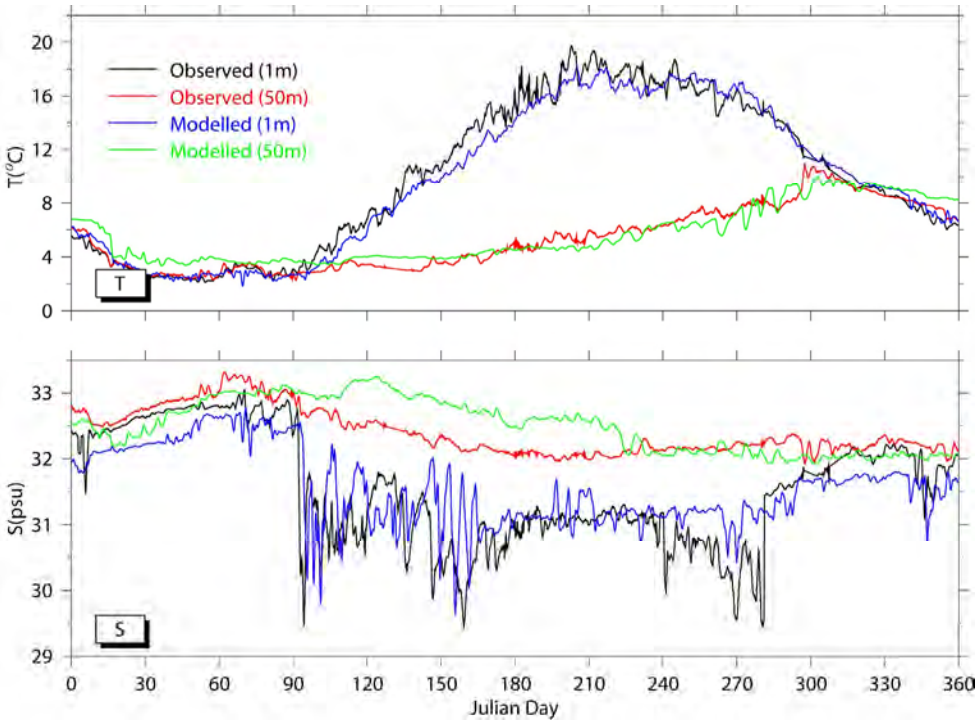

Figure 3.10. Modeled and observed temperature and salinity at GoMOOS Buoy A in 2004.

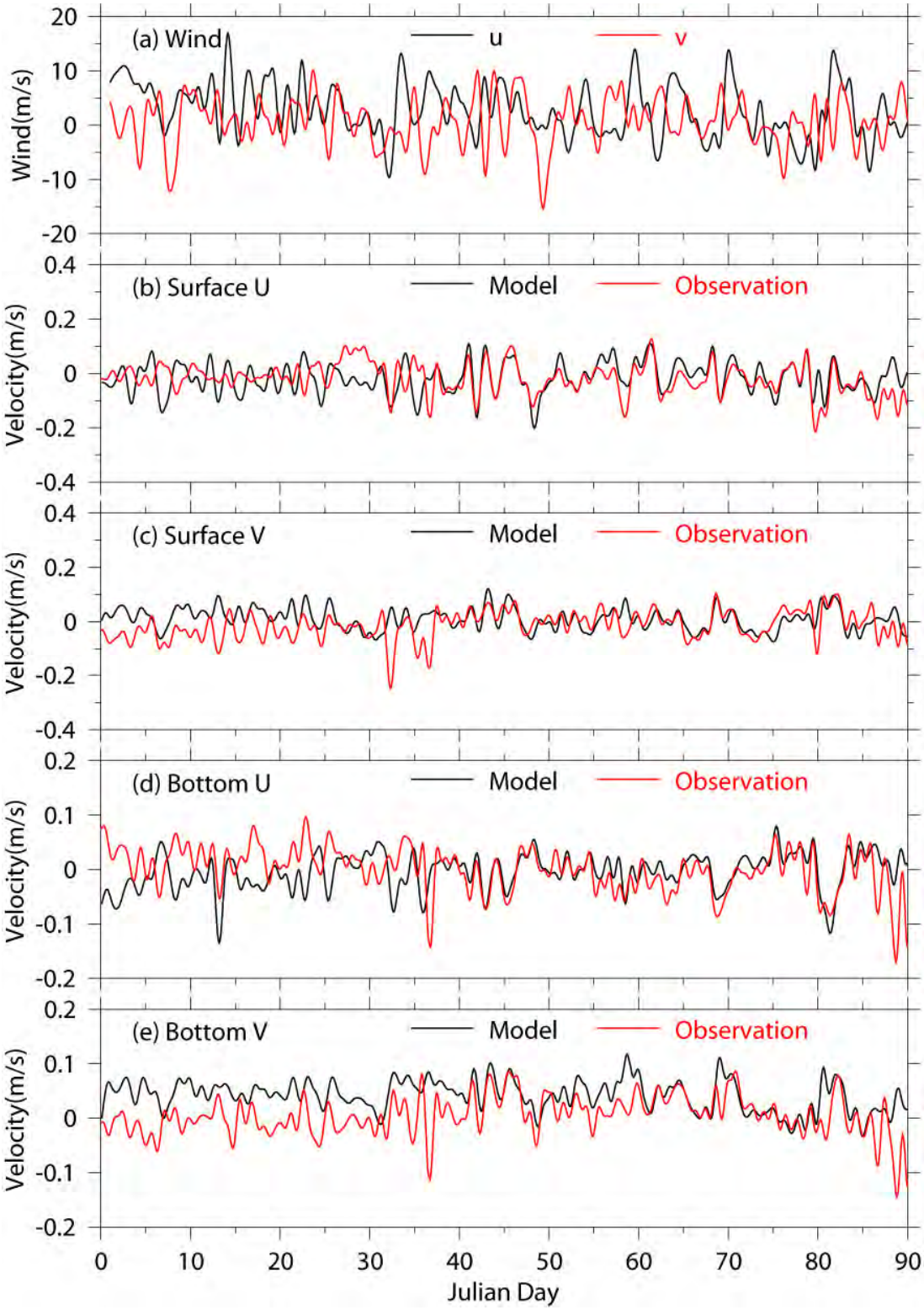

Figure 3.11. Winds at NOAA 44013 and currents at USGS Buoy A in Jan.-Mar. 2002, (a) Wind, (b) surface E-W velocity, (c) surface N-S velocity, (d) bottom E-W velocity, (e) bottom N-S velocity.

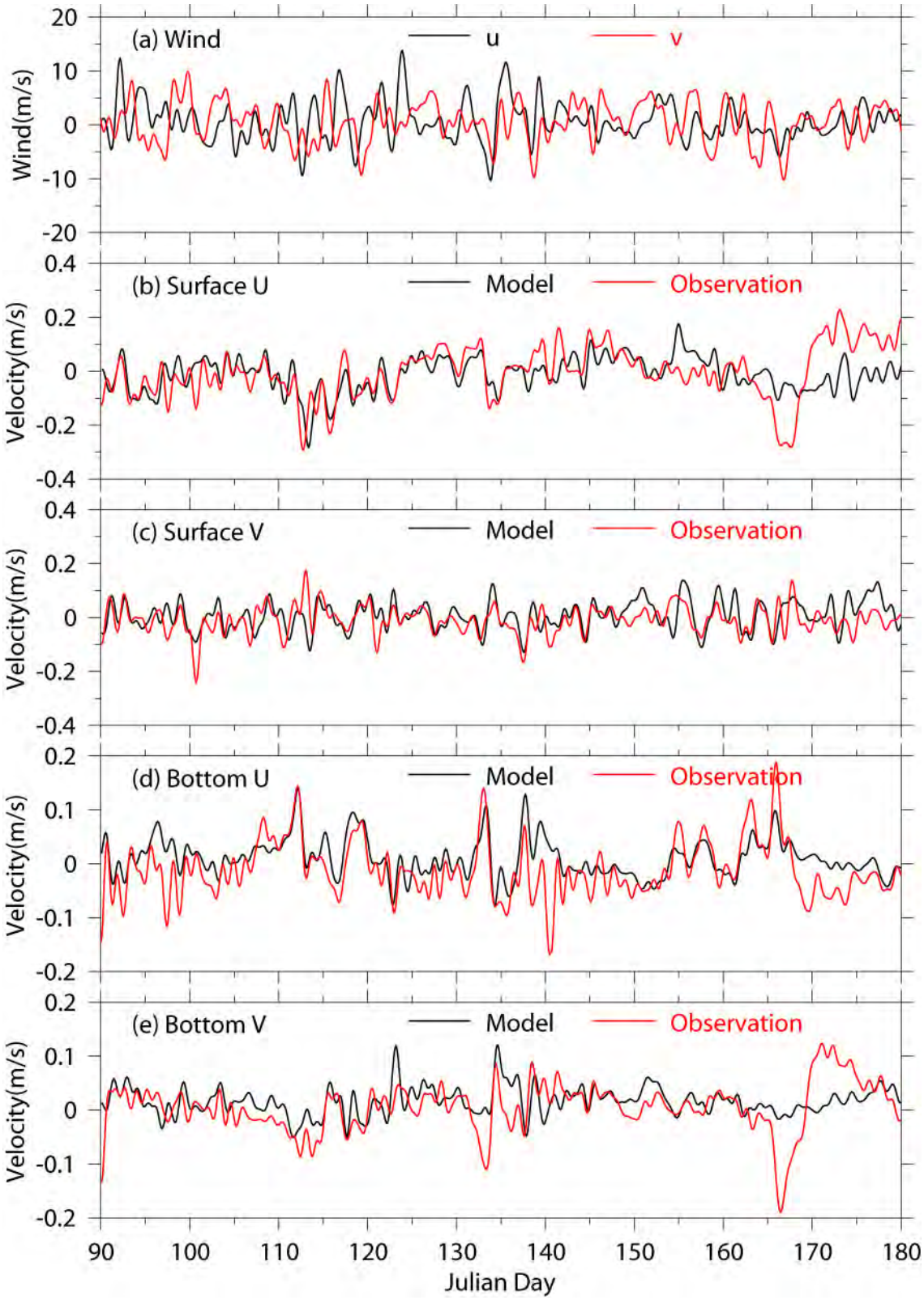

Figure 3.12. Winds at NOAA 44013 and currents at USGS Buoy A in Apr.-Jun. 2002, (a) Wind, (b) surface E-W velocity, (c) surface N-S velocity, (d) bottom E-W velocity, (e) bottom N-S velocity.

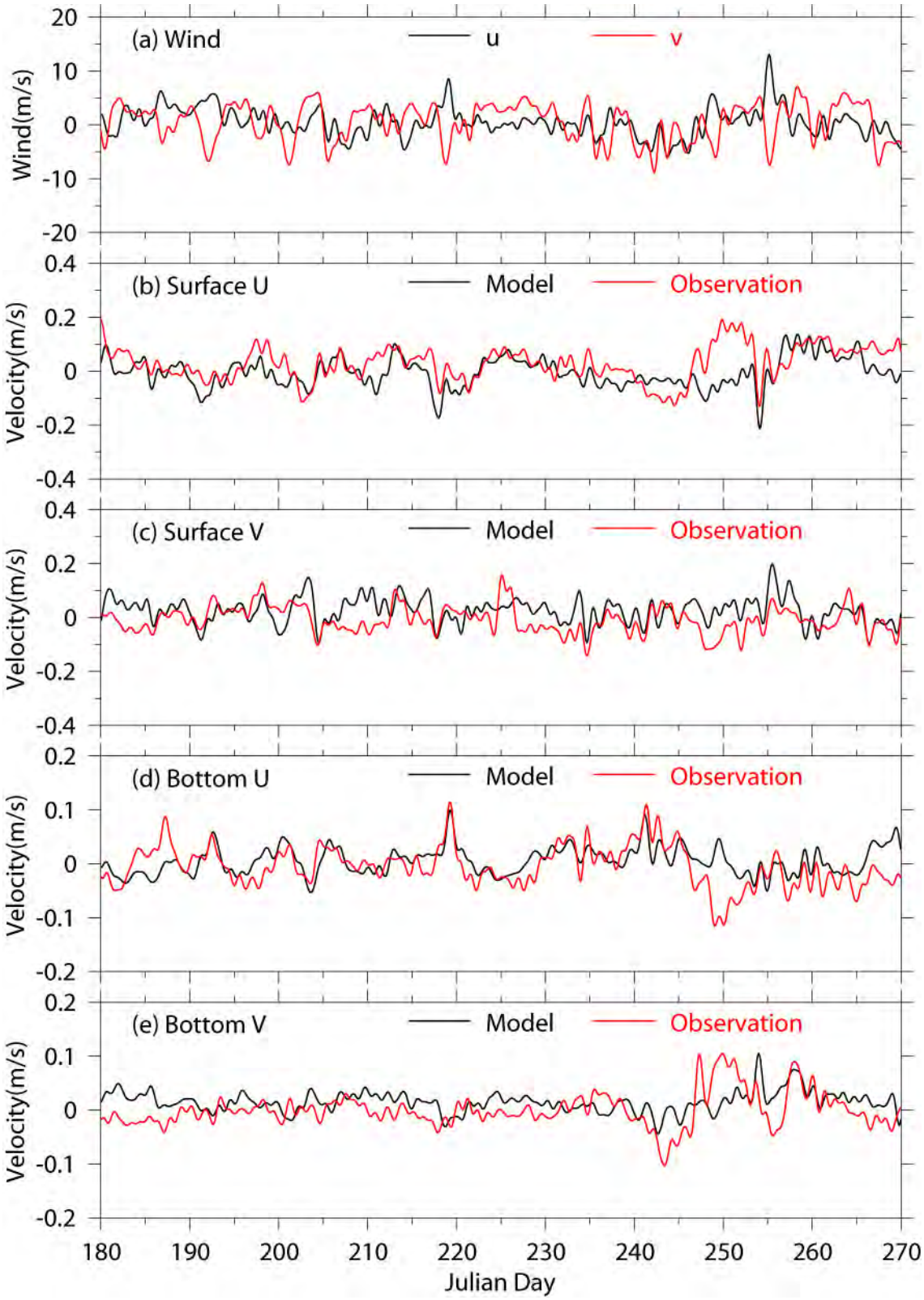

Figure 3.13. Winds at NOAA 44013 and currents at USGS Buoy A in Jul.-Sep. 2002, (a) Wind, (b) surface E-W velocity, (c) surface N-S velocity, (d) bottom E-W velocity, (e) bottom N-S velocity.

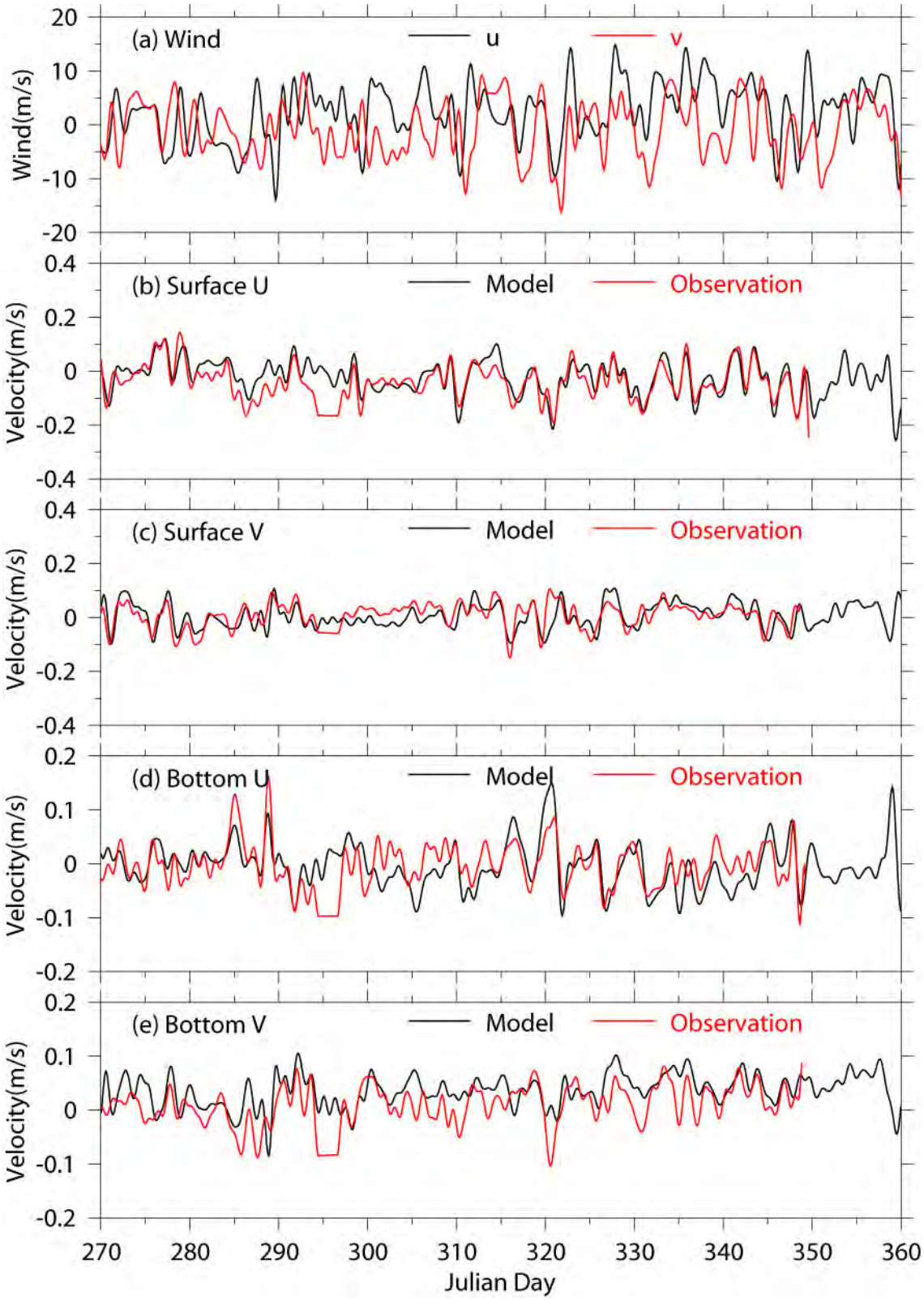

Figure 3.14. Winds at NOAA 44013 and currents at USGS Buoy A in Oct.-Dec. 2002, (a) Wind, (b) surface E-W velocity, (c) surface N-S velocity, (d) bottom E-W velocity, (e) bottom N-S velocity.

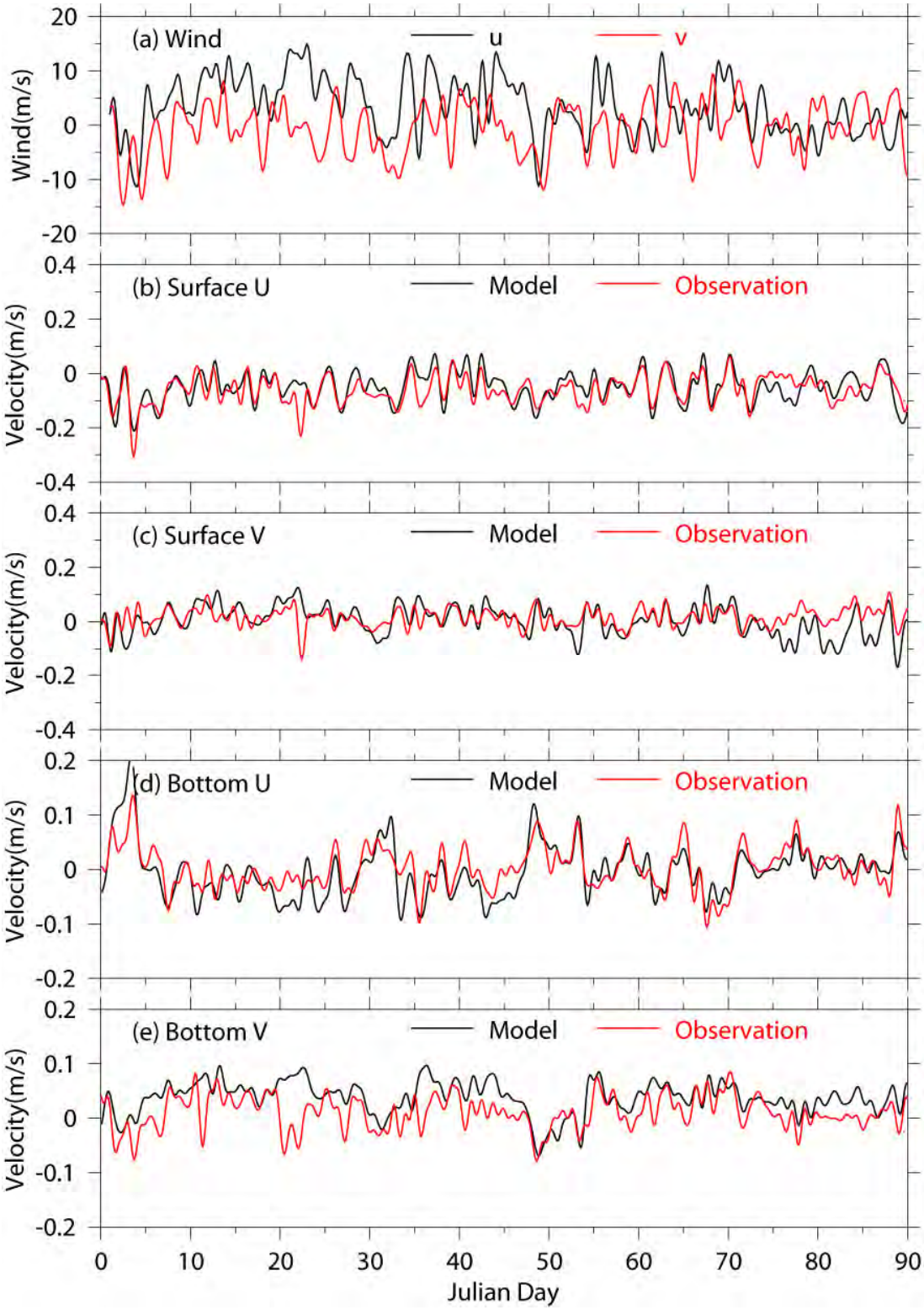

Figure 3.15. Winds at NOAA 44013 and currents at USGS Buoy A in Jan.-Mar. 2003, (a) Wind, (b) surface E-W velocity, (c) surface N-S velocity, (d) bottom E-W velocity, (e) bottom N-S velocity.

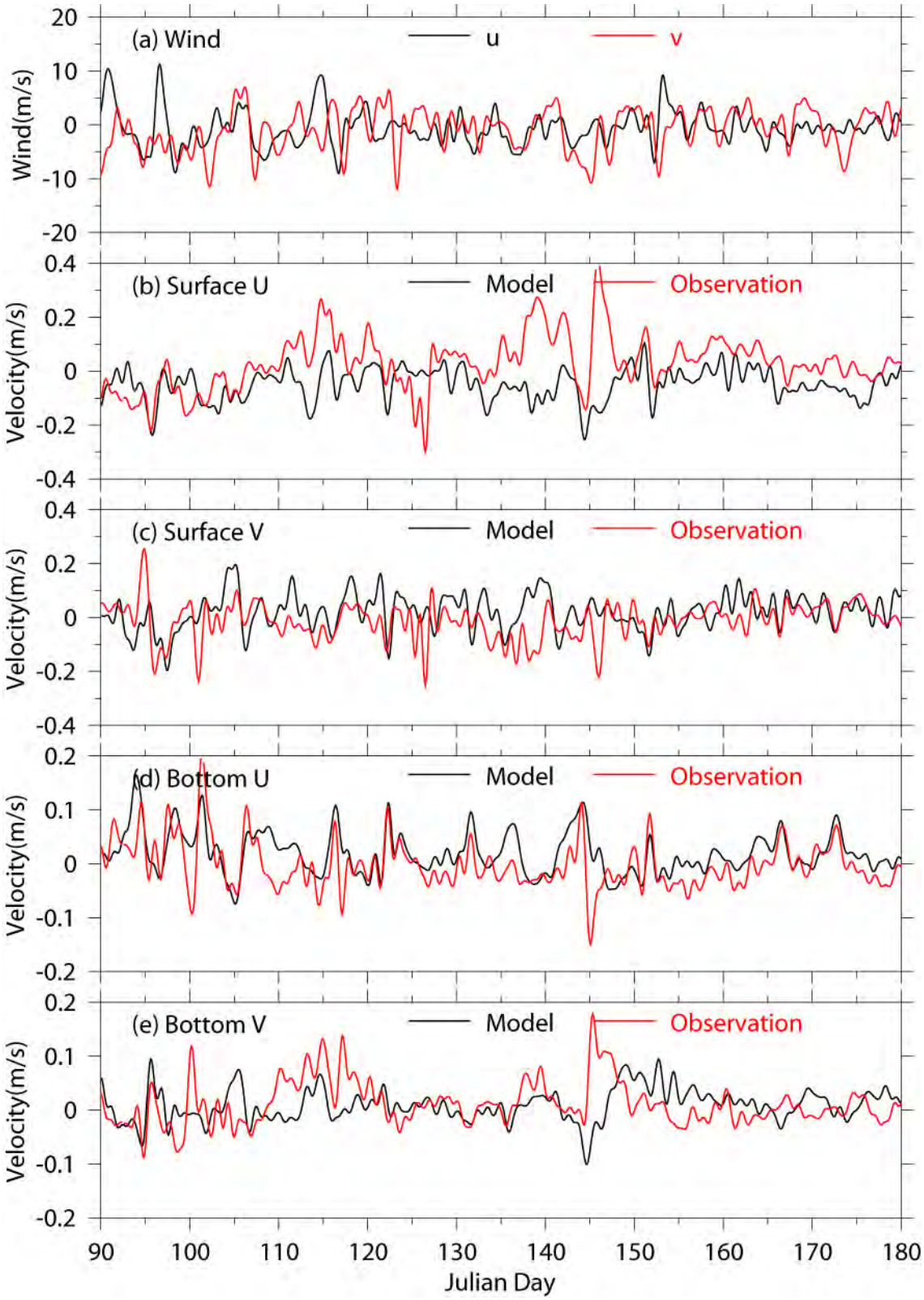

Figure 3.16. Winds at NOAA 44013 and currents at USGS Buoy A in Apr.-Jun. 2003, (a) Wind, (b) surface E-W velocity, (c) surface N-S velocity, (d) bottom E-W velocity, (e) bottom N-S velocity.

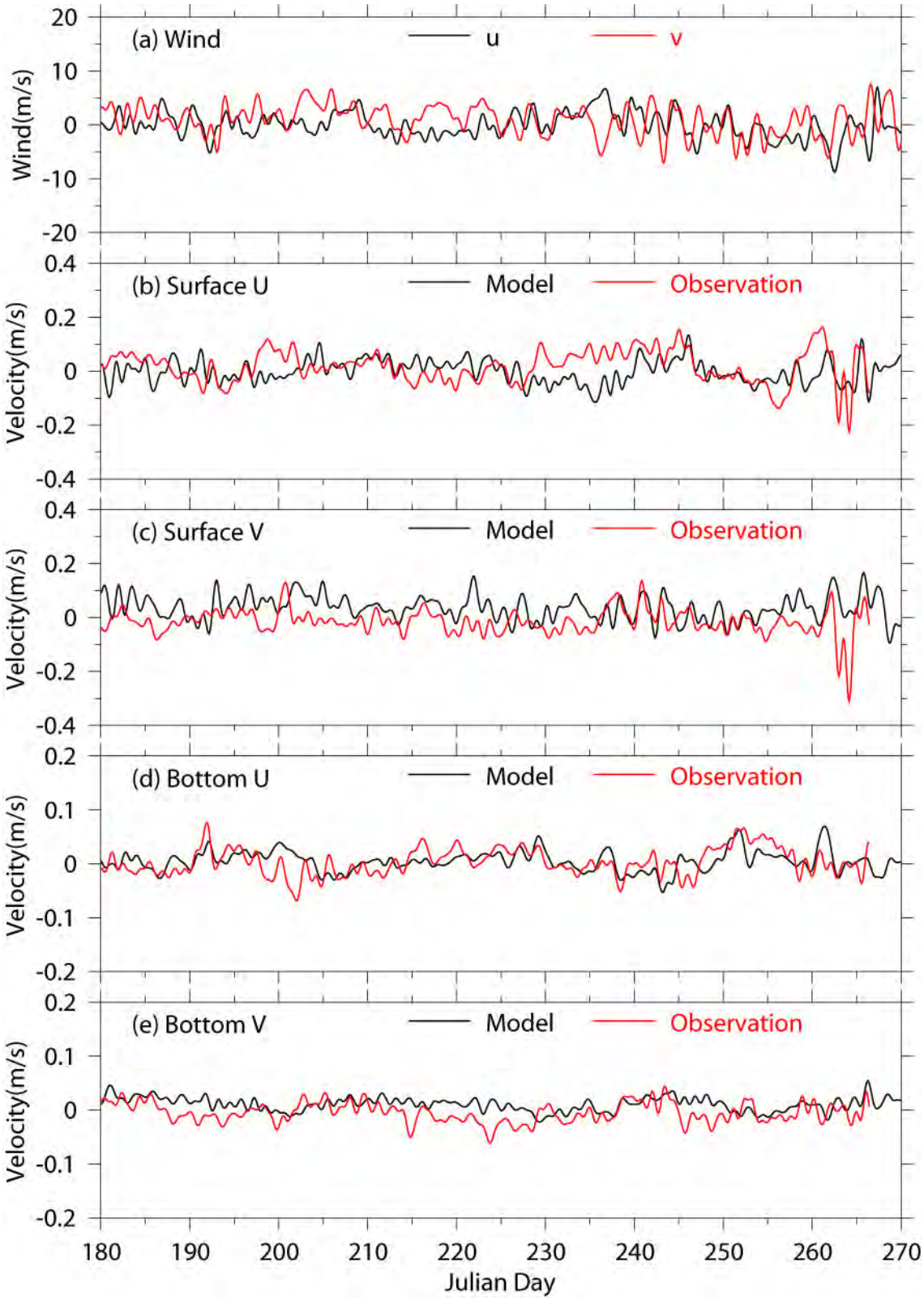

Figure 3.17. Winds at NOAA 44013 and currents at USGS Buoy A in Jul.-Sep. 2003, (a) Wind, (b) surface E-W velocity, (c) surface N-S velocity, (d) bottom E-W velocity, (e) bottom N-S velocity.

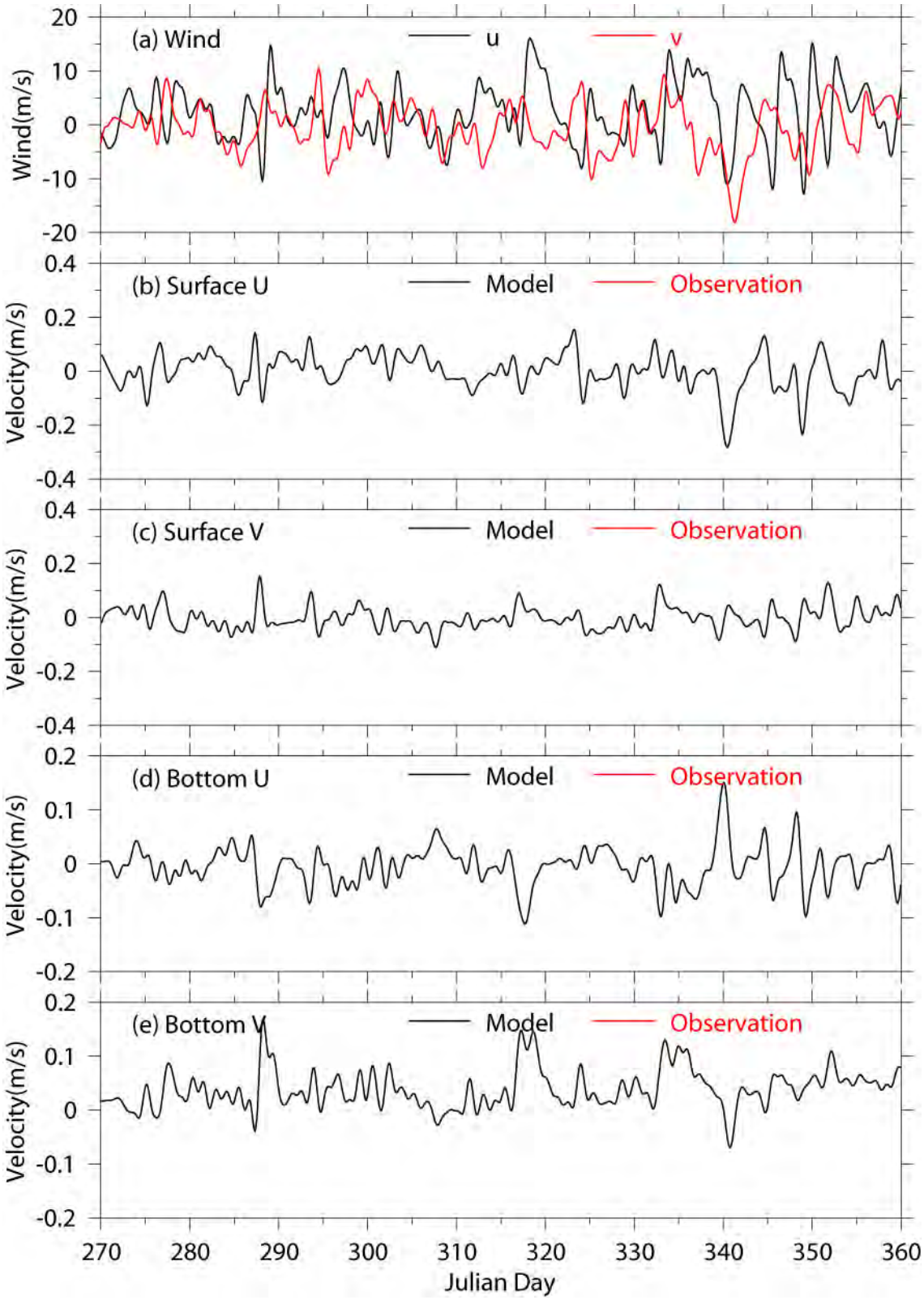

Figure 3.18. Winds at NOAA 44013 and currents at USGS Buoy A in Oct.-Dec. 2003, (a) Wind, (b) surface E-W velocity, (c) surface N-S velocity, (d) bottom E-W velocity, (e) bottom N-S velocity.

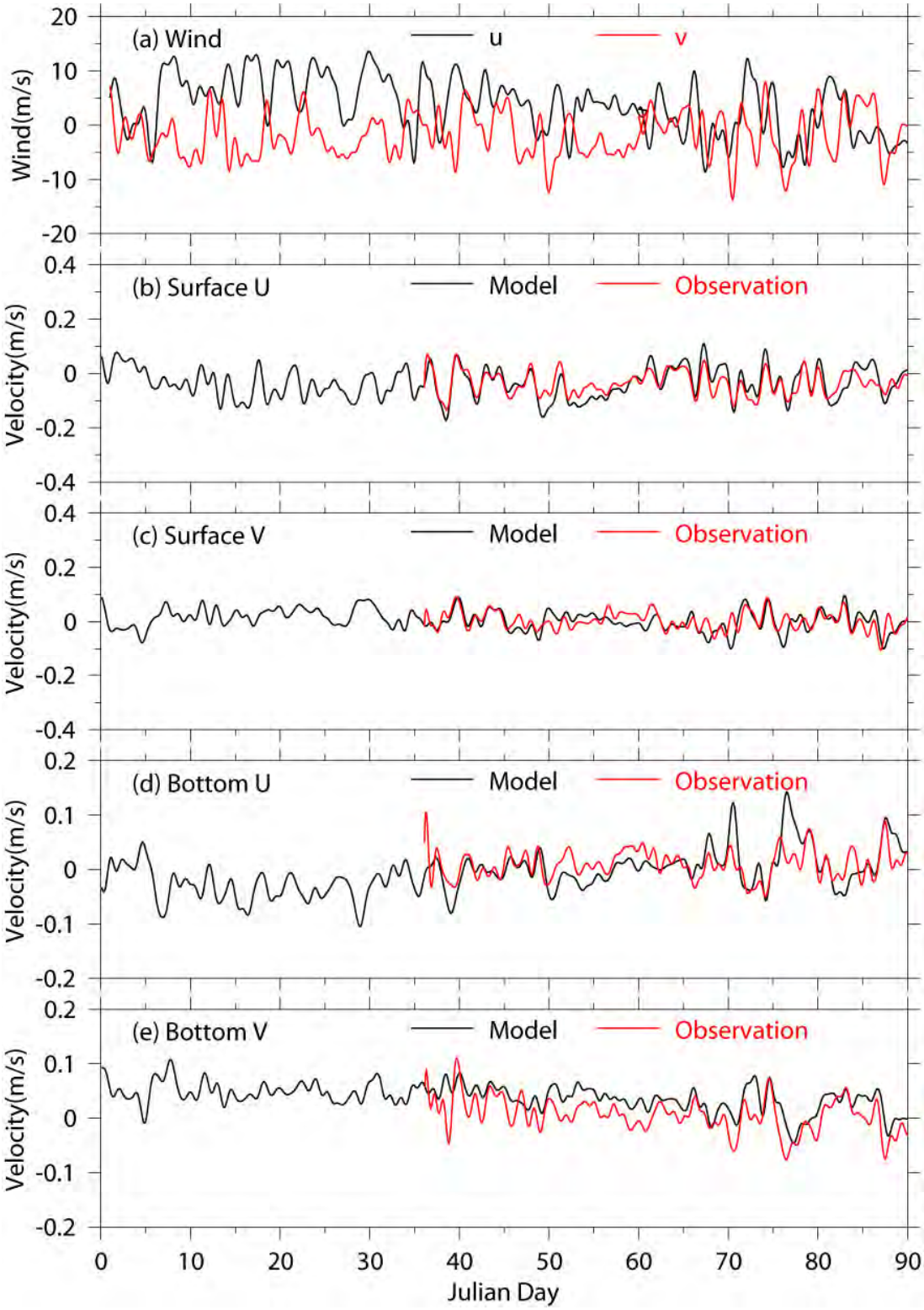

Figure 3.19. Winds at NOAA 44013 and currents at USGS Buoy A in Jan.-Mar. 2004, (a) Wind, (b) surface E-W velocity, (c) surface N-S velocity, (d) bottom E-W velocity, (e) bottom N-S velocity.

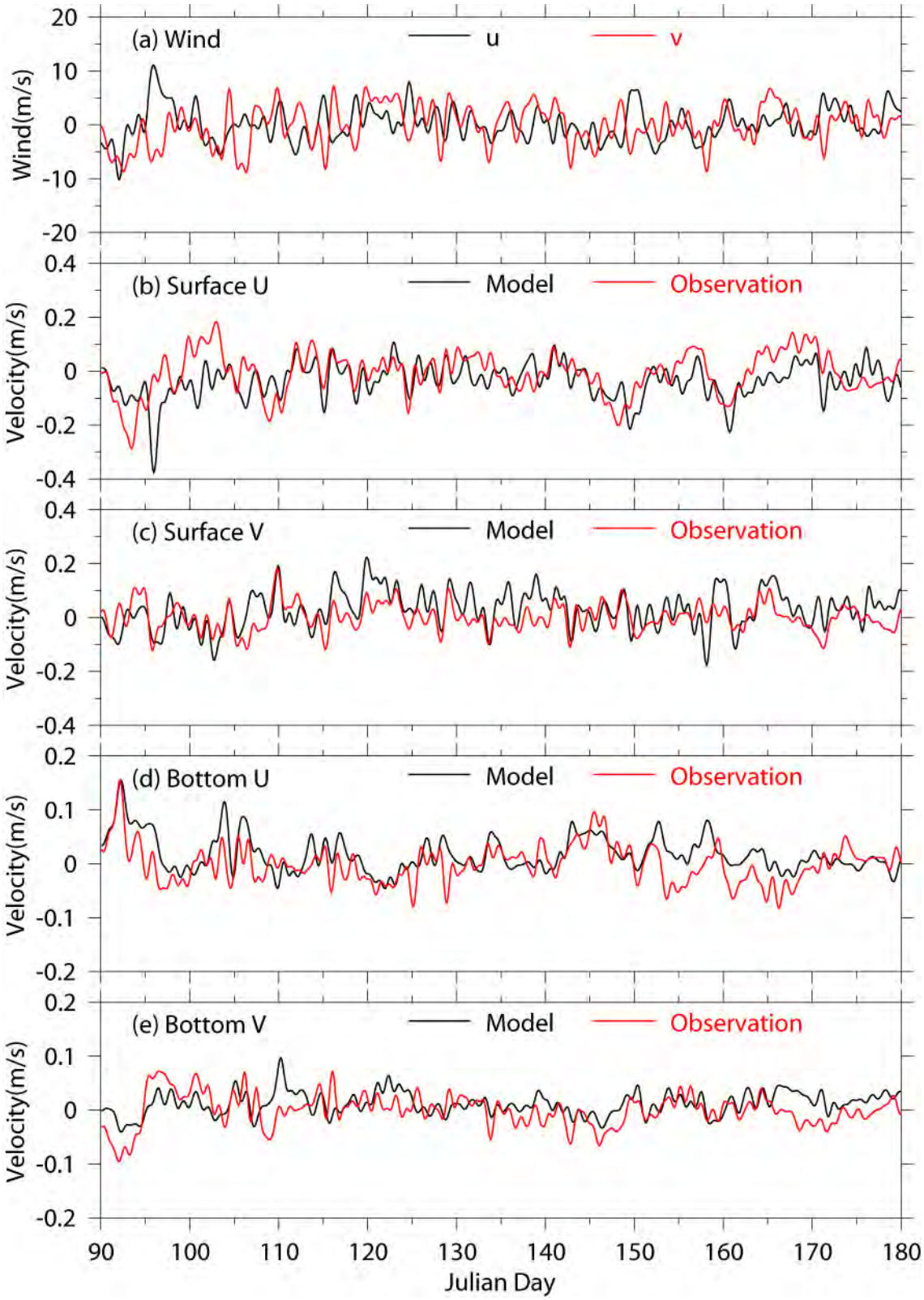

Figure 3.20. Winds at NOAA 44013 and currents at USGS Buoy A in Apr.-Jun. 2004, (a) Wind, (b) surface E-W velocity, (c) surface N-S velocity, (d) bottom E-W velocity, (e) bottom N-S velocity.

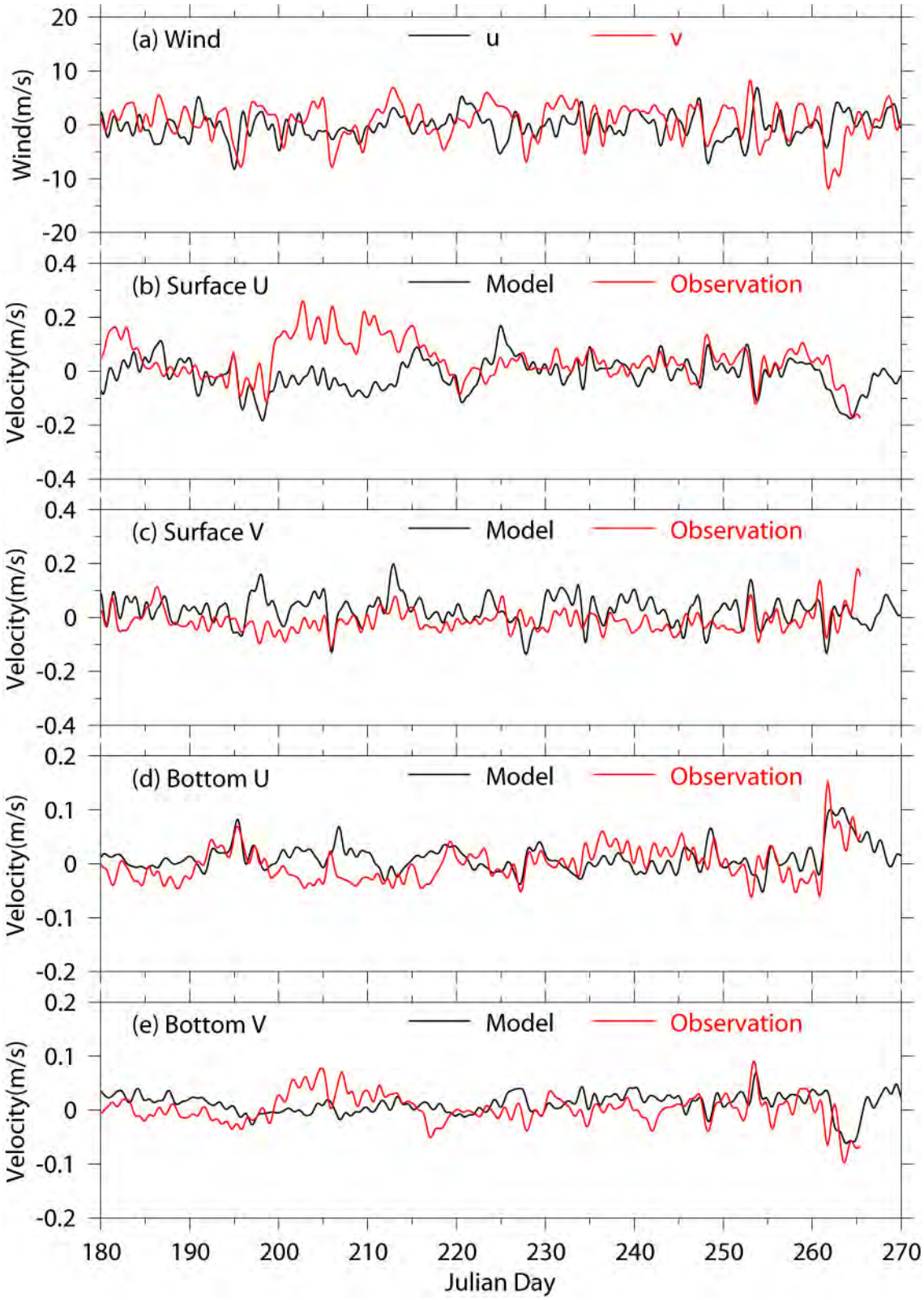

Figure 3.21. Winds at NOAA 44013 and currents at USGS Buoy A in Jul.-Sep. 2004, (a) Wind, (b) surface E-W velocity, (c) surface N-S velocity, (d) bottom E-W velocity, (e) bottom N-S velocity.

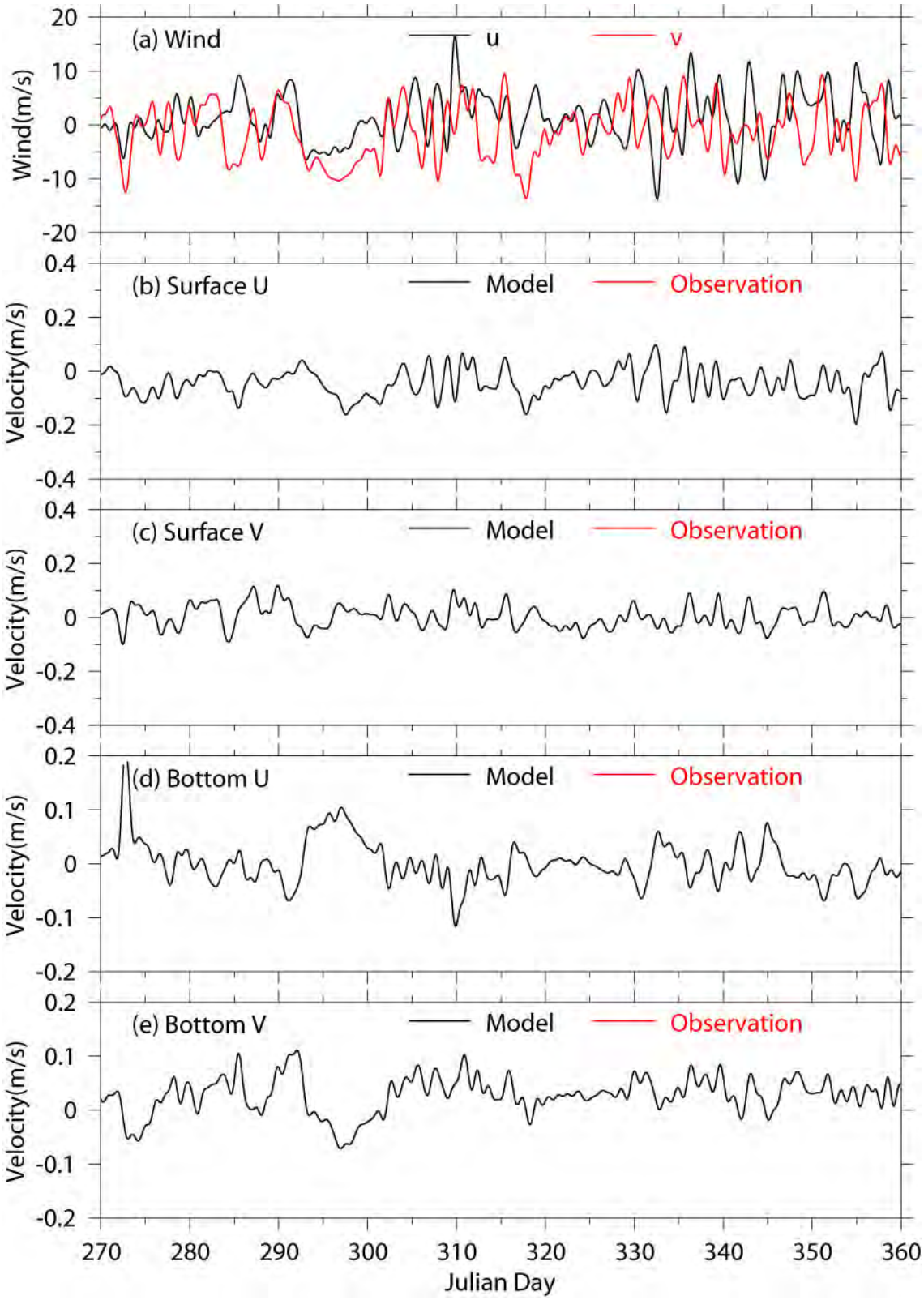

Figure 3.22. Winds at NOAA 44013 and currents at USGS Buoy A in Oct.-Dec. 2004, (a) Wind, (b) surface E-W velocity, (c) surface N-S velocity, (d) bottom E-W velocity, (e) bottom N-S velocity.

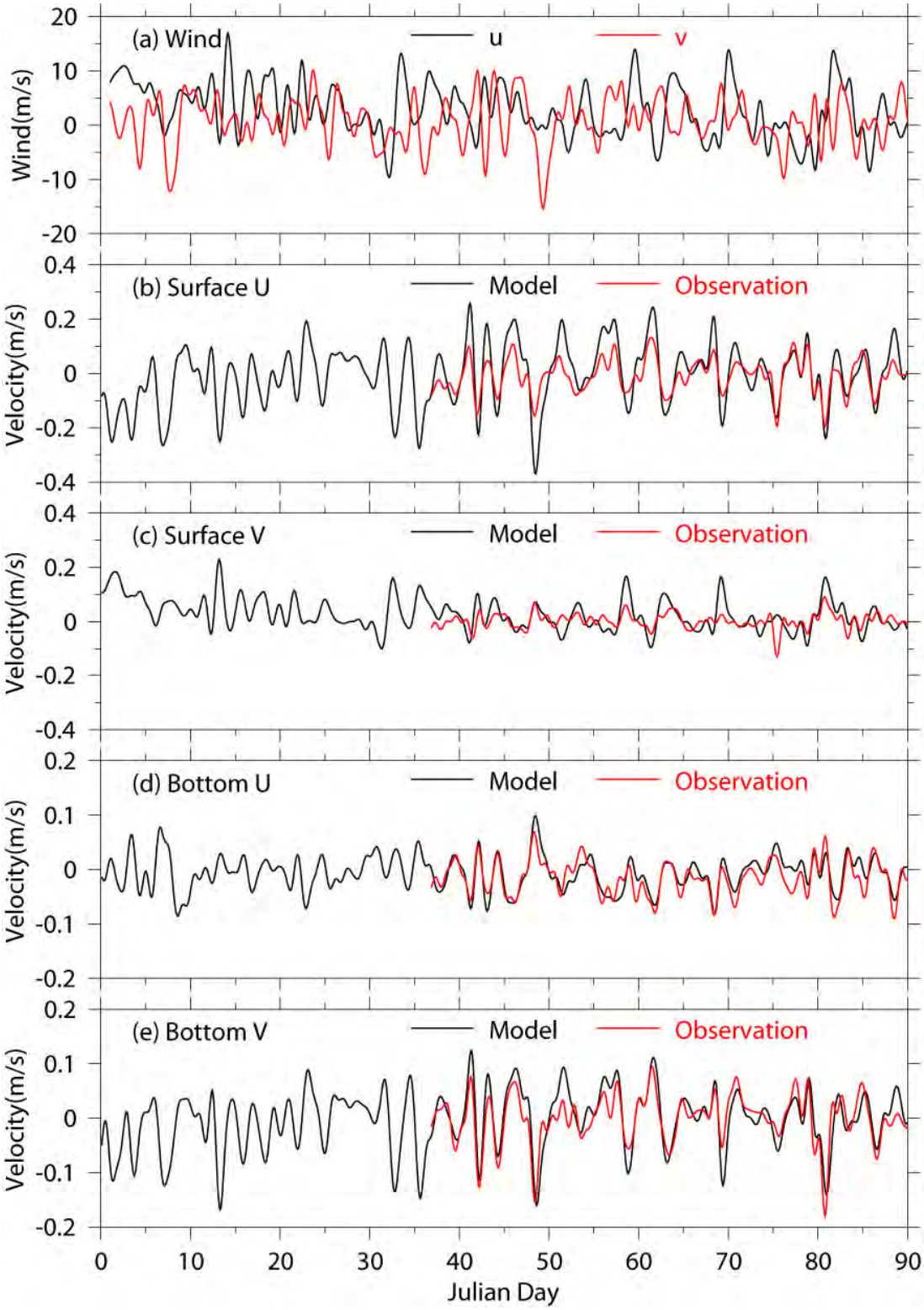

Figure 3.23. Winds at NOAA 44013 and currents at USGS Buoy B in Jan.-Mar. 2002, (a) Wind, (b) surface E-W velocity, (c) surface N-S velocity, (d) bottom E-W velocity (e) bottom N-S velocity.

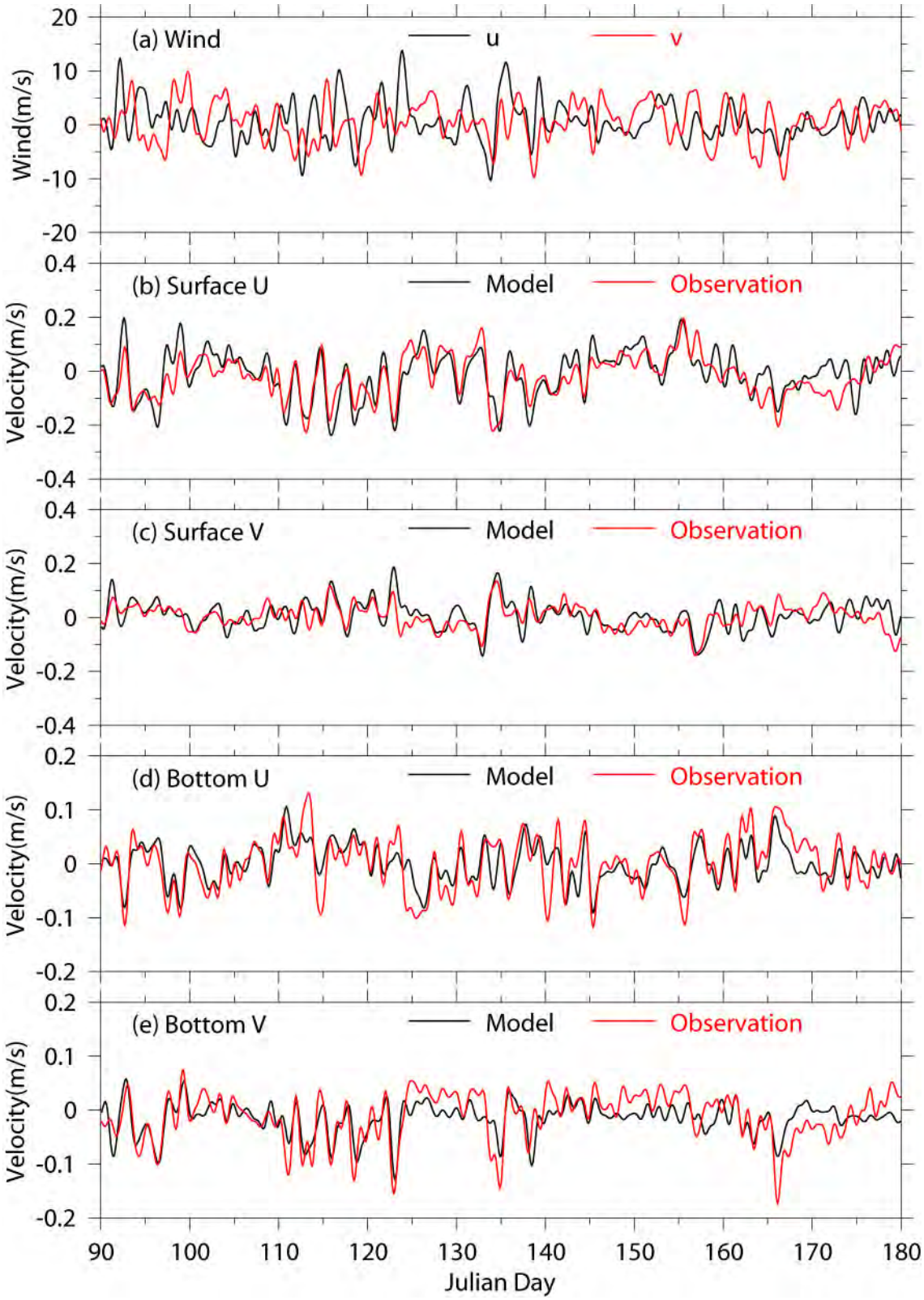

Figure 3.24. Winds at NOAA 44013 and currents at USGS Buoy B in Apr.-Jun. 2002, (a) Wind, (b) surface E-W velocity, (c) surface N-S velocity, (d) bottom E-W velocity, (e) bottom N-S velocity.

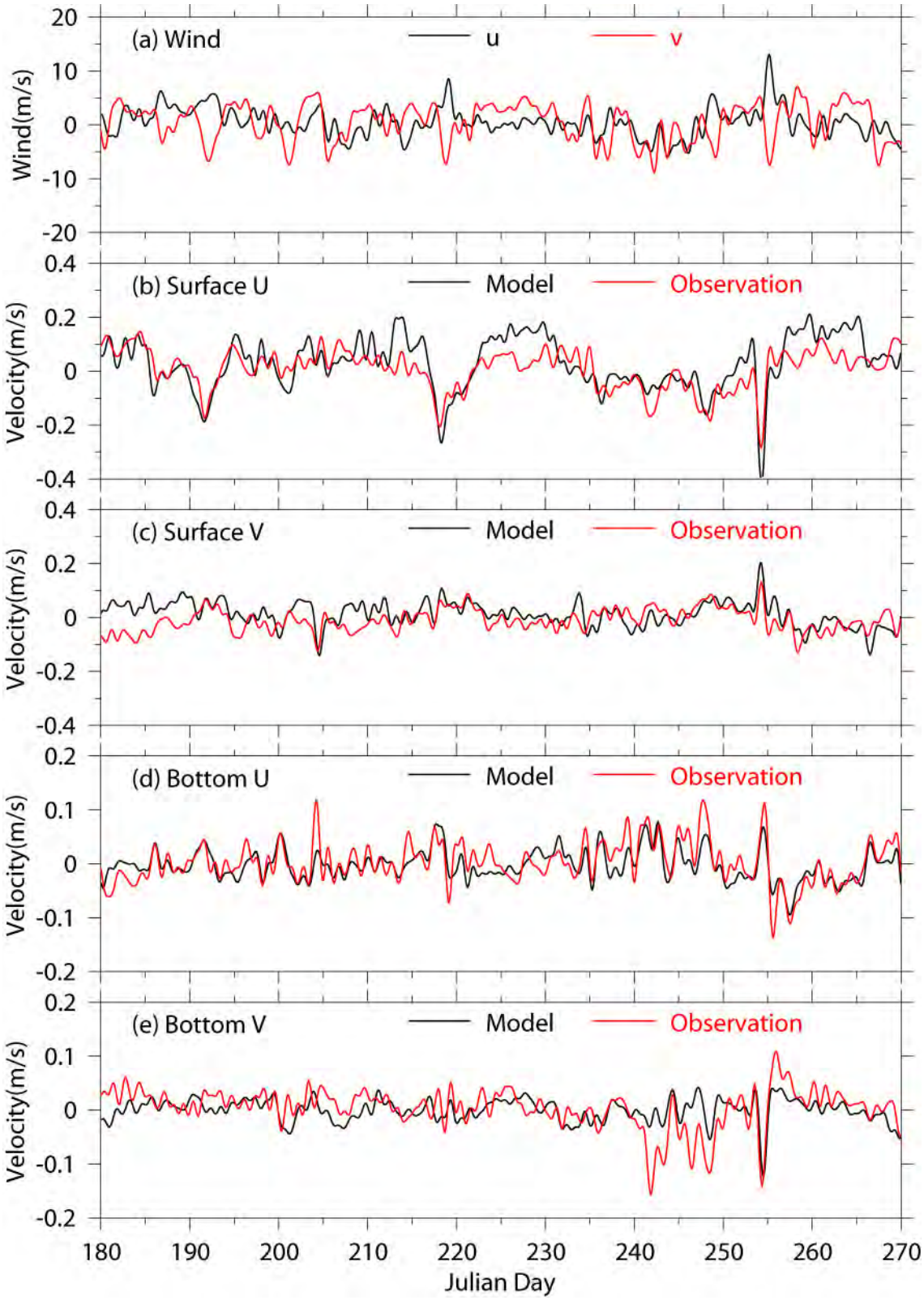

Figure 3.25. Winds at NOAA 44013 and currents at USGS Buoy B in Jul.-Sep. 2002, (a) Wind, (b) surface E-W velocity, (c) surface N-S velocity, (d) bottom E-W velocity (e) bottom N-S velocity.

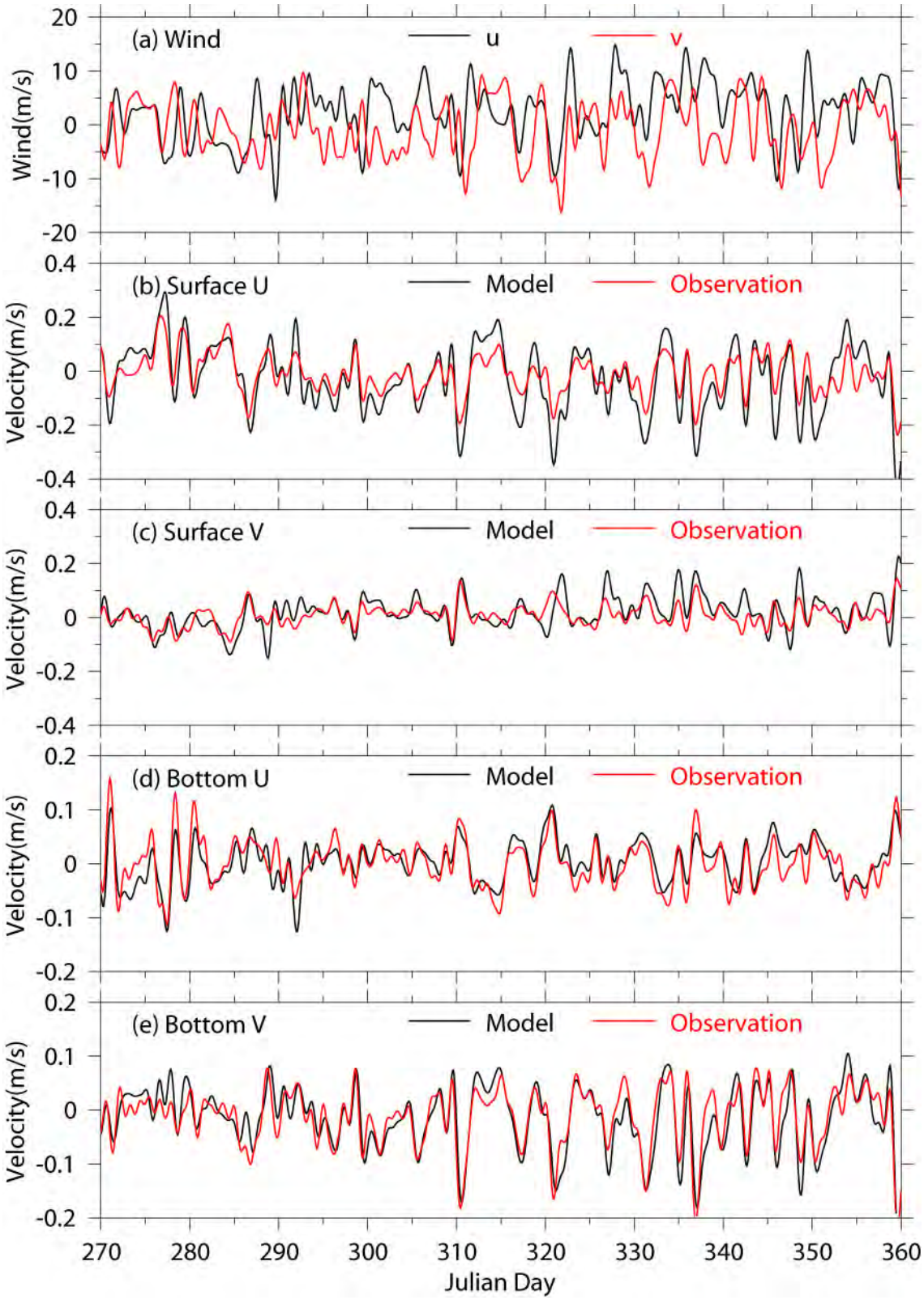

Figure 3.26. Winds at NOAA 44013 and currents at USGS Buoy B in Oct.-Dec. 2002, (a) Wind, (b) surface E-W velocity, (c) surface N-S velocity, (d) bottom E-W velocity, (e) bottom N-S velocity.

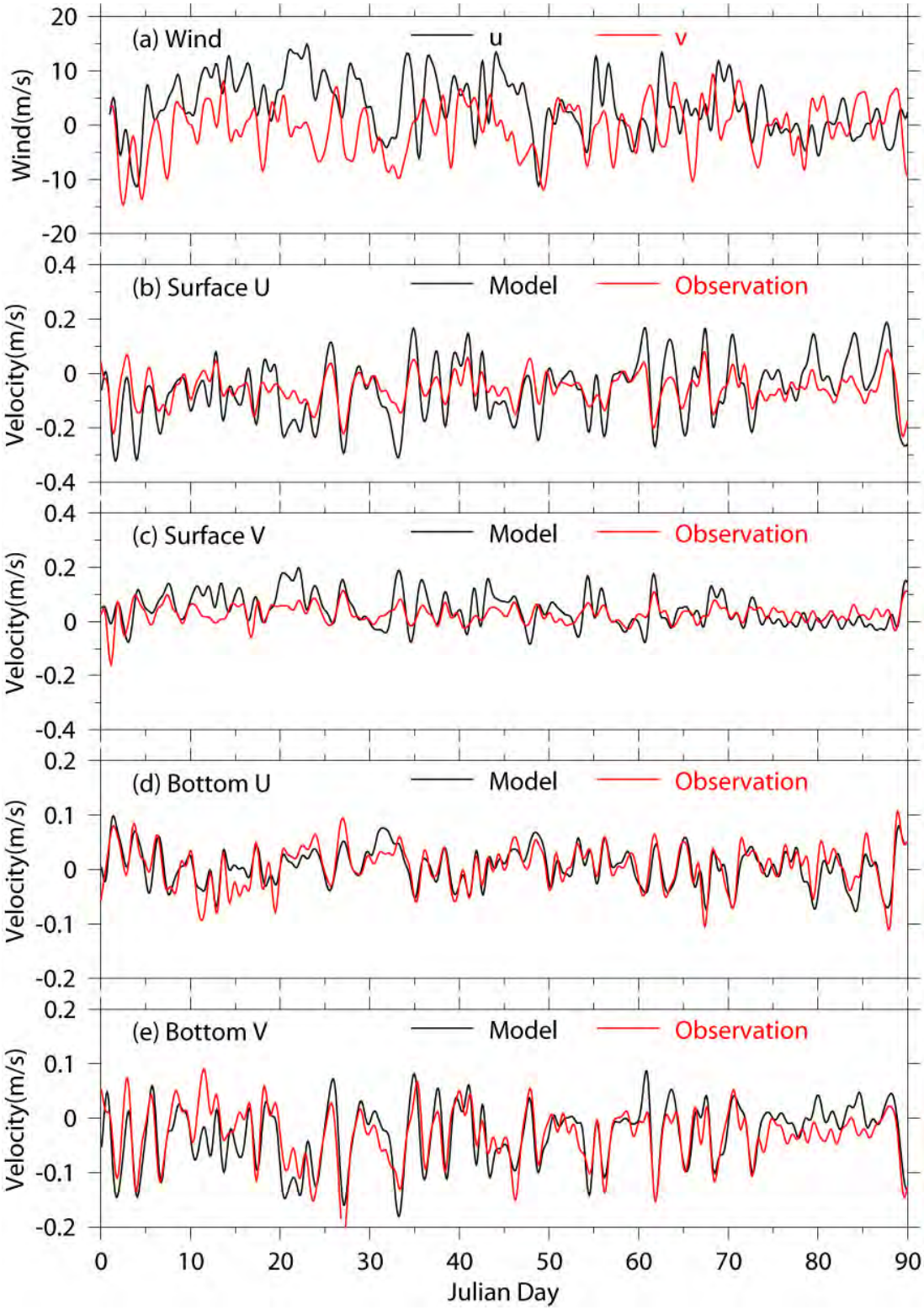

Figure 3.27. Winds at NOAA 44013 and currents at USGS Buoy B in Jan.-Mar. 2003, (a) Wind, (b) surface E-W velocity, (c) surface N-S velocity, (d) bottom E-W velocity (e) bottom N-S velocity.

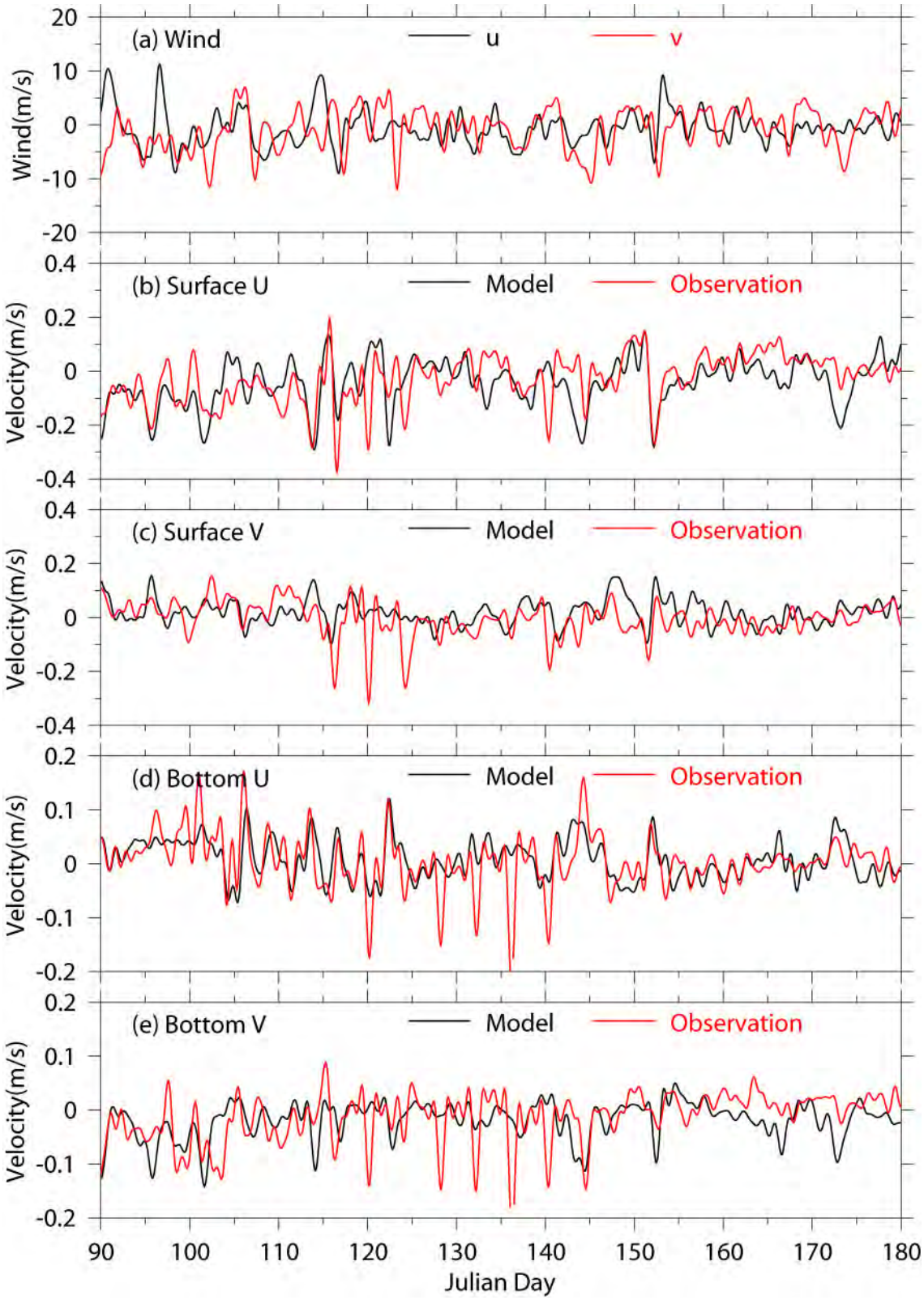

Figure 3.28. Winds at NOAA 44013 and currents at USGS Buoy B in Apr.-Jun. 2003, (a) Wind, (b) surface E-W velocity, (c) surface N-S velocity, (d) bottom E-W velocity, (e) bottom N-S velocity.

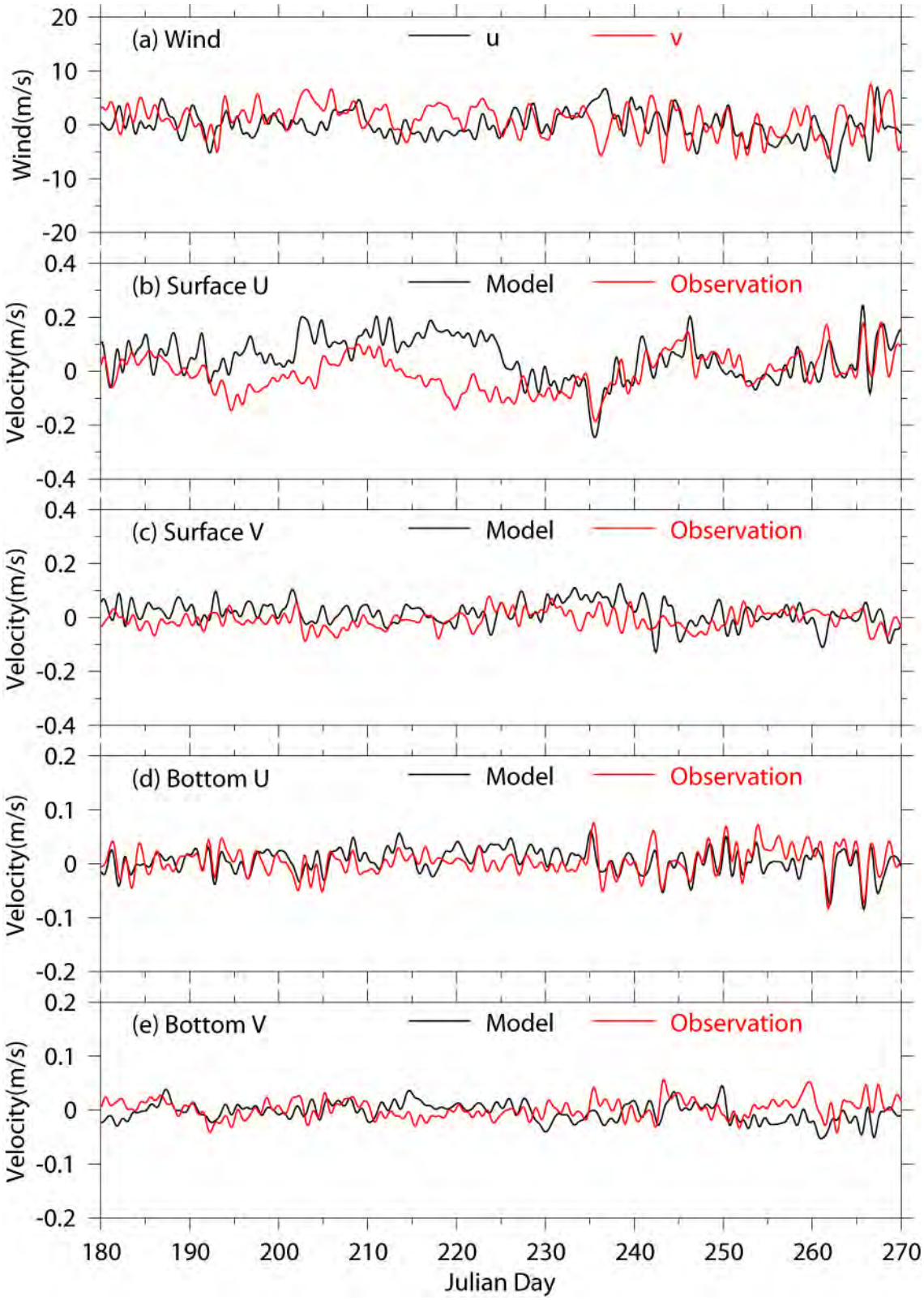

Figure 3.29. Winds at NOAA 44013 and currents at USGS Buoy B in Jul.-Sep. 2003, (a) Wind, (b) surface E-W velocity, (c) surface N-S velocity, (d) bottom E-W velocity (e) bottom N-S velocity.

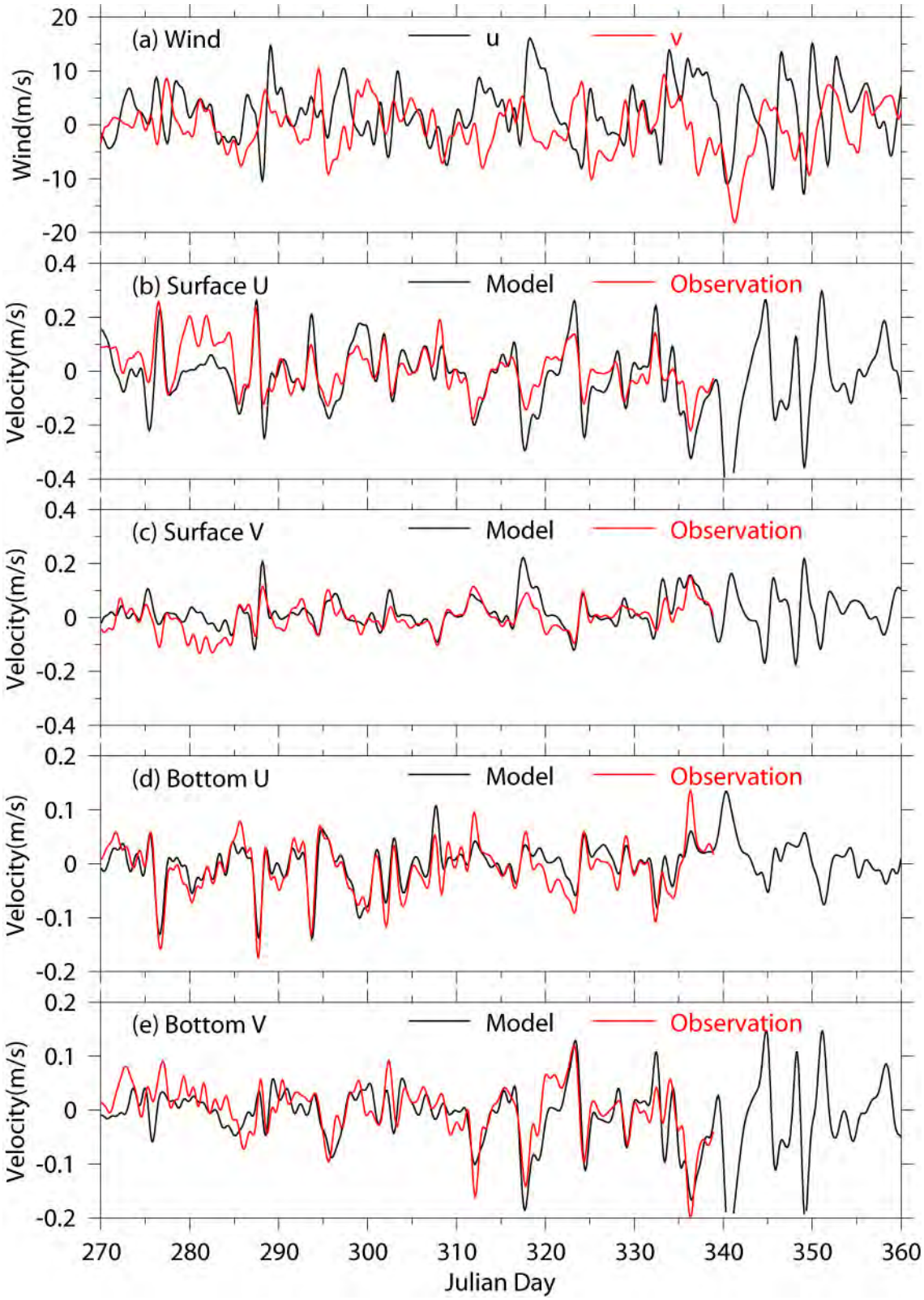

Figure 3.30. Winds at NOAA 44013 and currents at USGS Buoy B in Oct.-Dec. 2003, (a) Wind, (b) surface E-W velocity, (c) surface N-S velocity, (d) bottom E-W velocity, (e) bottom N-S velocity.

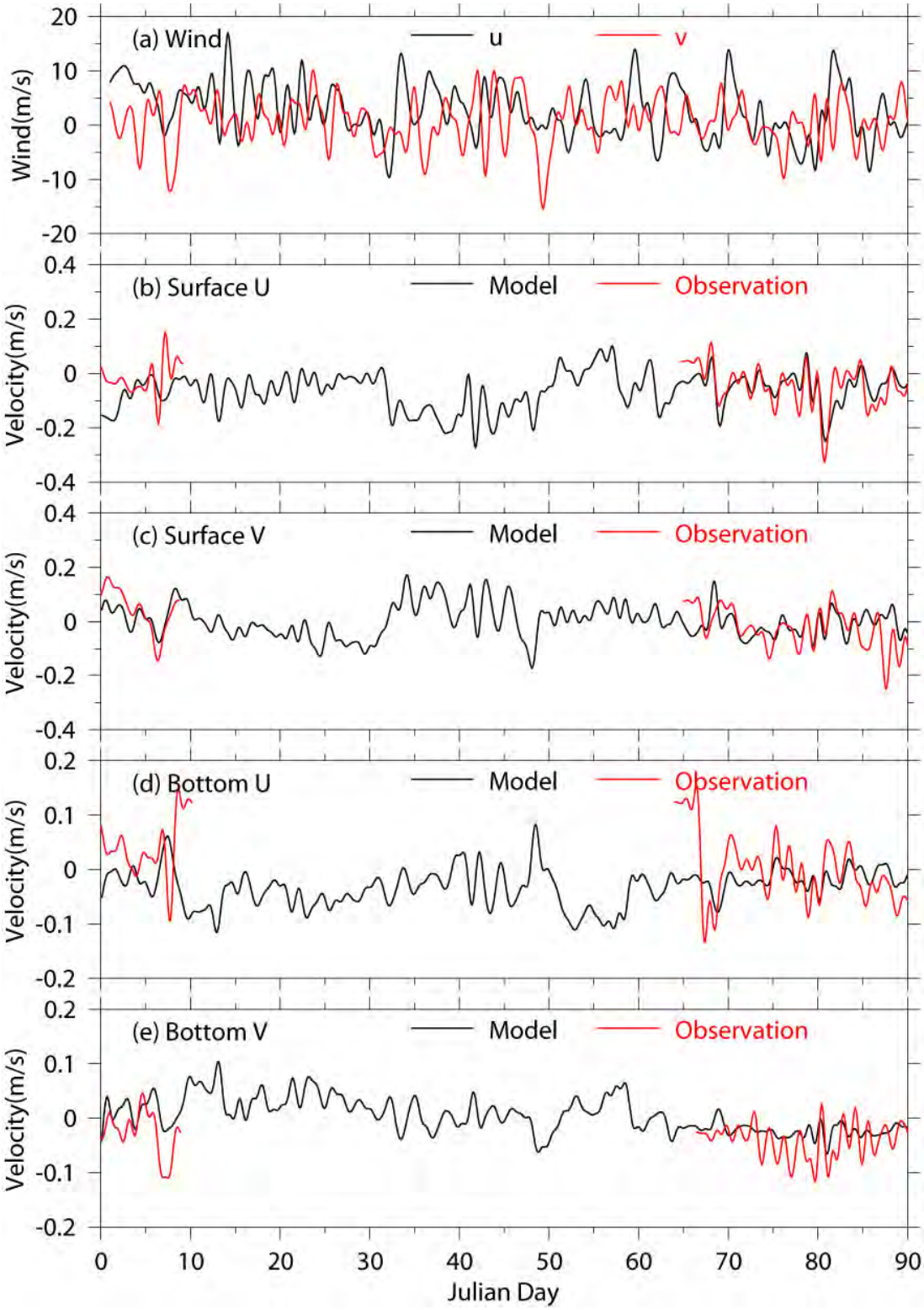

Figure 3.31. Winds at NOAA 44013 and currents at GoMOOS A in Jan.-Mar. 2002, (a) Wind, (b) surface E-W velocity, (c) surface N-S velocity, (d) bottom E-W velocity (e) bottom N-S velocity.

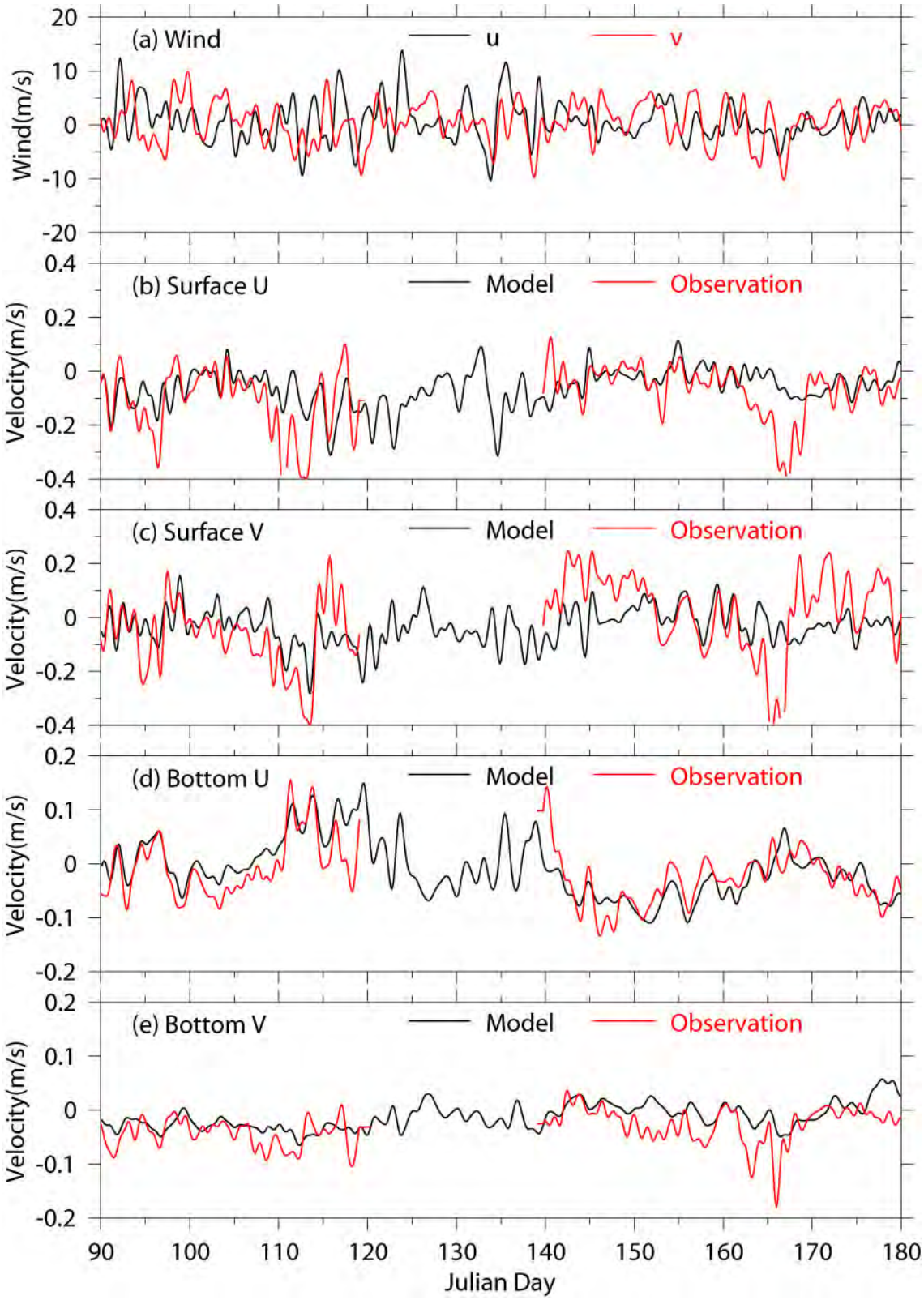

Figure 3.32. Winds at NOAA 44013 and currents at GoMOOS A in Apr.-Jun. 2002, (a) Wind, (b) surface E-W velocity, (c) surface N-S velocity, (d) bottom E-W velocity, (e) bottom N-S velocity.

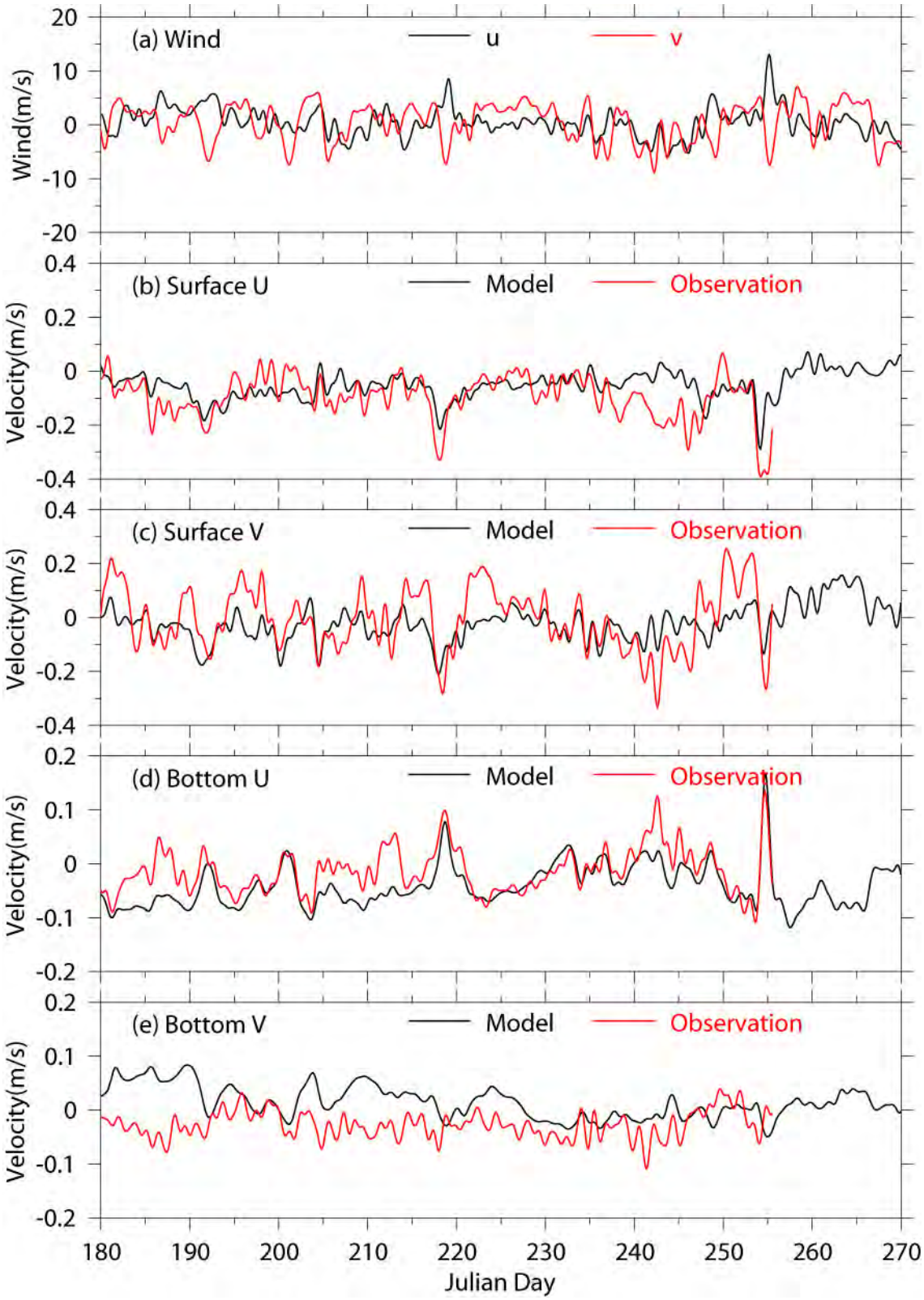

Figure 3.33. Winds at NOAA 44013 and currents at GoMOOS A in Jul.-Sep. 2002, (a) Wind, (b) surface E-W velocity, (c) surface N-S velocity, (d) bottom E-W velocity (e) bottom N-S velocity.

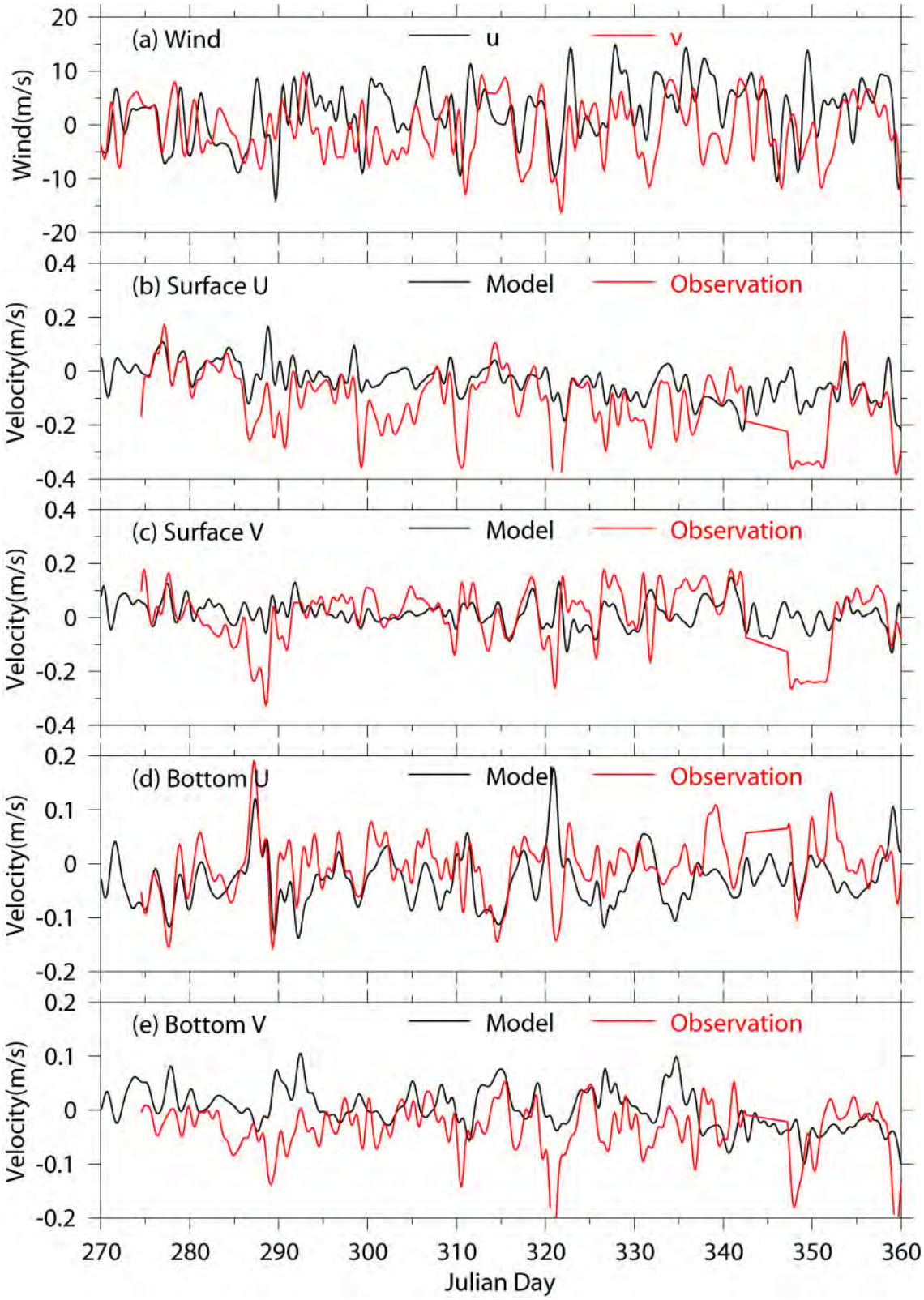

Figure 3.34. Winds at NOAA 44013 and currents at GoMOOS A in Oct.-Dec. 2002, (a) Wind, (b) surface E-W velocity, (c) surface N-S velocity, (d) bottom E-W velocity, (e) bottom N-S velocity.

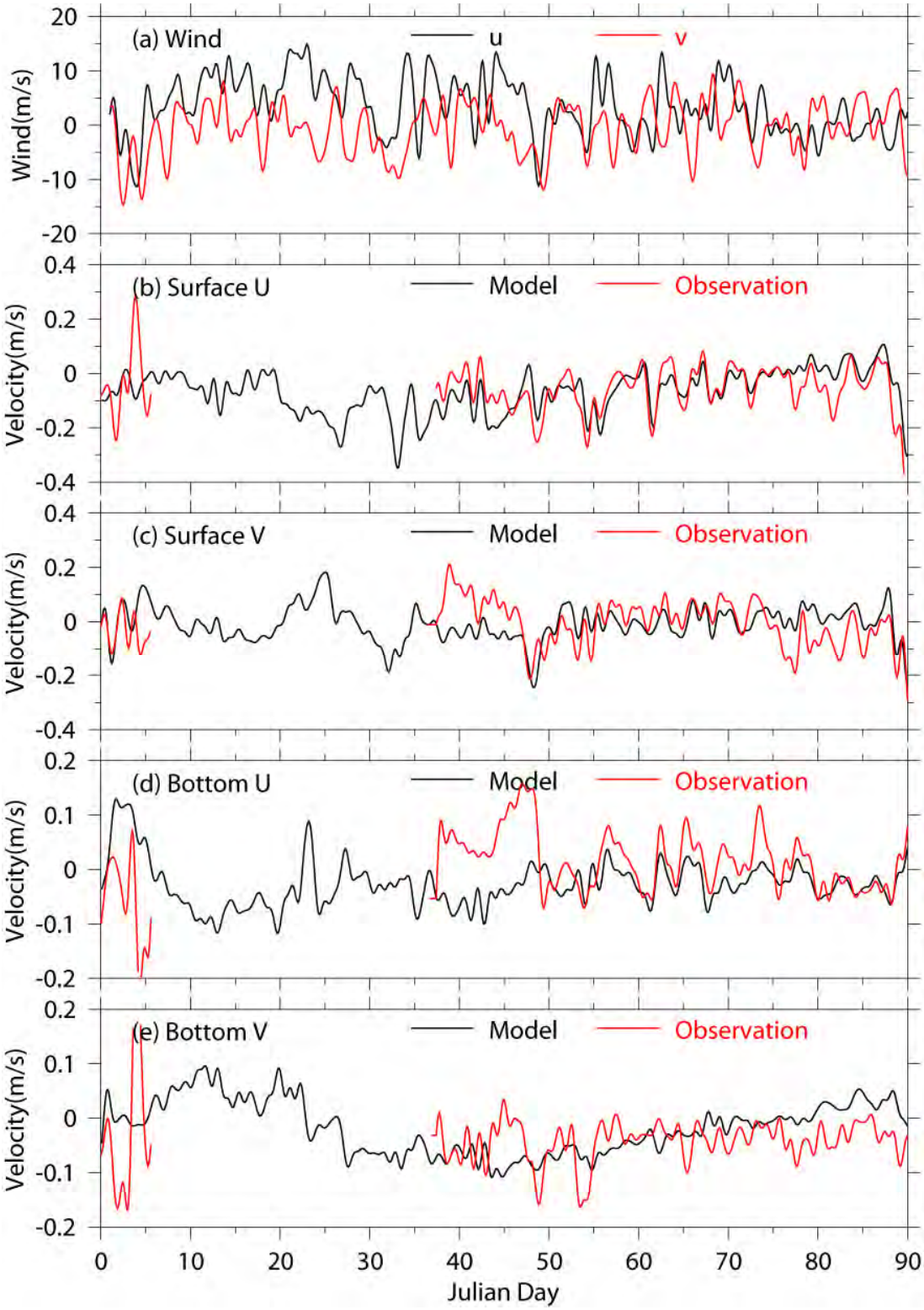

Figure 3.35. Winds at NOAA 44013 and currents at GoMOOS A in Jan.-Mar. 2003, (a) Wind, (b) surface E-W velocity, (c) surface N-S velocity, (d) bottom E-W velocity (e) bottom N-S velocity.

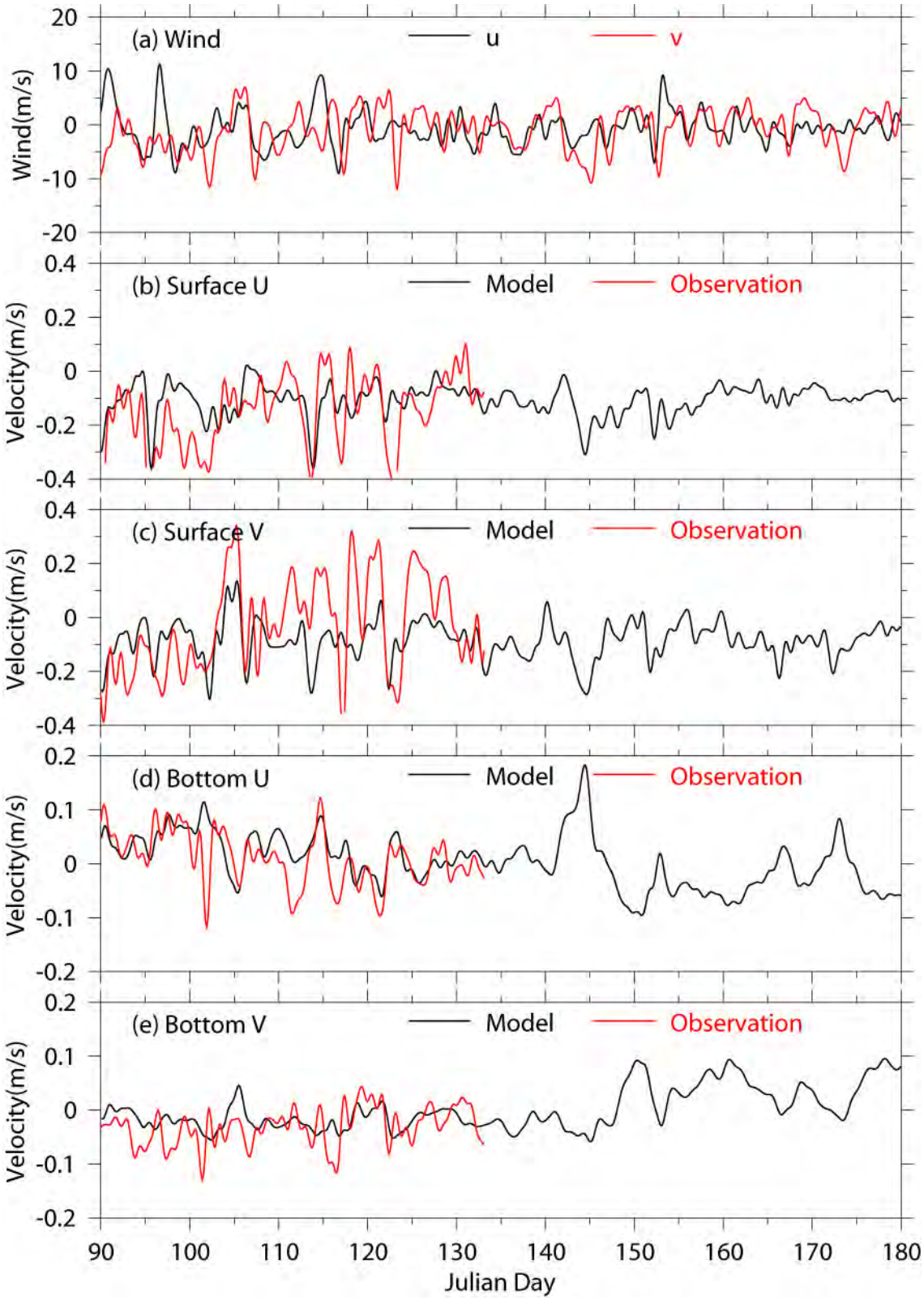

Figure 3.36. Winds at NOAA 44013 and currents at GoMOOS A in Apr.-Jun. 2003, (a) Wind, (b) surface E-W velocity, (c) surface N-S velocity, (d) bottom E-W velocity, (e) bottom N-S velocity.

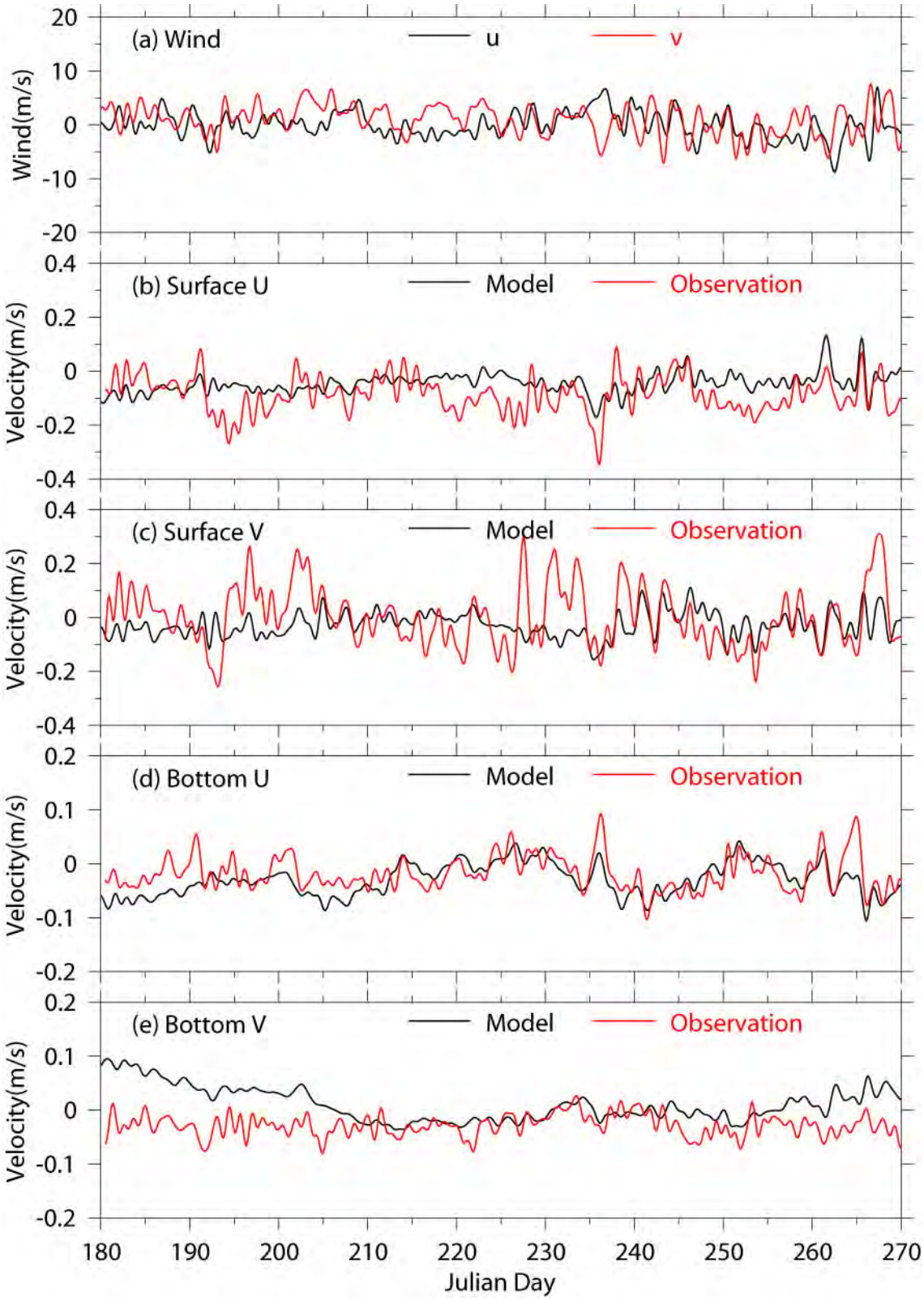

Figure 3.37. Winds at NOAA 44013 and currents at GoMOOS A in Jul.-Sep. 2003, (a) Wind, (b) surface E-W velocity, (c) surface N-S velocity, (d) bottom E-W velocity (e) bottom N-S velocity.

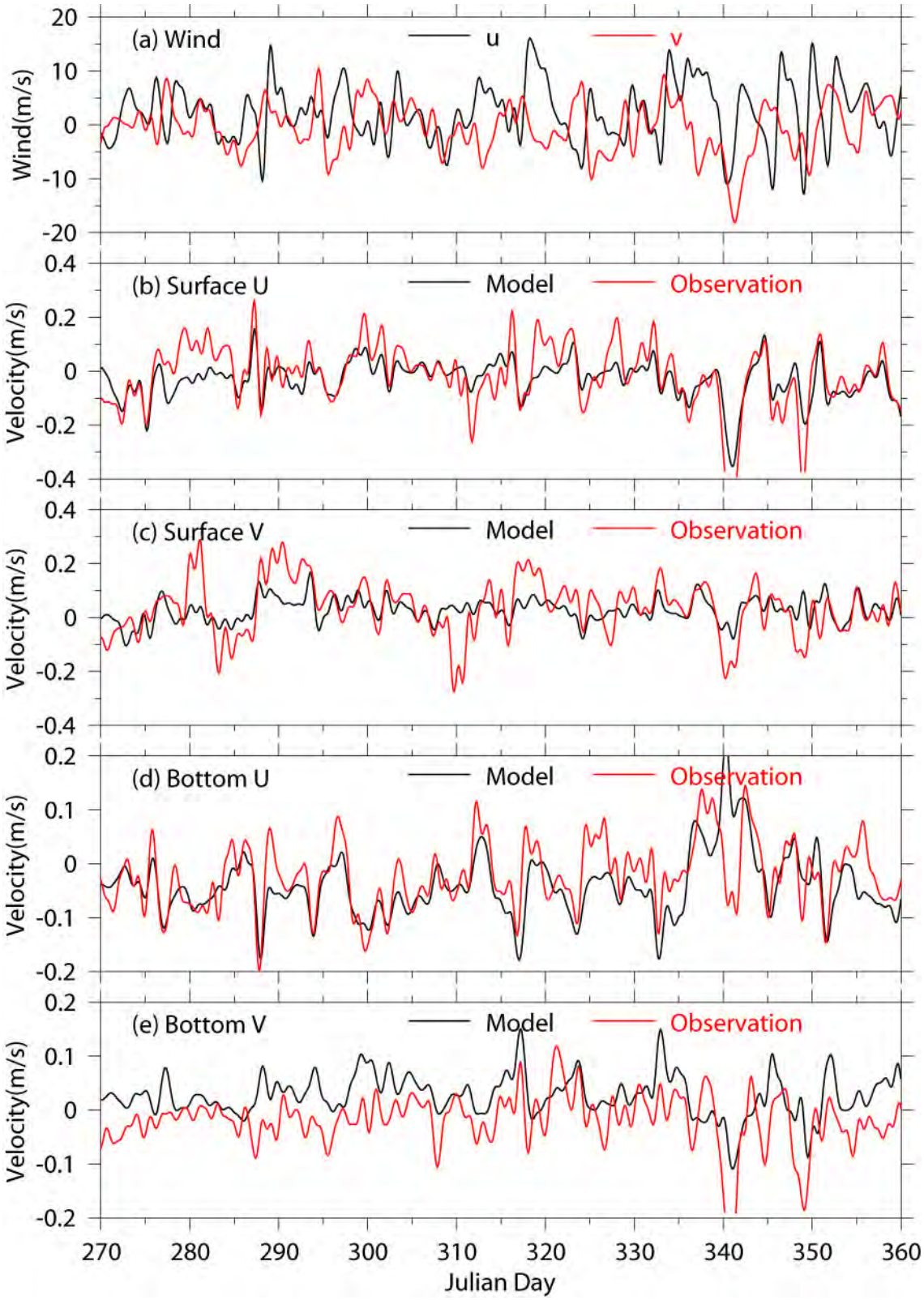

Figure 3.38. Winds at NOAA 44013 and currents at GoMOOS A in Oct.-Dec. 2003, (a) Wind, (b) surface E-W velocity, (c) surface N-S velocity, (d) bottom E-W velocity, (e) bottom N-S velocity.

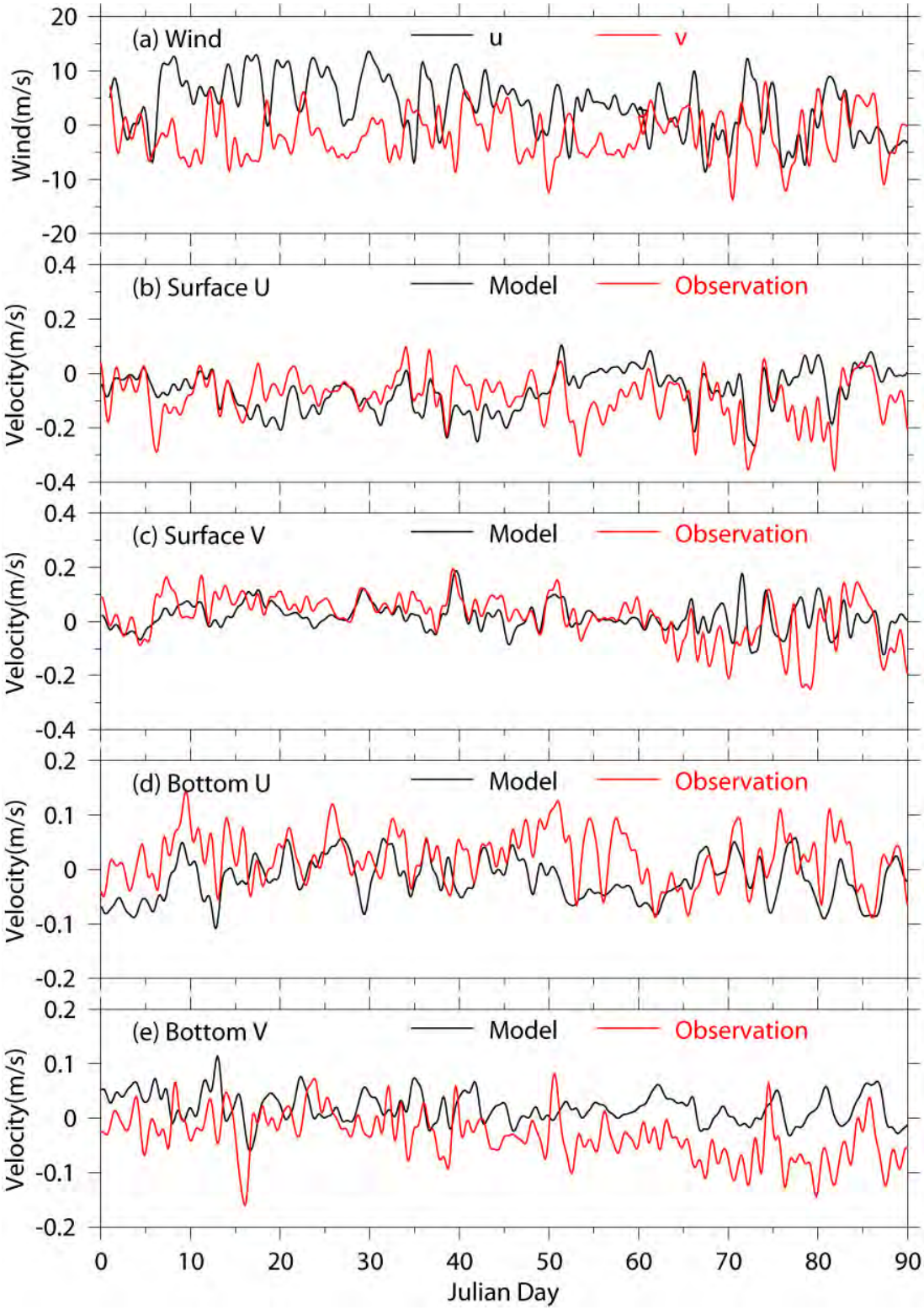

Figure 3.39. Winds at NOAA 44013 and currents at GoMOOS A in Jan.-Mar. 2004, (a) Wind, (b) surface E-W velocity, (c) surface N-S velocity, (d) bottom E-W velocity (e) bottom N-S velocity.

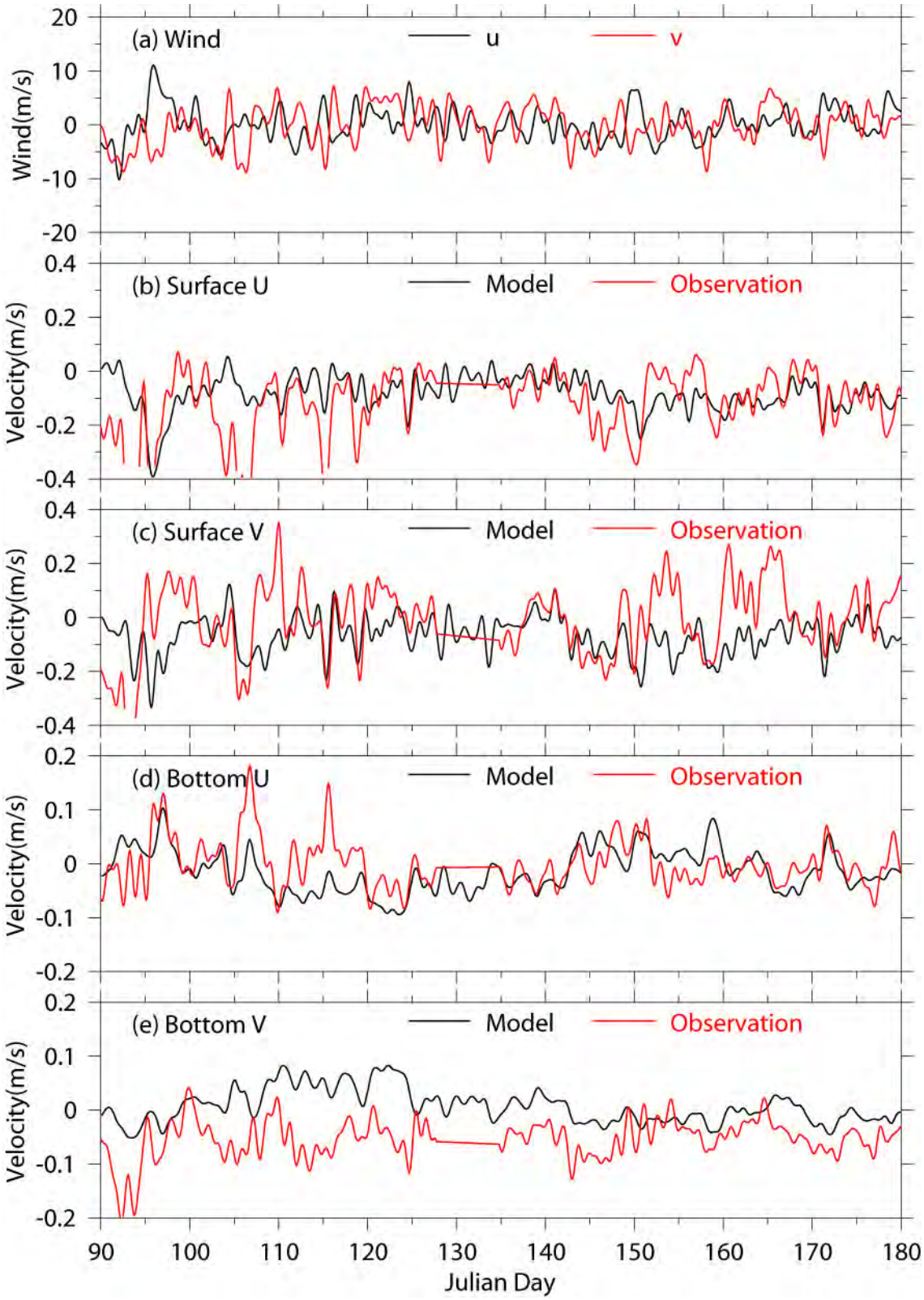

Figure 3.40. Winds at NOAA 44013 and currents at GoMOOS A in Apr.-Jun. 2004, (a) Wind, (b) surface E-W velocity, (c) surface N-S velocity, (d) bottom E-W velocity, (e) bottom N-S velocity.

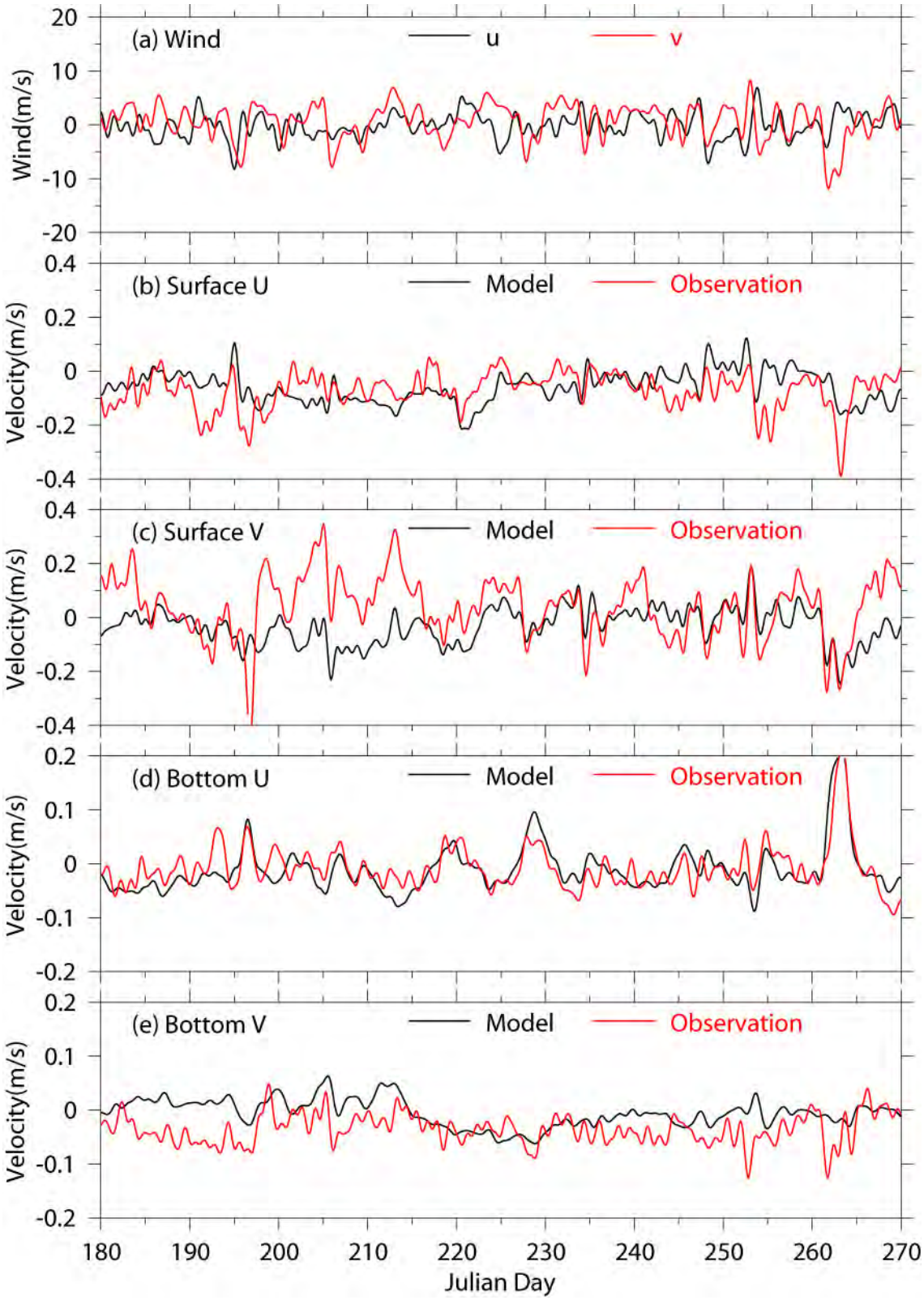

Figure 3.41. Winds at NOAA 44013 and currents at GoMOOS A in Jul.-Sep. 2004, (a) Wind, (b) surface E-W velocity, (c) surface N-S velocity, (d) bottom E-W velocity (e) bottom N-S velocity.

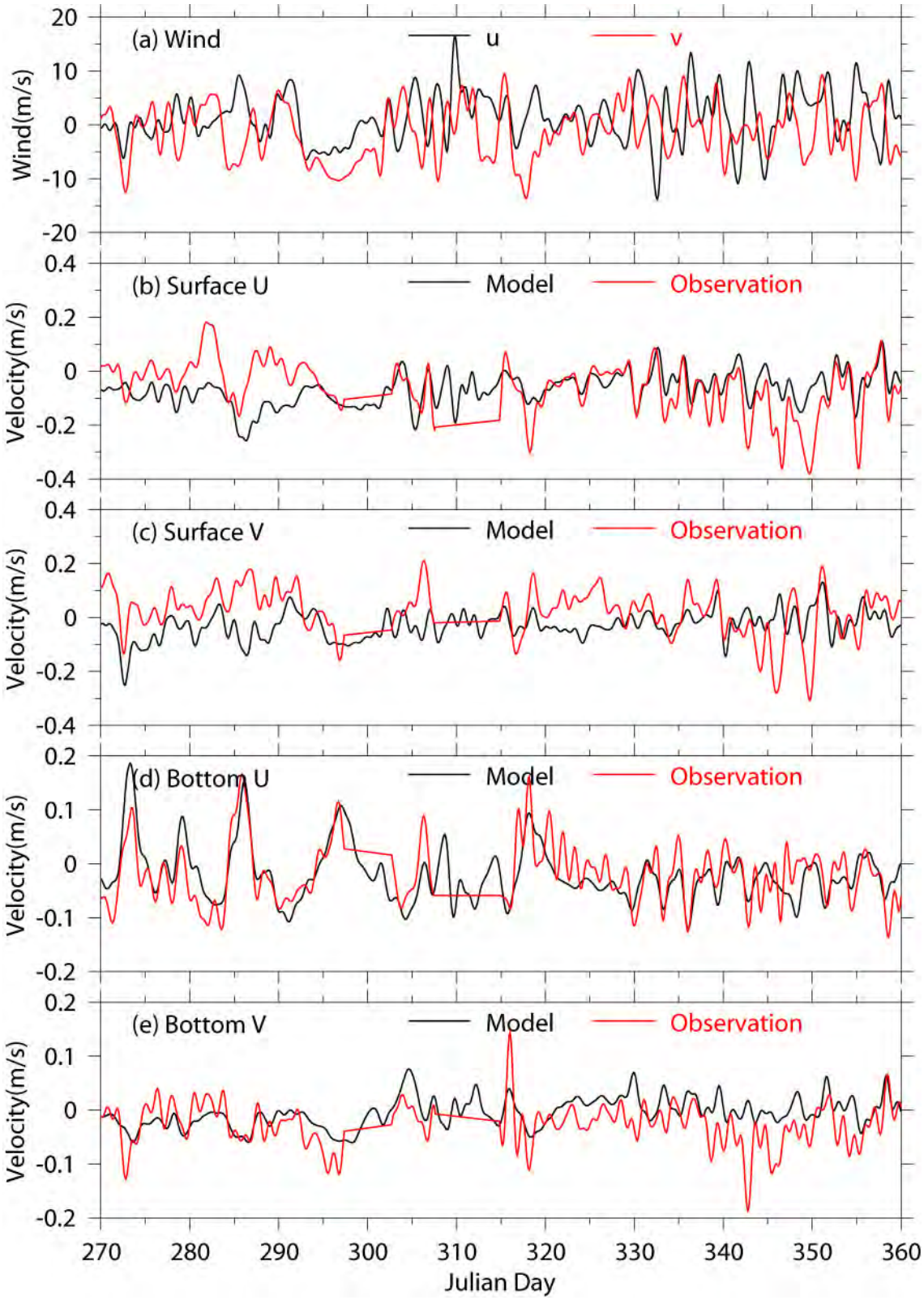

Figure 3.42. Winds at NOAA 44013 and currents at GoMOOS A in Oct.-Dec. 2004, (a) Wind, (b) surface E-W velocity, (c) surface N-S velocity, (d) bottom E-W velocity, (e) bottom N-S velocity.

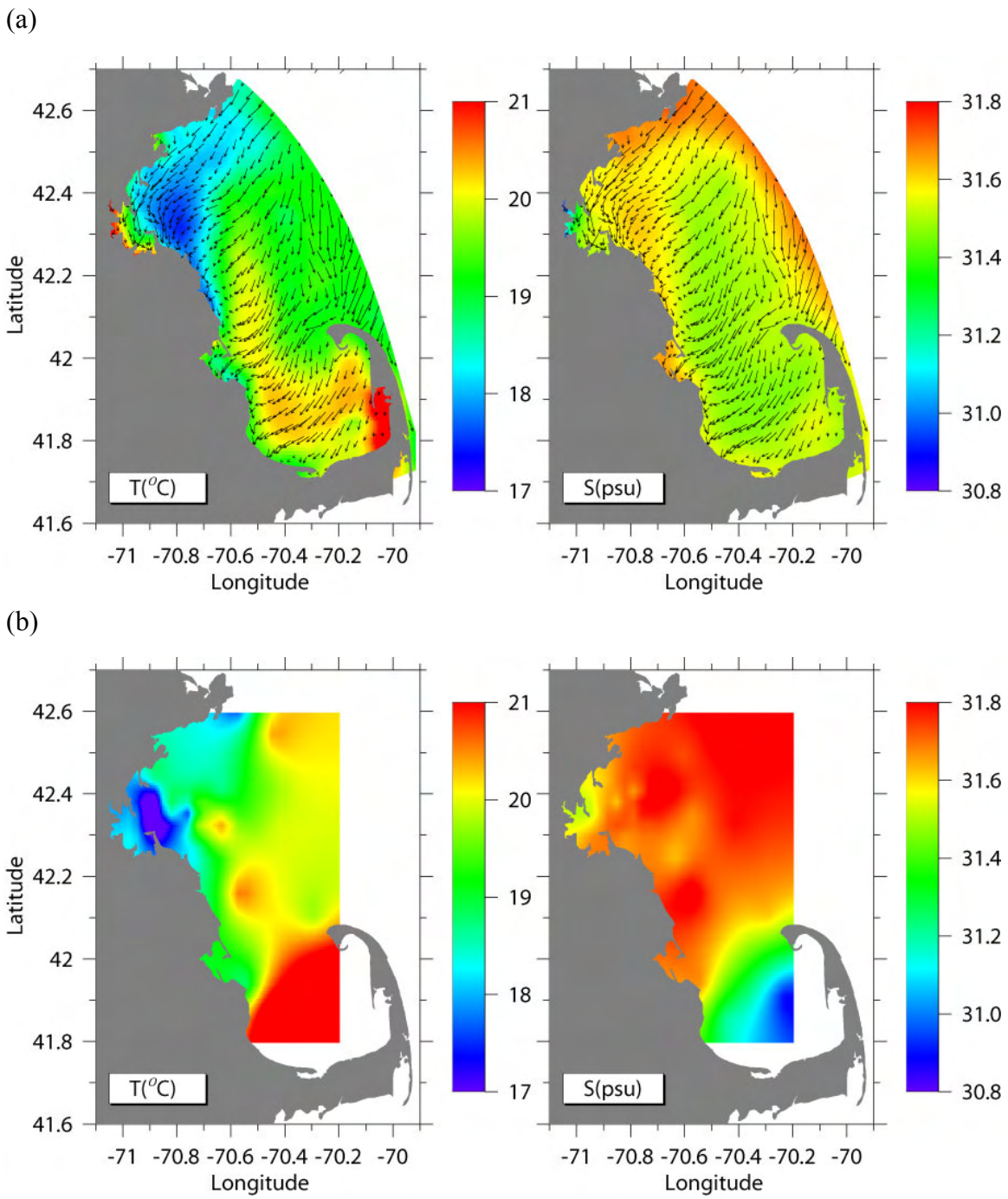

Figure 3.43. Modeled and observed surface temperature and salinity: (a) modeled results on August 21, 2002 and (b) observations in August 19-22, 2002.

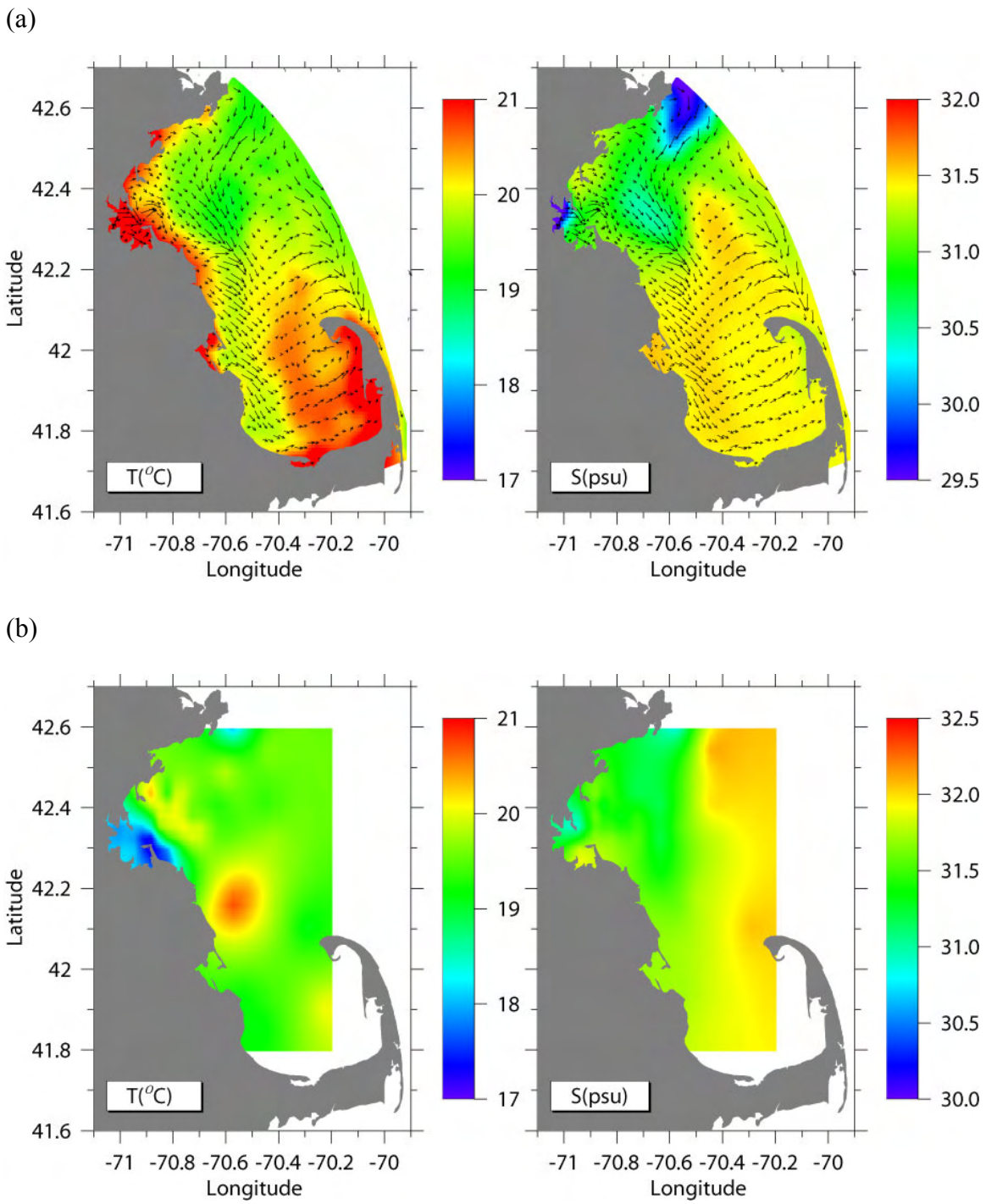

Figure 3.44. Modeled and observed surface temperature and salinity: (a) modeled results on August 20, 2003, and (b) observations in August 18-21, 2003.

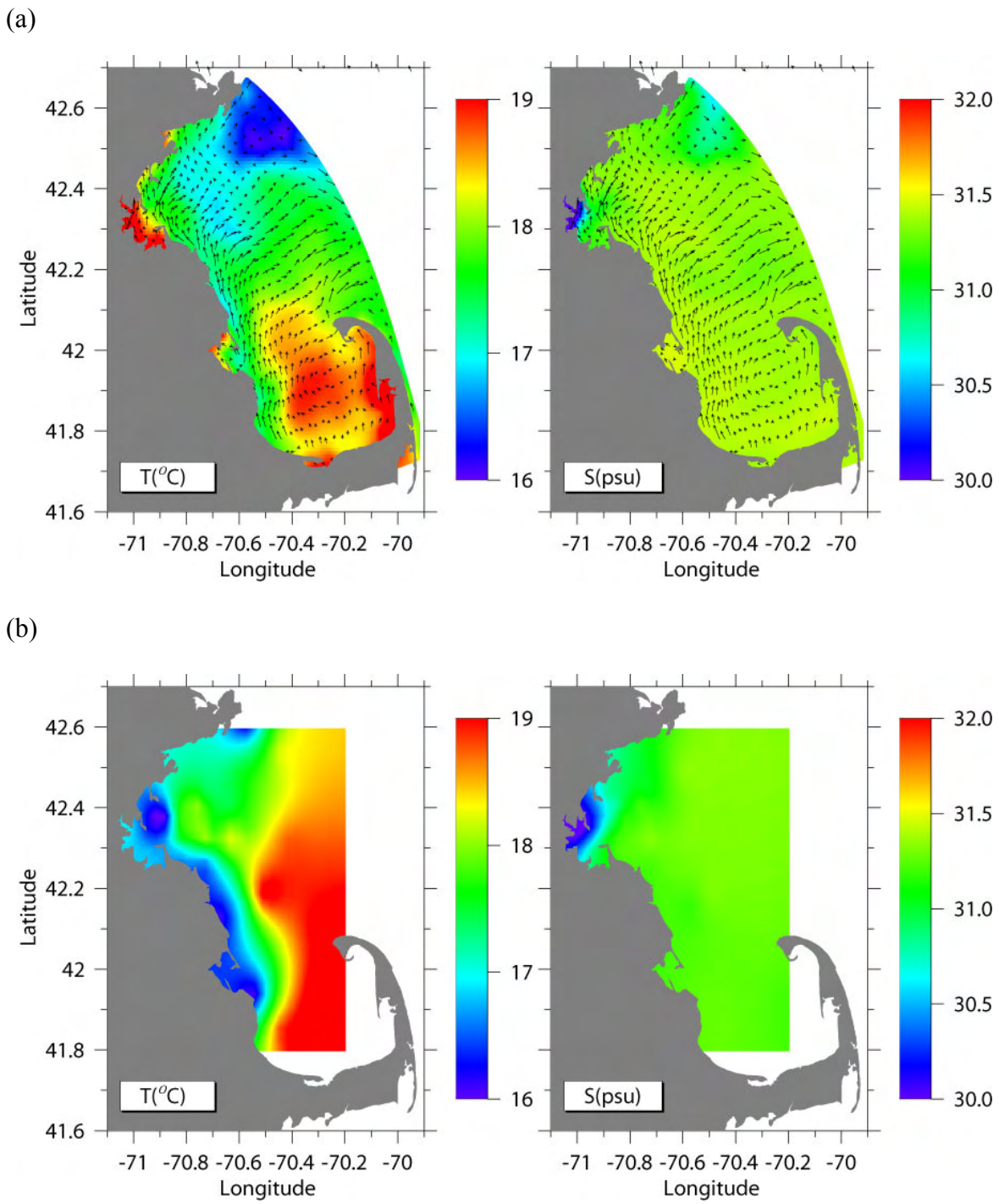

Figure 3.45. Modeled and observed surface temperature and salinity: (a) modeled results on August 18, and (b) observations in August 16-19, 2004.

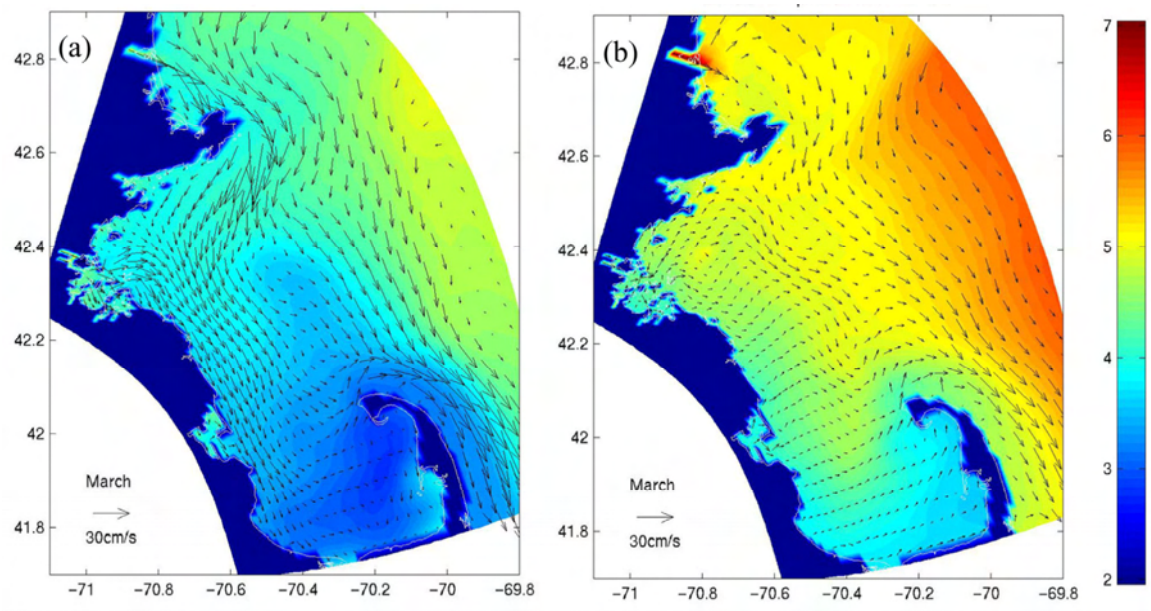

Figure 3.46. Modeled surface temperature (color) and currents in (a) March, 2000 and (b) March, 2002.

4. MODEL ENHANCEMENT AND SENSITIVITY EXPERIMENTS

4.1 Data assimilation

It is well recognized that upstream boundary conditions are important for modeling Massachusetts Bay circulation and water quality (Jiang and Zhou, 2004b, 2004c). We expect that model improvement can be made when measurements with better spatial and temporal coverages along the open boundary are available. The time-series of measurement at GoMOOS buoy B near the model open boundary can be used for improving the short-term model behavior through data assimilation. We compare the model results of the experiment with assimilation of GoMOOS buoy B measurements and the experiment without assimilation (referred to as no-nudging hereafter).

The temperature and salinity at USGS buoys A and B between nudging and no-nudging experiments for 2002 are shown in Figure 4.1a and 4.1b, respectively (see section 2.4.4 for details in the assimilation method). The assimilation significantly improves the modeled salinities at both stations, especially in late spring and early summer when river discharges were largest, whereas temperature results are essentially the same. This indicates that the salinity in the MBS is largely controlled by the intruding GOM waters through the open boundary, while water temperature in the MBS is mostly controlled by local heating and cooling processes.

The currents at USGS buoys A and B from experiments with and without data assimilation are shown in Figures 4.2-4.9. The results with data assimilation are smoother at both locations than that without assimilation. The model results with data assimilation were significantly improved during periods when the model tended to overestimate currents (e.g., surface currents during days 30-90 and 310-340).

4.2 Effects of vertical model resolution

In this section, we examine effects of the model vertical resolution by increasing the number of sigma layers from 12 to 22. The thicknesses of original and new sigma layers are shown in Table 4.1. We modified the vertical distribution of the river discharges accordingly to best mimic the distribution in the 12-layer simulation. The model results at the end of 2001 produced by the 2001 simulation were linearly interpolated into new sigma layers to provide initial conditions for

the 22-layer simulation.

The temperature and salinity at USGS buoys A and B from the 12-layer simulation and 22-layer simulation are shown in Figures 4.10 and 4.11, respectively. Both experiments simulated the springtime freshening equally well, and both under-estimated the strengths of summer upwelling/downwelling events, especially at the buoy A, and under-estimated salinity in winter. The high salinity of the MWRA shipboard measurement at the N21 during November and December appears to be outliers. Similarly, the 22-layer model did not have significant improvement in modeled currents (not shown).

The effect of vertical resolution on vertical thermohaline structures is examined through time series of vertical temperature and salinity profiles. The change may be most significant in summer when vertical stratification is strongest. Here we present the comparison of summer stratification produced by the two experiments at buoy A (Figures 4.12-4.13), and buoy B (Figures 4.14-4.15), respectively. Both experiments produced very similar results except that the 22-layer experiment produced stronger vertical movement of thermocline and slightly stronger stratification at both locations. Overall, the 22-layer model did not produce significant differences in temperature, salinity and currents distributions. In some cases, it appears that the results with higher resolution are a bit worse in comparing with the data (e.g., 12m temperature at USGS buoy B in days 180-270 of 2002).

It is not particularly surprising that a model with finer vertical resolution does not produce better results since this experiment merely changes the vertical grid resolution. The increase of vertical resolution will increase both vertical current shear and vertical gradients temperature and salinity, which have opposite effects on the vertical mixing such that the final effects are uncertain. On the other hand, physical processes have strong correlation in their horizontal and vertical scales. The horizontal resolution needs to be proportionally increased in order to resolve the coastal upwelling process.

4.3 Near real-time forecasting

The forecast of coastal marine environment will provide invaluable and timely information with high spatial-temporal resolutions for the needs of coastal zone management, fisheries, emergency rescue and pollution control. We have developed an operational forecast system for the Massachusetts Bay physical environment, which is providing experimental 2-day forecast for

Massachusetts Bay physical conditions including sea level, temperature, salinity, and currents (http://www.harbor1.umb.edu/forecast). The system also produces hindcasts of the physical conditions based on updated observational data. A comparison of forecasted and hindcasted fields is shown in Figure 4.16, which agree with each other in general. The forecast significantly relies on meteorological forecast, and the forecasted and hindcasted fields may be different when weather forecasts are different from actual conditions.

The forecast system has five consecutive components: (1) acquisition of observed and forecasted meteorological and oceanographic data, (2) data processing to produce model input, (3) model implementation, (4) model output processing to generate products for users, and (5) web display. The executions of these components are controlled by a central command system, which starts the data acquisition at specified time, and then triggers subsequent processes after successful executions of previous processes. The hindcast and forecast computations are in fact an integrative rolling-over process that updates forecasted fields with updated forcing conditions from observations, which prevents model from drifting and accumulating errors. The observed data including river discharges, meteorological parameters measured at NDBC 44013 and Logan Airport and temperature, salinity and currents measurements GoMOOS buoy B, are updated up to the moment of model runs. The 4-day meteorological forecasts provided by the National Weather Services are used as the meteorological conditions. Climatological means are used for other future conditions such as river discharges and open boundary conditions. The time-delays between the model run and the acquisition times of data including real measurements and meteorological forecast are listed in Table 4.2.

The hydrodynamic model has been developed in the last 10 years, which provides a solid basis for the success of the forecast system. Further improvements include: (a) use of NCEP forecasted 2-D wind fields and heat fluxes instead of meteorological conditions at a single station, (b) assimilation of satellite SST, (c) prediction of solar radiation based on forecasted cloud coverage and astronomical formulations, and (d) nesting with the GoMOOS operational model to provide real-time open boundary conditions (Xue et al., 2005).

Table 4.1 Sigma layers of original (12 layers) and new model (22 layers)

Sigma layer (k)	Control	New
1	0	0
2	0.01	0.01
3	0.04	0.03
4	0.1	0.06
5	0.2	0.1
6	0.3	0.15
7	0.4	0.2
8	0.5	0.25
9	0.6	0.3
10	0.7	0.35
11	0.8	0.4
12	0.9	0.45
13	1.0	0.5
14	-	0.55
15	-	0.6
16	-	0.65
17	-	0.7
18	-	0.75
19	-	0.8
20	-	0.85
21	-	0.9
22	-	0.95
23	-	1.0

Table 4.2 Time-delays between acquisition times of data and forecast

Forcing	Time Delay
River discharges	15 min.-3 hours
NDBC (winds, air pressure, air temperature)	10 min.
WHOI Solar radiation	Climatological mean
Logan airport (relative humidity)	Climatological mean
NCEP meteorological forecast	10 min.
GoMOOS buoy B (t, s, currents)	10 min.

(a)

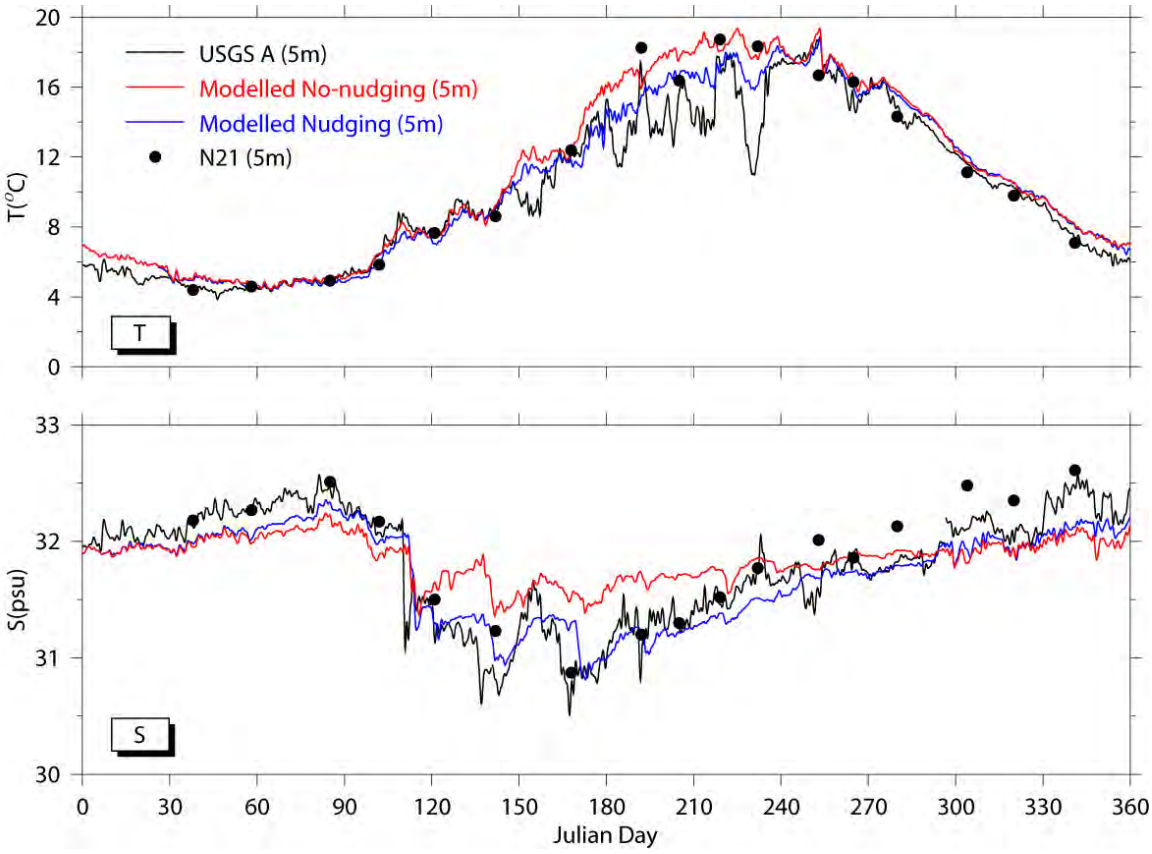

Figure 4.1. Modeled temperature and salinity between no-nudging and nudging cases at (a) Buoy A and (b) Buoy B in 2002.

(b)

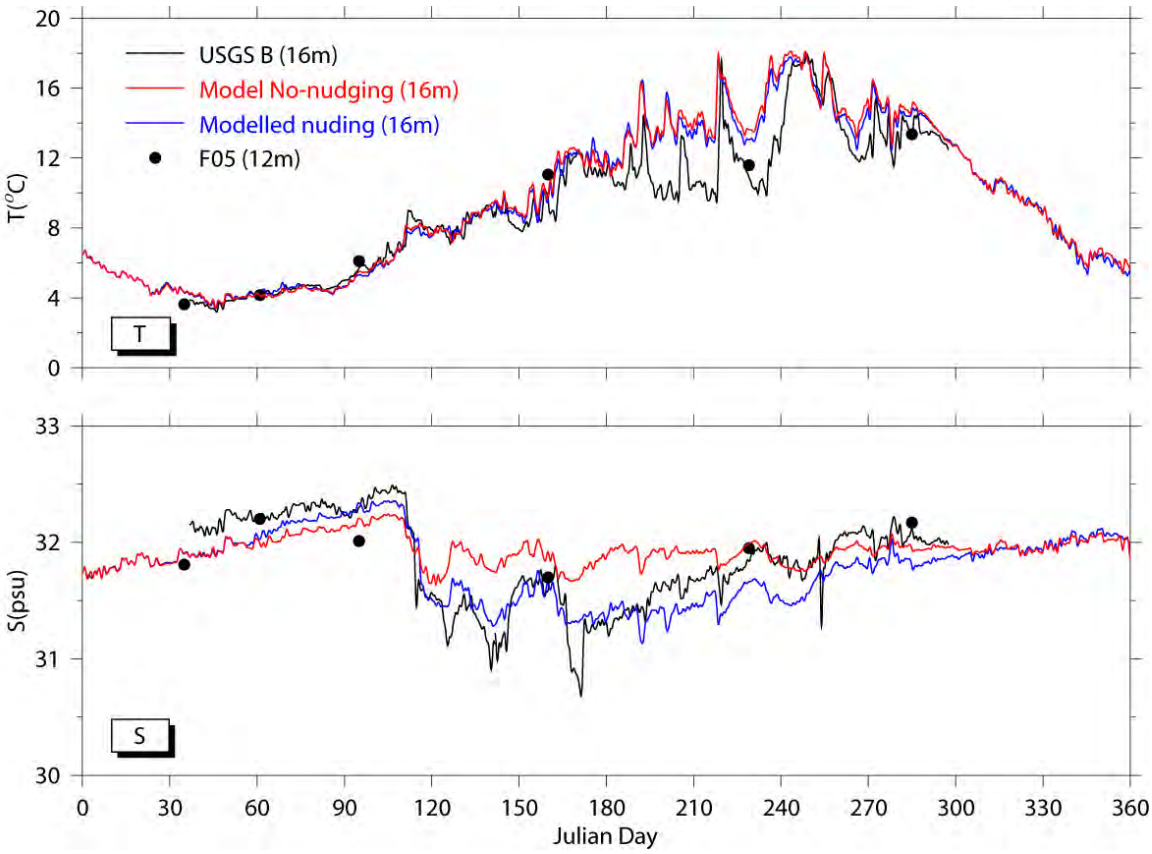

Figure 4.1. Continued.

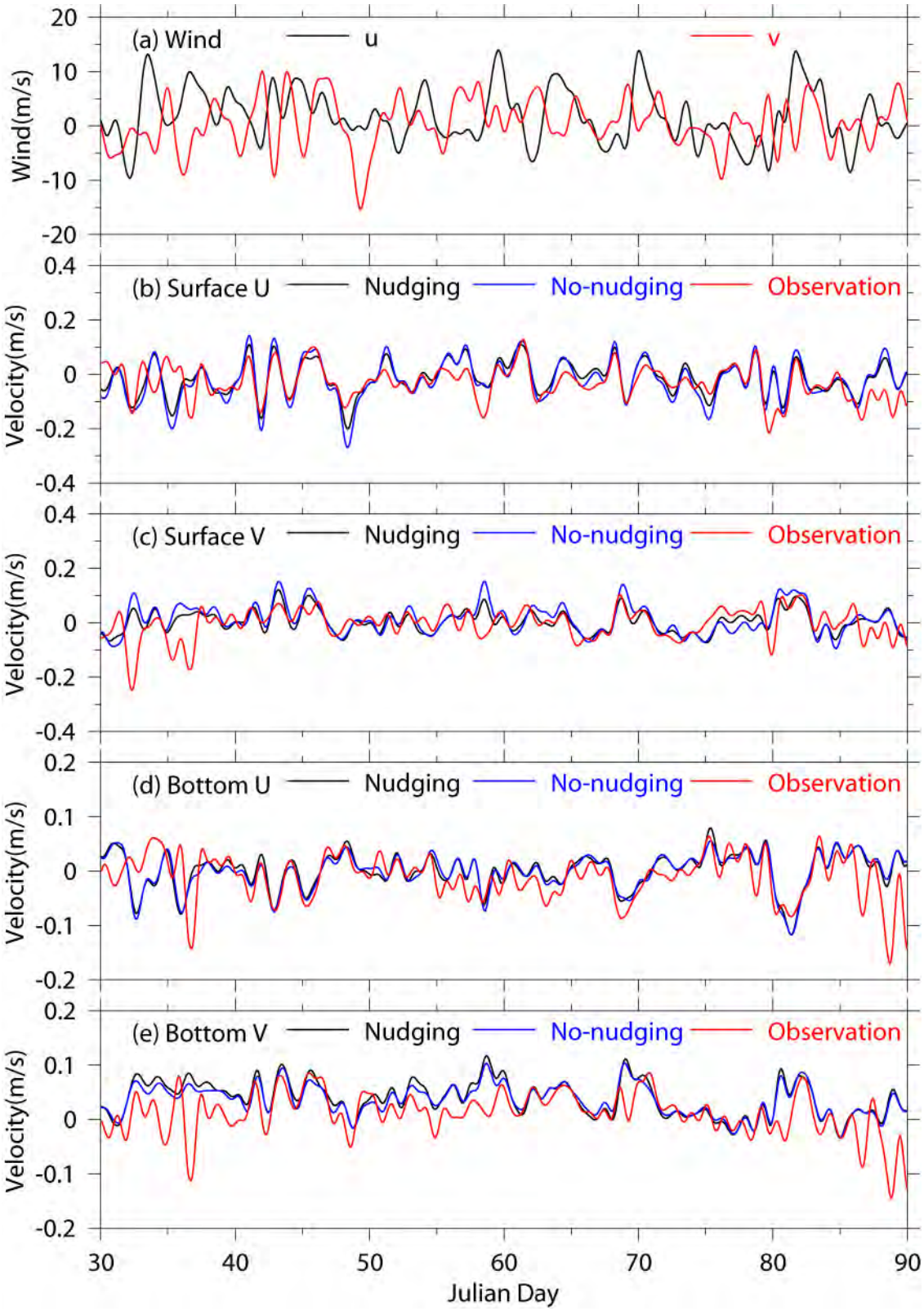

Figure 4.2. Winds at NOAA 44013 and currents at USGS Buoy A in Jan.-Mar. 2002, (a) Wind, (b) surface E-W velocity, (c) surface N-S velocity, (d) bottom E-W velocity, (e) bottom N-S velocity.

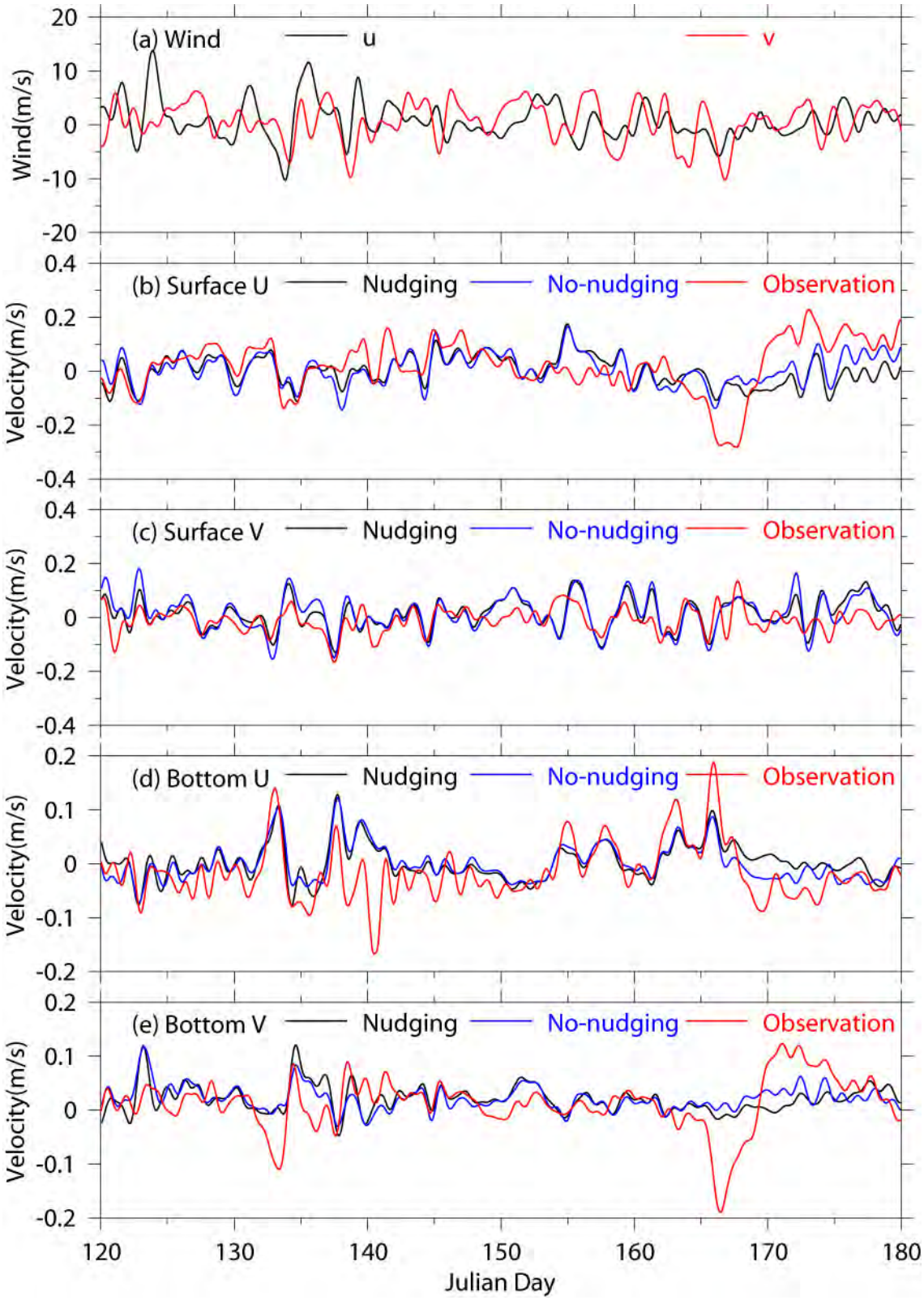

Figure 4.3. Winds at NOAA 44013 and currents at USGS Buoy A in Apr.-Jun. 2002, (a) Wind, (b) surface E-W velocity, (c) surface N-S velocity, (d) bottom E-W velocity, (e) bottom N-S velocity.

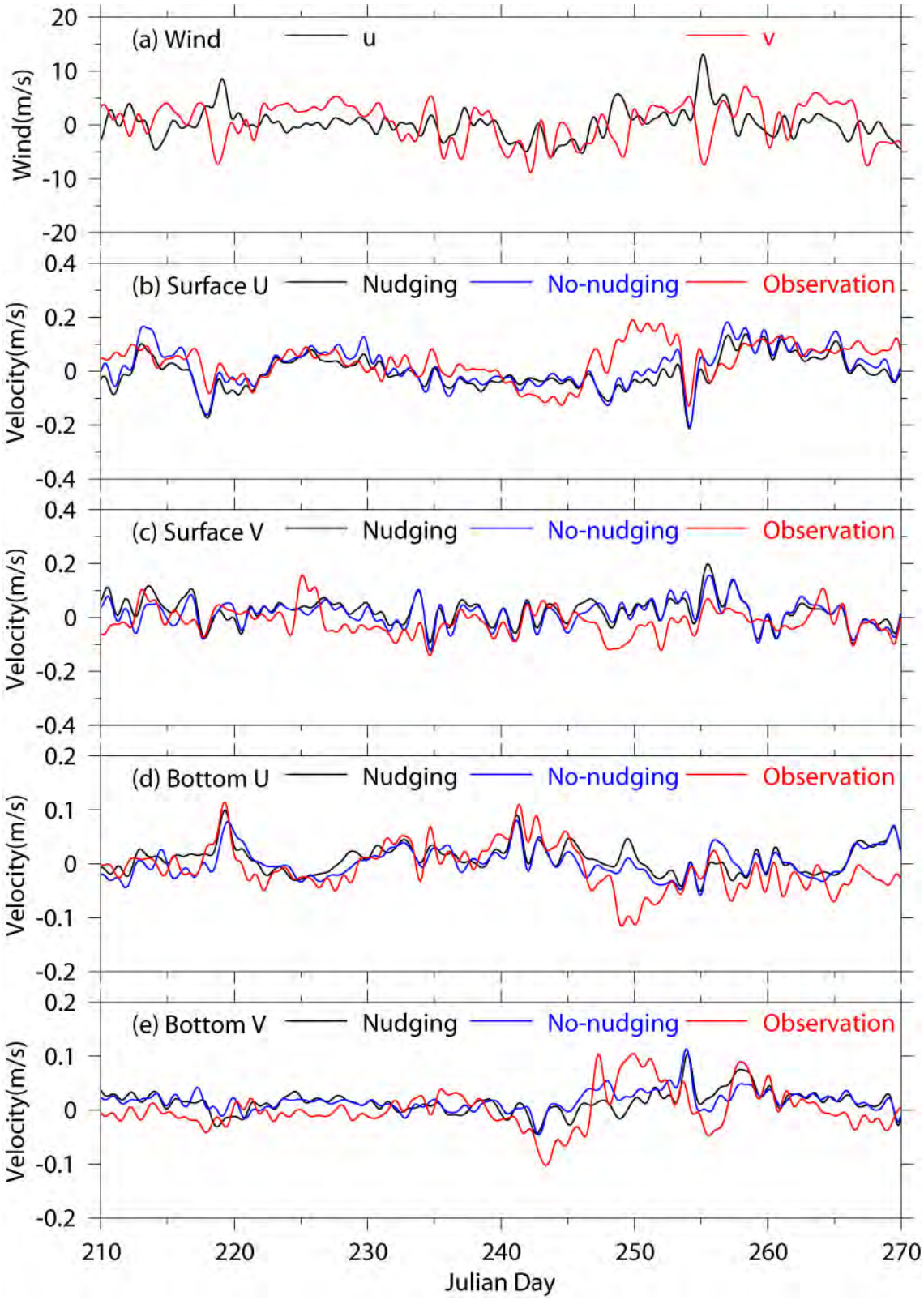

Figure 4.4. Winds at NOAA 44013 and currents at USGS Buoy A in Jul.-Sep. 2002, (a) Wind, (b) surface E-W velocity, (c) surface N-S velocity, (d) bottom E-W velocity, (e) bottom N-S velocity.

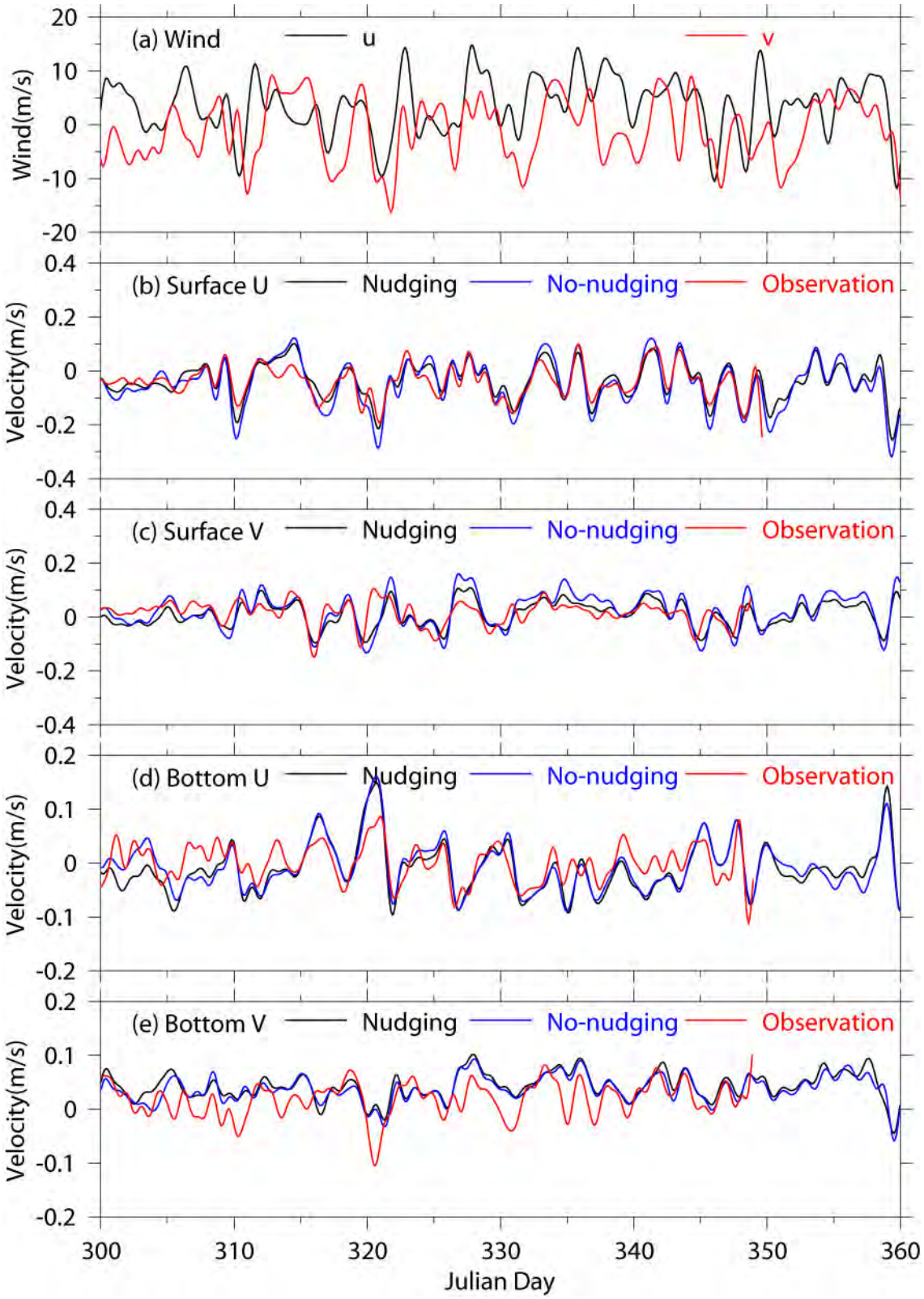

Figure 4.5. Winds at NOAA 44013 and currents at USGS Buoy A in Oct.-Dec. 2002, (a) Wind, (b) surface E-W velocity, (c) surface N-S velocity, (d) bottom E-W velocity, (e) bottom N-S velocity.

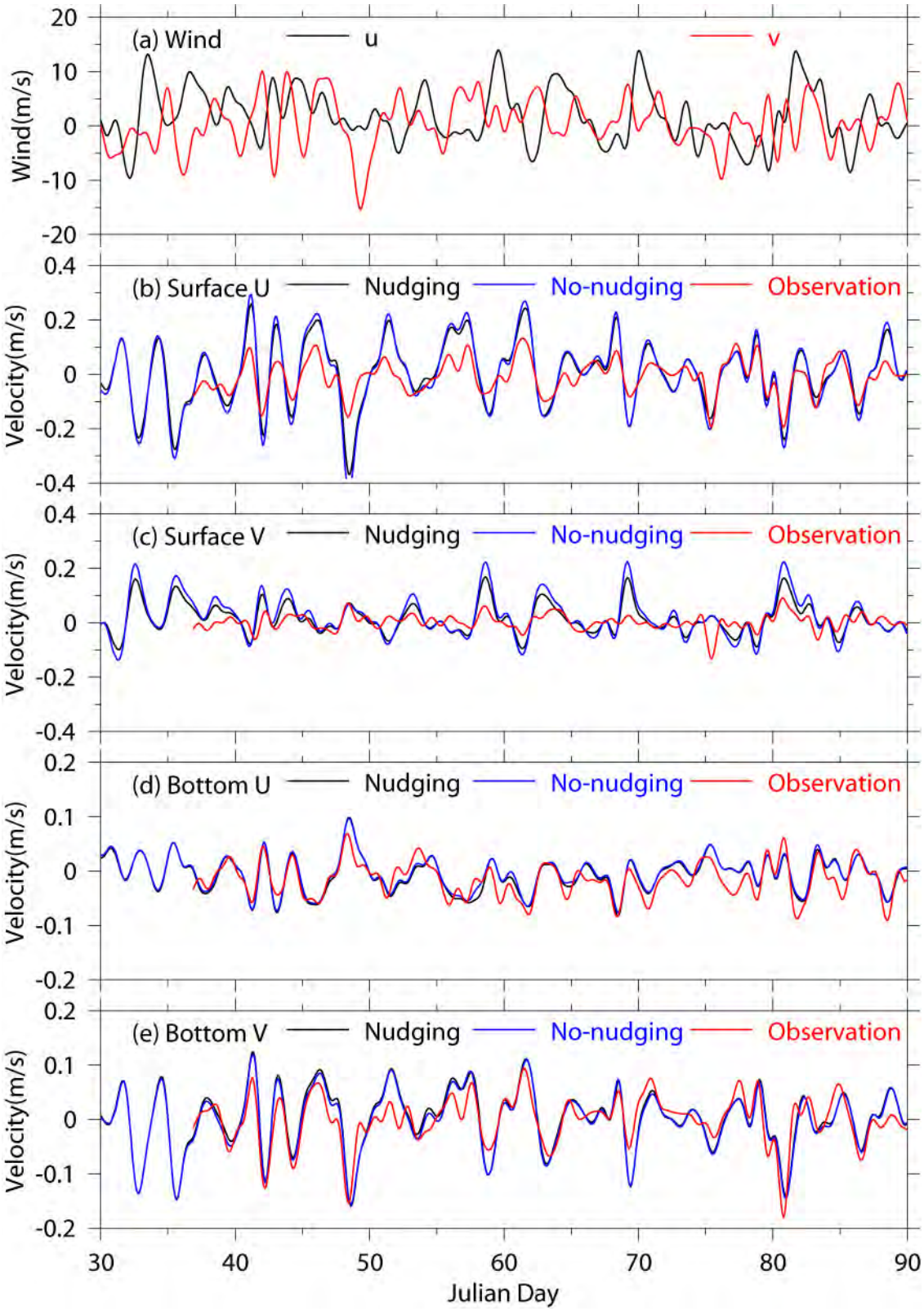

Figure 4.6. Winds at NOAA 44013 and currents at USGS Buoy B in Jan.-Mar. 2002, (a) Wind, (b) surface E-W velocity, (c) surface N-S velocity, (d) bottom E-W velocity, (e) bottom N-S velocity.

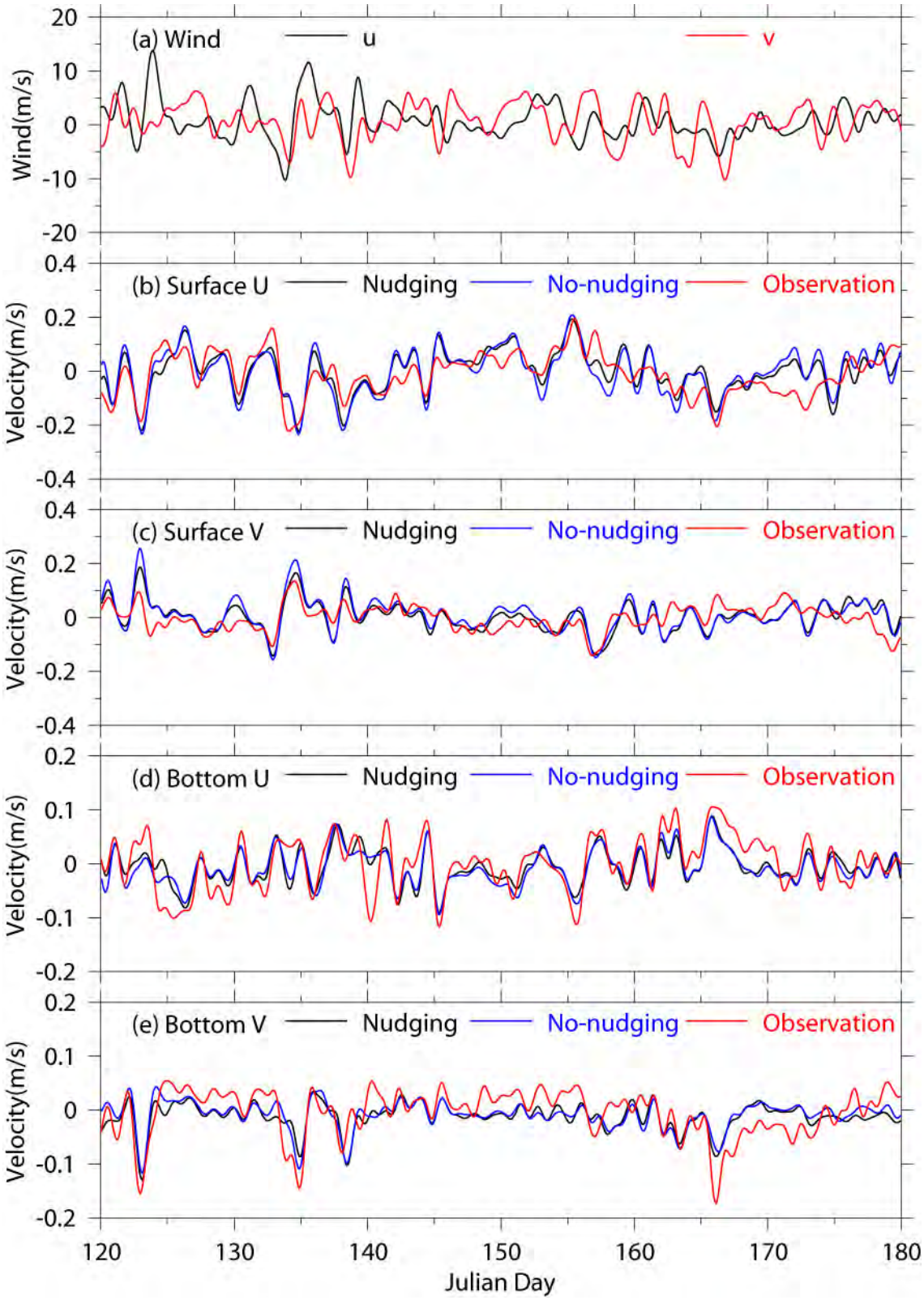

Figure 4.7. Winds at NOAA 44013 and currents at USGS Buoy B in Apr.-Jun. 2002, (a) Wind, (b) surface E-W velocity, (c) surface N-S velocity, (d) bottom E-W velocity, (e) bottom N-S velocity.

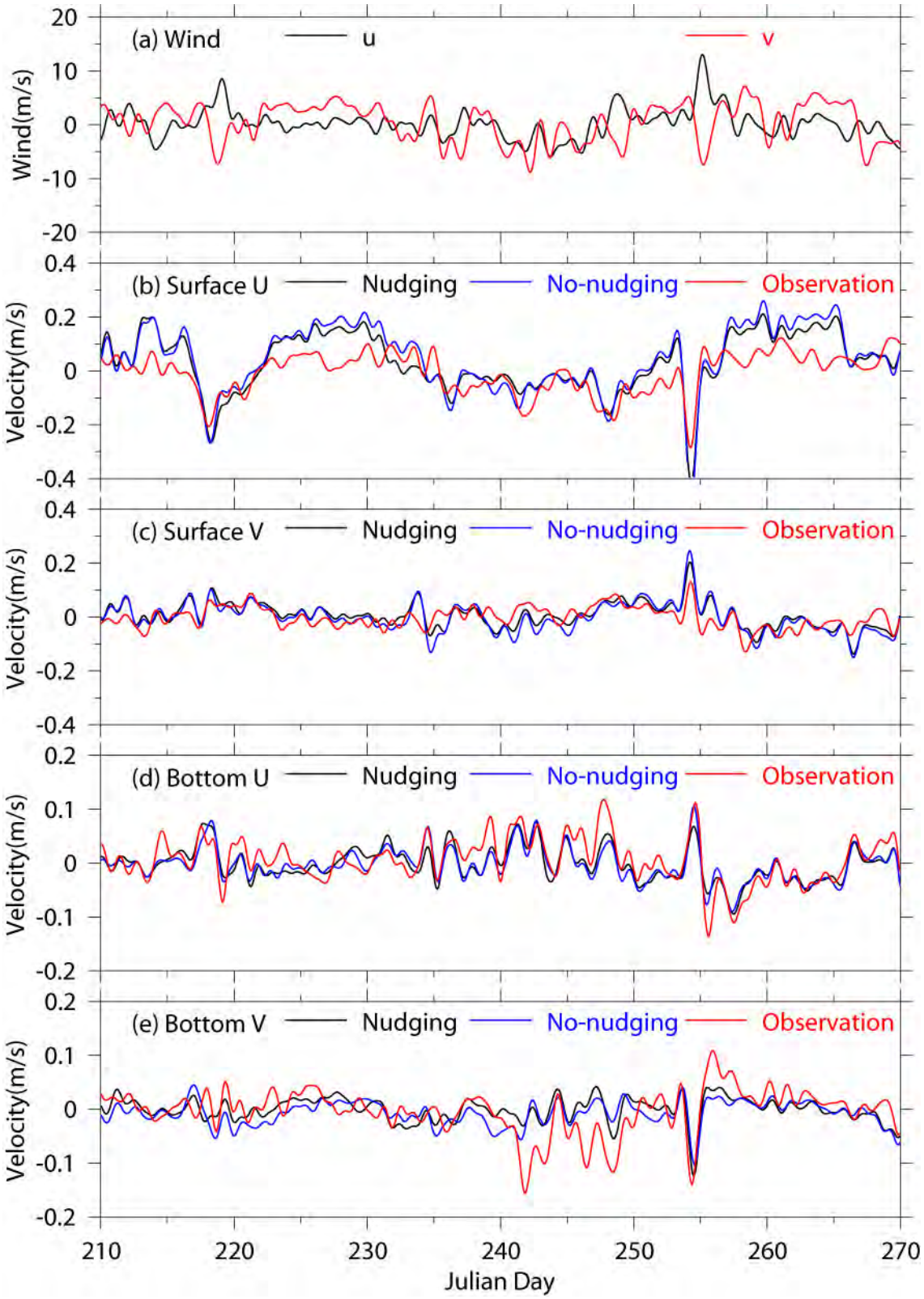

Figure 4.8. Winds at NOAA 44013 and currents at USGS Buoy B in Jul.-Sep. 2002, (a) Wind, (b) surface E-W velocity, (c) surface N-S velocity, (d) bottom E-W velocity, (e) bottom N-S velocity.

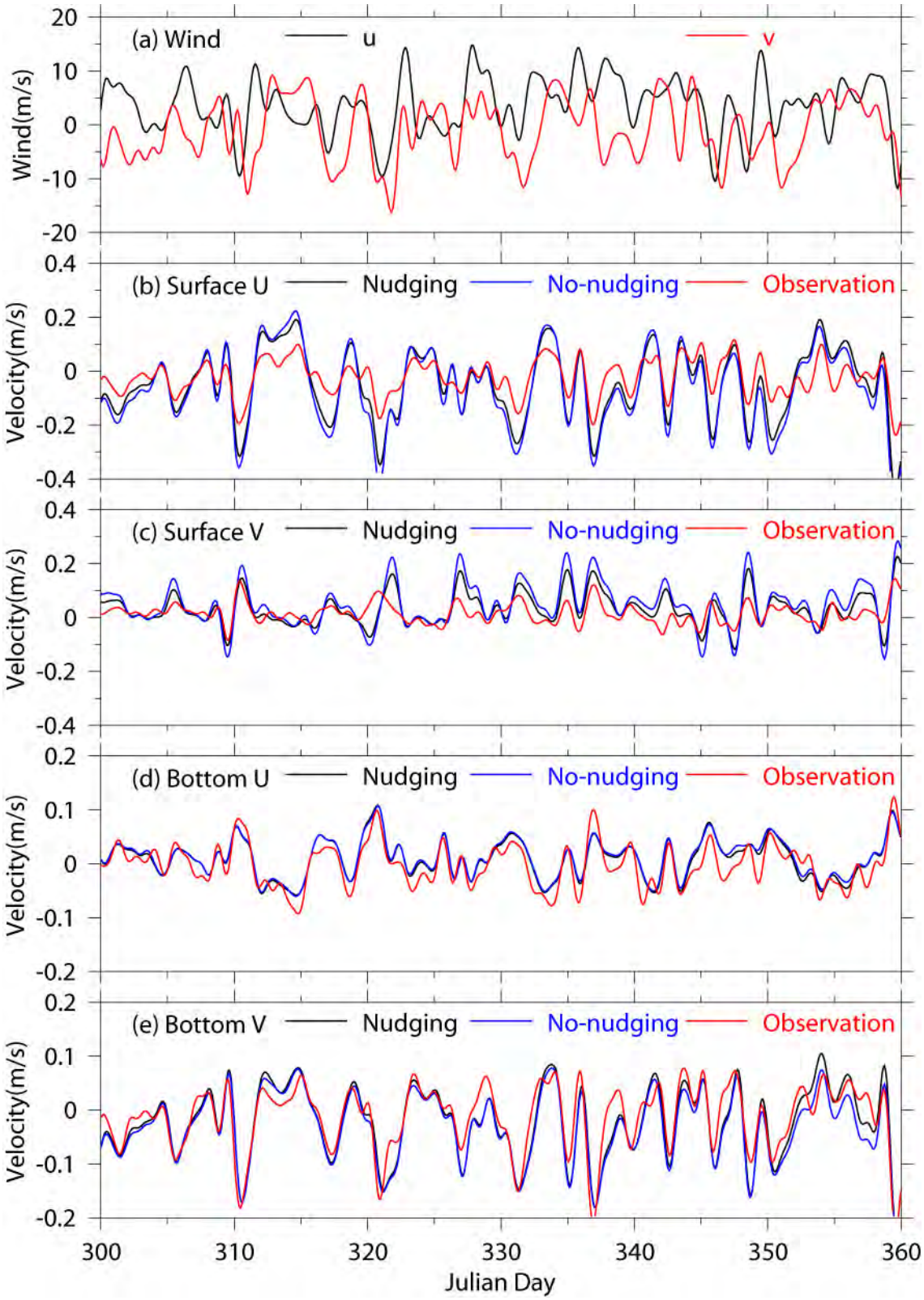

Figure 4.9. Winds at NOAA 44013 and currents at USGS Buoy B in Oct.-Dec. 2002, (a) Wind, (b) surface E-W velocity, (c) surface N-S velocity, (d) bottom E-W velocity, (e) bottom N-S velocity.

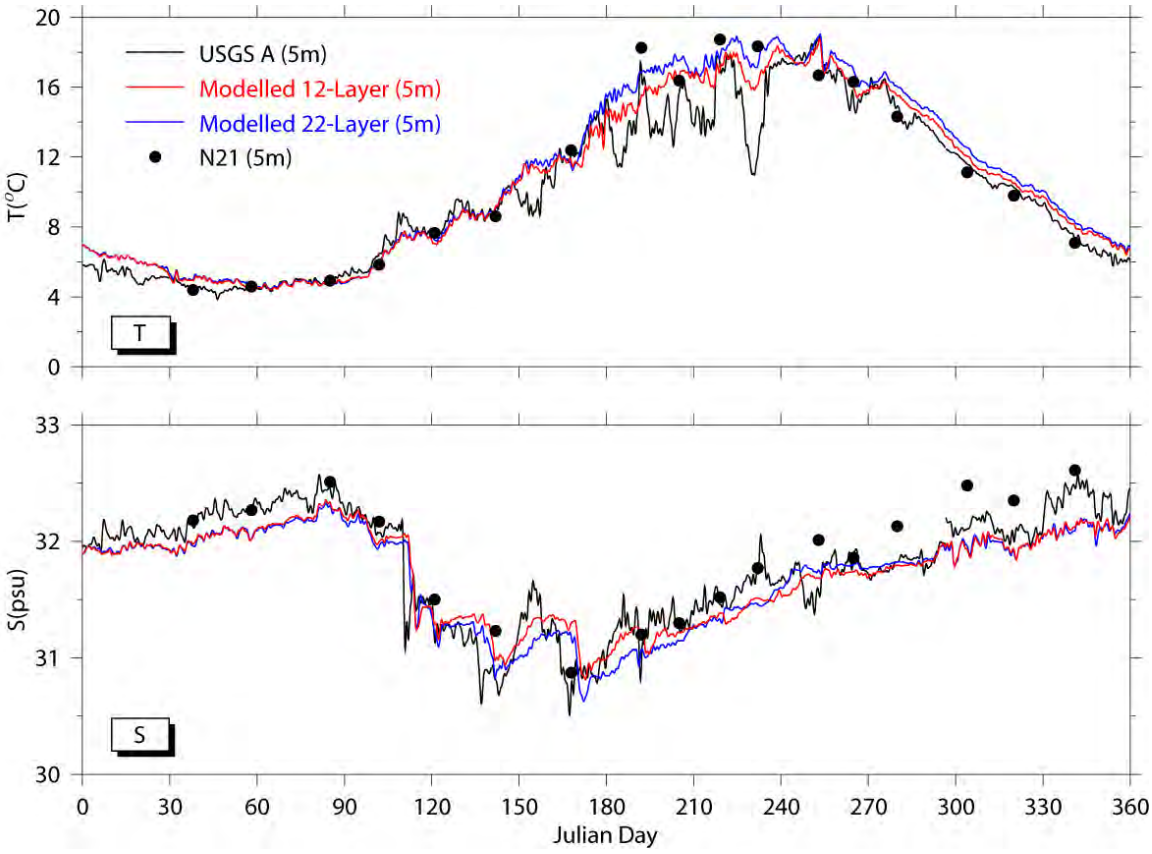

Figure 4.10. Modeled temperature and salinity at USGS Buoy A (5m) in 2002.

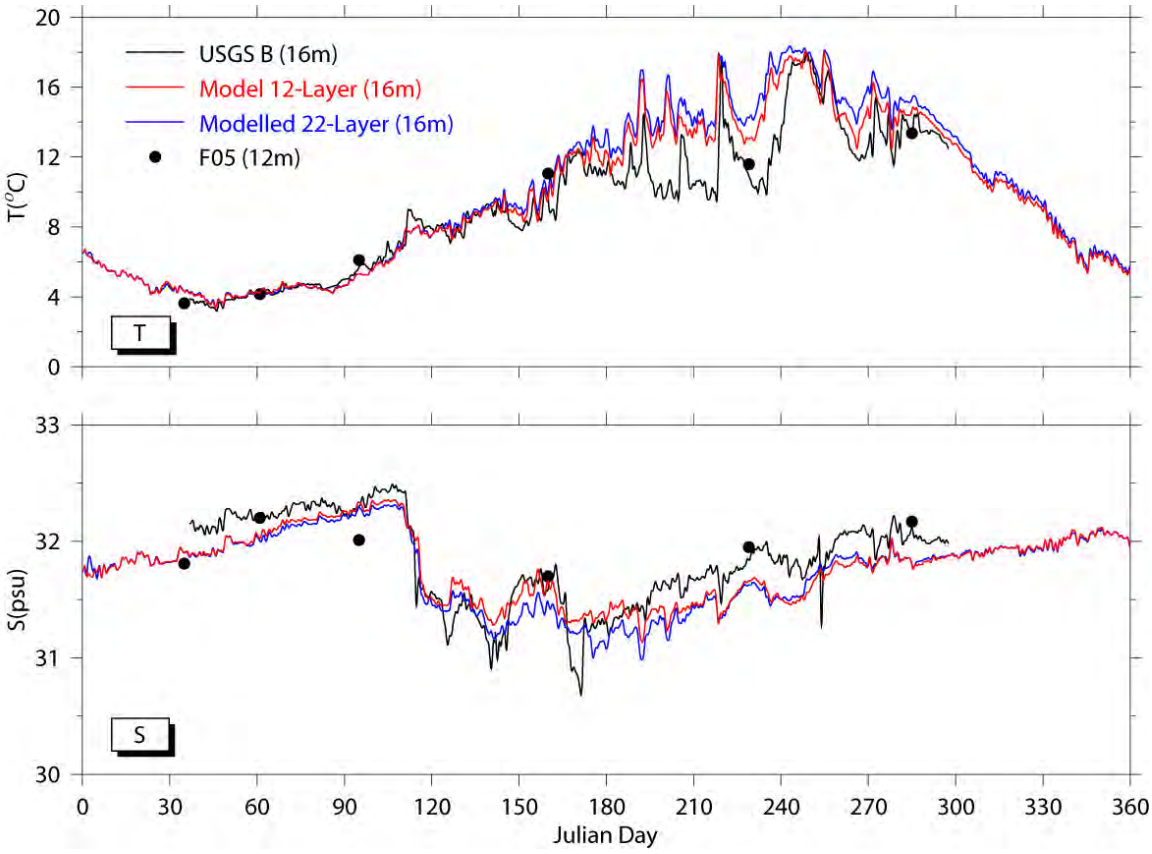

Figure 4.11. Modeled temperature and salinity at USGS Buoy B (16m) in 2002.

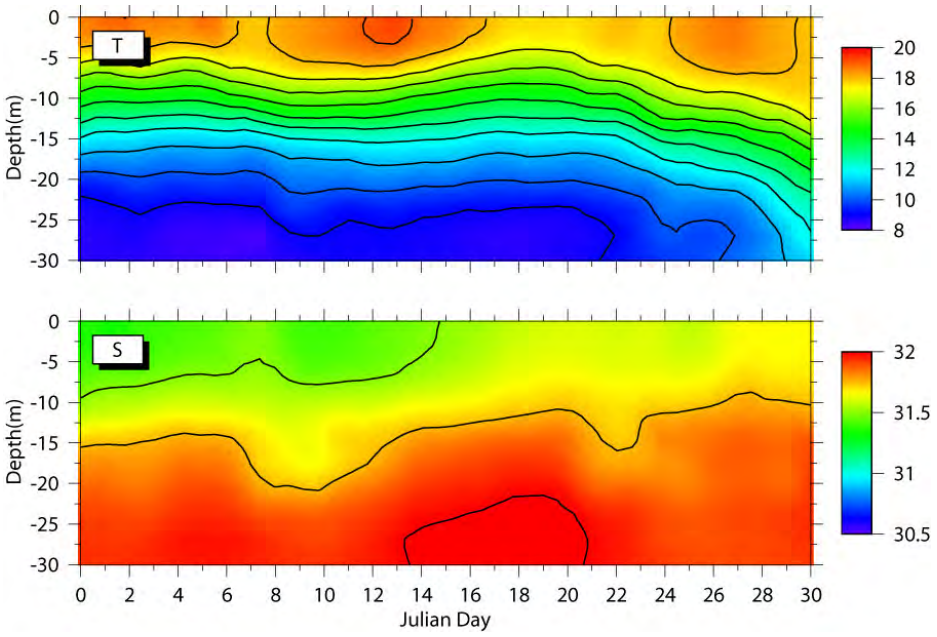

Figure 4.12. Modeled temperature and salinity at USGS Buoy A in August 2002 (12-Layer).

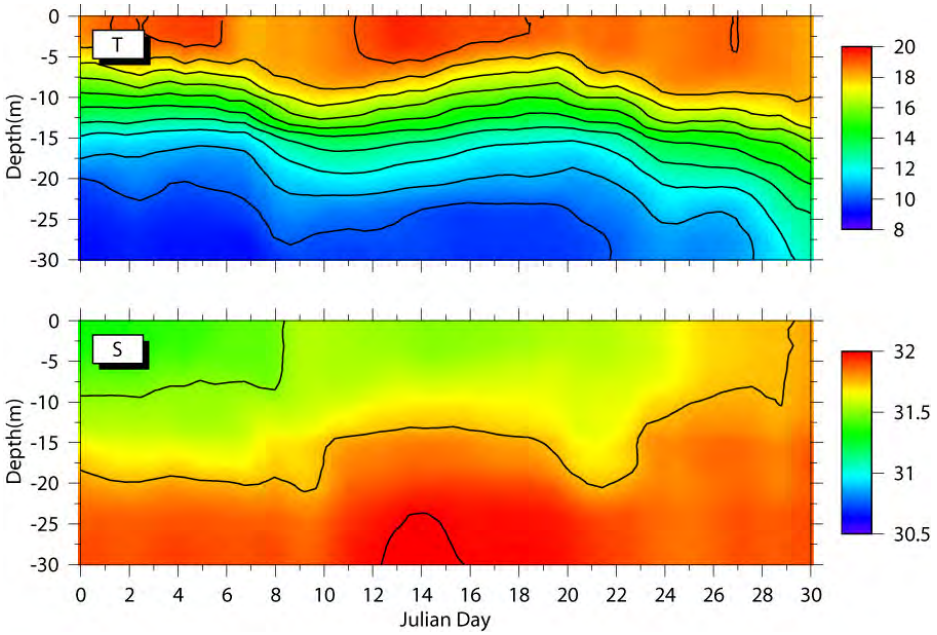

Figure 4.13. Modeled temperature and salinity at USGS Buoy A in August 2002 (22-Layer).

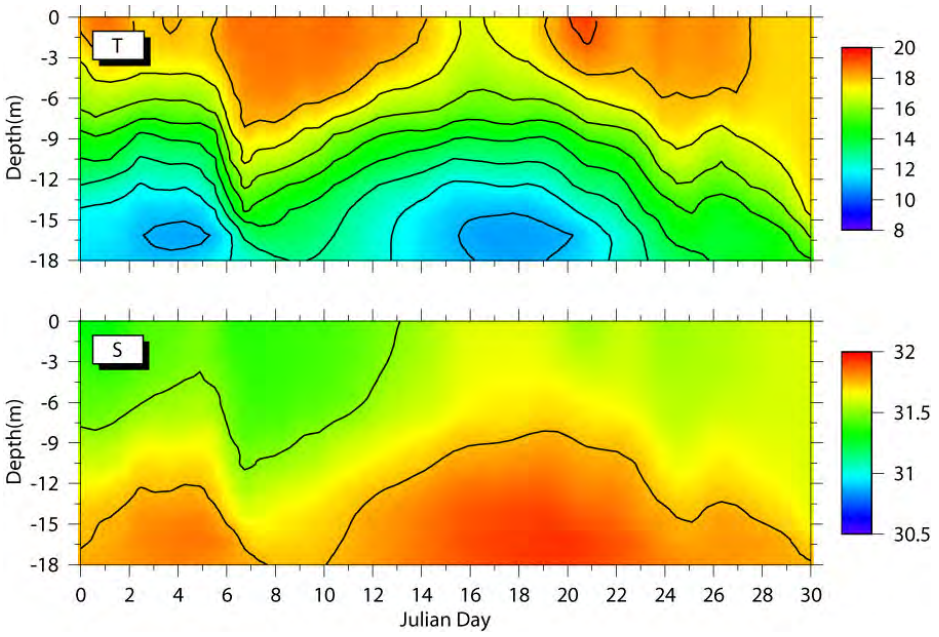

Figure 4.14. Modeled temperature and salinity at USGS Buoy B in August 2002 (12-Layer).

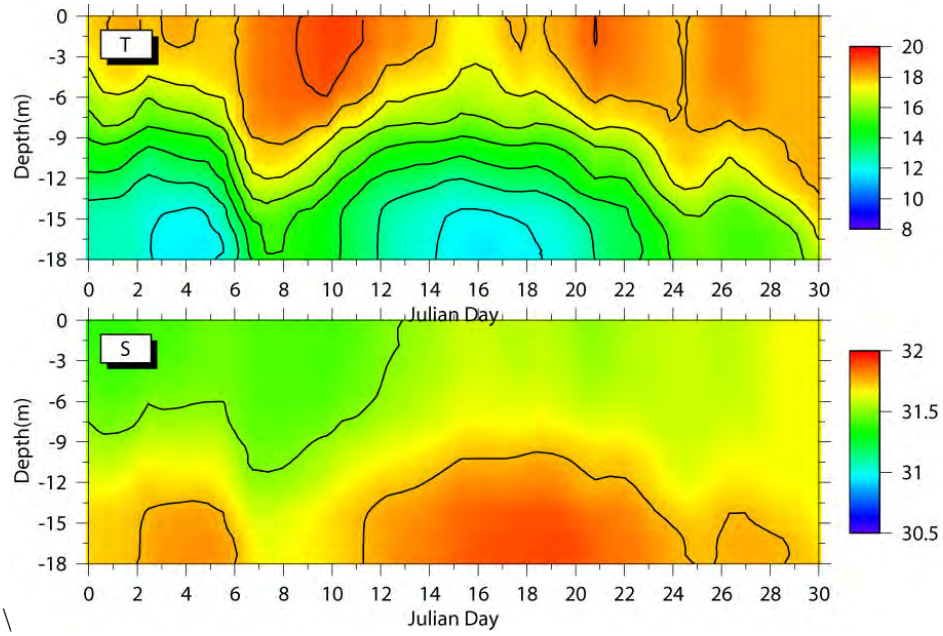

Figure 4.15. Modeled temperature and salinity at USGS Buoy B in August 2002 (22-Layer).

(a)

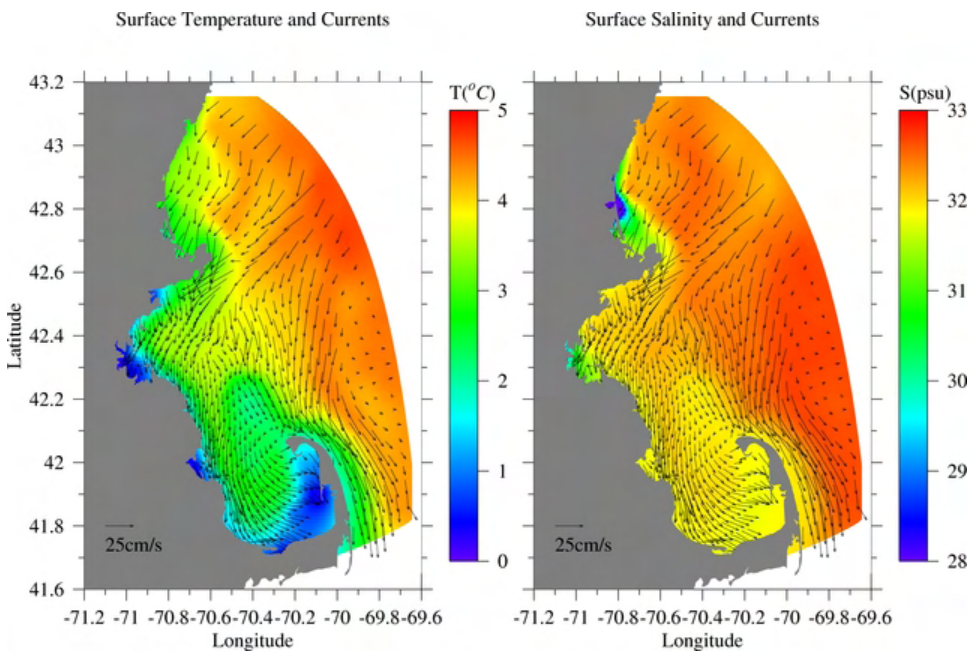

(b)

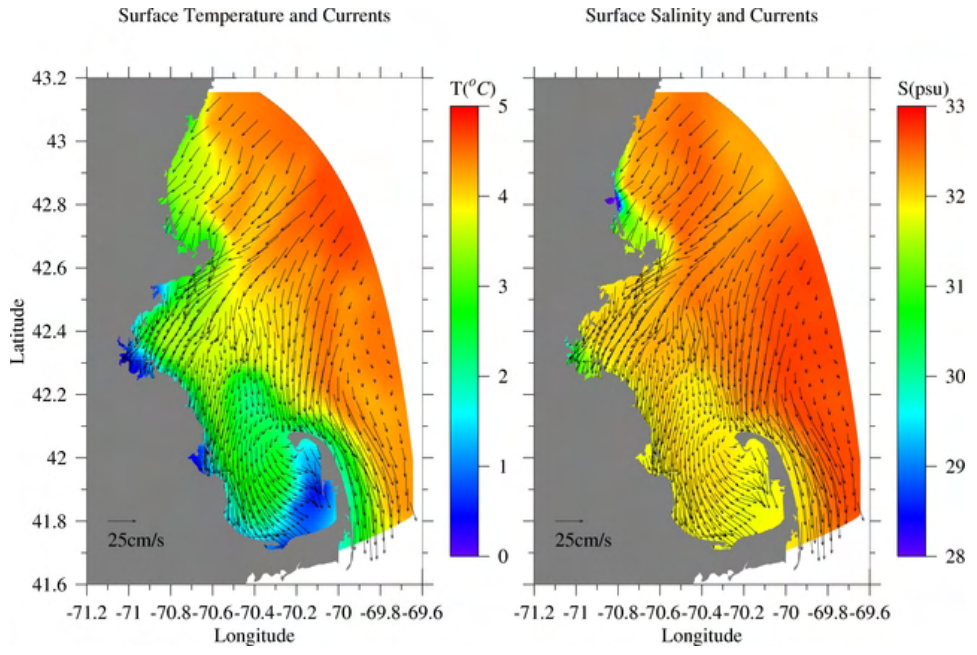

Figure 4.16. (a) Forecast temperature and salinity on March 5, 2006. (b) Hindcast temperature and salinity on March 5, 2006.

5. SUMMARY AND RECOMMENDATIONS

5.1 Summary

This report presents the calibration and simulation results of the MBS hydrodynamic model for years 2002-2004. Overall, the modeled temperature, salinity and currents are well compared with observations from moorings and surveys in response to both seasonal changes in meteorological forcing, freshwater inputs and boundary forcing, and short-term wind events. The validation of modeled results indicates again that the MB hydrodynamic model is robust, and ready for applications in various environmental studies.

The discrepancies between model results and observations in temperature, salinity and currents in western MB suggest the need of more detailed open boundary conditions and the need of studies on the freshwater plume dynamics near Cape Ann. Over-smoothed open boundary conditions have caused under-estimated water exchanges between MB and the GOM that in spring can lead to under-estimation of Merrimack River plume and hence the overestimation of salinity in western MB. Interactions between the topography, coastal currents, surface winds and freshwater plume are likely controlling the bifurcation and intrusion of WMCC near Cape Ann, but the specific mechanisms remain unclear.

The model simulates weaker stratification and summer upwelling along the western coast, which might be due to inadequate grid resolution. Numerical experiment suggests that simply increasing vertical resolution does not improve the model results. The reason for this is that coastal upwelling strength in late spring and summer is determined by both vertical stratification and horizontal upwelling front, which requires high horizontal resolution.

The model has been enhanced by assimilating measurements at GoMOOS buoy B, which improves the upstream boundary conditions. A simple nudging scheme has been developed for assimilating temperature, salinity, and currents. This method has significantly improved the modeled salinity and currents in spring and early summer.

An operation forecast has been developed to provide real-time forecast for MBS physical environment. The system has been operational and provides reasonably well forecast.

5.2 Recommendations

Improving open boundary conditions. The lack of short-term variability in the open conditions will cause 1) less short-term variability in modeled currents, and 2) overestimation of

salinity in western MB due to under-estimated freshwater plume from the Merrimack River. Assimilation of measurements at GoMOOS buoy B has significantly improved the modeled salinity and currents. However, information along most of the open boundary is still lacking. Nesting the MB model in a GOM model may improve open boundary conditions and hence model results.

Improving both vertical and horizontal grid resolutions. The increase in horizontal resolution can lead to a decrease in grid-related horizontal numerical diffusion, an increase in horizontal density gradient, a better representation of baroclinic instability, and current-topographic interactions. The strength of upwelling/downwelling events may be under-estimated due to over-smoothed gradients of density and currents by overestimated horizontal and vertical mixing.

Process studies. Analyses of model results and observations have indicated rich mesoscale processes in the MBS such as mesoscale eddies, and upwelling/downwelling wind events. For example, during the relaxation period of a northeasterly wind event, a mesoscale anticyclone of 15~20 km is frequently produced in the north shore region, translates southwestward at a translation speed of several km per day along the coast and then dissipates near Scituate. Another example is the bifurcation of the WMCC near Cape Ann, which determines the volume transport of the GOM waters into MB. However, the mechanism leading to the bifurcation is unclear. The impacts of these translating mesoscale eddies and volume transport of the GOM waters into MB on biogeochemical processes and the fate of the MWRA effluent have not been well studied. A better understanding of these processes will lead to a better prediction of frontal locations, spatial and temporal scales of an eddy, the volume transport, and the fate of effluent.

Integration between model forecast and field surveys in MB. While scientists are challenged to make a better model, the managers are challenged to integrate contemporary mathematical and model tools and results into their management. Traditionally in oceanography we have conducted surveys over fixed stations in last 100 years, and have been challenged by the spatial and temporal biases between stations, missing short-term critical events and frequent unexpected values from field surveys, which are critical during decision-making. With the calibrated model, we can, in a certain degree of confidence, forecast the physical fields, assimilate data into the model at real time, and guide surveys for resolving physical fields at any small-meso-basin scales so that managers will have best information for making decisions. The MB model has been developed and calibrated in the last 10 years and cost over million dollars. While its

scientific contributions will be continuously evaluated by peer-reviewed publications, its applications in management tasks have not been sufficiently explored.

6. REFERENCES

Bigelow, H.B. 1927. Physical oceanography of the Gulf of Maine (Part II). Bulletin of the Bureau of Fisheries, 40: 511-1027.

Blumberg, A.F. and G. L. Mellor, 1987. A description of a three-dimensional coastal ocean circulation model. In: Three-Dimensional Coastal Ocean Models, Coastal and Estuarine Sciences, Vol.4, N. Heaps (Ed.), American Geophysical Union, Washington, D.C., 1-6.

Butman, B., 1976. Hydrography and low frequency currents associated with the spring runoff in Massachusetts Bay Memoires. Societe Royale des Sciences de Liege, 6: 247-275.

Butman, B., M.H. Bothner, F.L. Lightsom, B.T. Gutierrez, P.S. Alexander, M.A. Martini, and W.S. Strahle, 2002, Long-term Oceanographic Observations in Western Massachusetts Bay offshore of Boston, Massachusetts: Data Repor for 1989-2000, U.S. Geological Survey Digital Data Series 74.

Casulli, V., 1990, Semi-implicit finite difference methods fro the two-dimensional shallow water equations, J. Comput. Phys., 86: 56-74.

Galperin, B., L.H. Kantha, S. Hassid and A. Rosati, 1988. A quasi-equilibrium turbulent energy model for geophysical flows. J. Atmos. Sci., 45: 55-62.

Geyer, W. R., G.B. Gardner, W.S. Brown, J. Irish, B. Butman, T. Loder, and R.P. Signell, 1992. Physical oceanographic investigation of Massachusetts and Cape Cod Bays. Massachusetts Bay Program. MBP-92-03, 497pp.

HydroQual, Inc. 2000. Bays Eutrophication Model (BEM): modeling analysis for the period 1992-1994. Boston, Massachusetts Water Resources Authority. ENQUAD 2000-02, 158pp.

HydroQual, Inc. 2003. Bays Eutrophication Model (BEM): modeling analysis for the period 1998-1999. Boston, Massachusetts Water Resources Authority. ENQUAD 2003-03, 318pp.

HydroQual, Inc. and R.P. Signell, 2001. Calibration of the Massachusetts and Cape Cod Bays Hydrodynamic Model: 1998-1999. Boston, Massachusetts Water Resources Authority. ENQUAD 2001-12, 170pp.

Jiang, M. S. and M. Zhou, 2003. Massachusetts Bay Hydrodynamic Model and Water Quality Model results in 1998-99: Comparison Report between HydroQual and University of Massachusetts Boston Runs. Boston, Massachusetts Water Resources Authority. ENQUAD

2003-10, 42pp.

Jiang, M. S. and M. Zhou, 2004a. The summer Ekman pumping and its implications to the deep water renewal in Massachusetts and Cape Cod Bays. Proceedings of the 8th Estuarine Coatal Modeling. San Francisco. 11-3-2003.

Jiang, M.S. and M. Zhou, 2004b, Calibration of the Massachusetts and Cape Cod Bays Hydrodynamic Model: 2000-2001. Boston: Massachusetts Water Resources Authority. ENQUAD Report 2004-08. 71pp.

Jiang, M.S. and M. Zhou, 2004c. Calibration of the Massachusetts and Cape Cod Bays water quality model: 2000-2001. MWRA ENQUAD 2004-09. 90pp.

Large, W.G. and S. Pond, 1981. Open ocean momentum flux measurements in moderate to strong winds, J. Phys. Oceanogr. 11: 324-336.

Lynch, D. and C. Naime, 1993.The M2 tide and its residual on the outer banks of the Gulf of Maine, J. Phys. Oceanogr., 23: 2222-2253.

Lynch, D.R., Naimie, C.E. and Werner, F.E., 1996. Comprehensive coastal circulation model with application to the Gulf of Maine. Cont. Shelf Res., 12: 37-64.

Mellor, G. and T. Yamada, 1982. Development of a turbulence closure model for geophysical fluid problems, Rev. Geophys. Space Phys., 20: 851-875.

Pedlosky, J. (1987), *Geophysical Fluid Dynamics*. Springer-Verlag, 710pp.

Pettigrew, N. R., et al., 2005, The kinematic and hydrographic structure of the Gulf of Maine Coastal Current Deep-Sea Research II, 52: 2369–2391.

Shapiro, R., 1975. Linear filtering, Mathematics of Computation, 29, 1094-1097

Signell, R.P., H. L. Jenter, and A. F. Blumberg, 1996. Circulation and effluent dilution modeling in Massachusetts Bay: model implementation, verification and results. USGS Open File Report 96-015, U.S. Geological Survey, Woods Hole.

Smagorinsky, J. 1963. General circulation experiments with the primitive equations: I. The basic experiment. Monthly Weather Review, 91: 99-164.

Smolarkiewicz, P. K., 1984: A fully multidimensional positive definite advection transport algorithm with implicit diffusion. *J. Comput. Phys.*, 54: 325-362.

Taylor, D.I. 2005. Patterns of wastewater, river and non-point source loadings to Boston Harbor, 1995 - 2003. Boston: Massachusetts Water Resources Authority. Report 2005-08. 52 pp.

Weller, R., D. Rudnick and N.J. Brink, 1995. Meteorological variability and air-sea fluxes at a

closely spaced array of surface moorings. J. Geophys. Res., 100: 4867-4883.

Werme, C. and C.D. Hunt, C. D. 2002, 2001 outfall monitoring overview..Boston: Massachusetts Water Resources Authority. ENQUAD 2002-18, 84pp.

Xue, H. J., F. Chai, and N. R. Pettigrew, 2000. A model study of the seasonal circulation in the Gulf of Maine. J. Phys. Oceanogr., 30: 1111-1135.

Xue, H. J., L. Shi, S. Cousins, and N.R. Pettigrew, 2005, The GoMOOS Nowcast/Forecast System, Cont. Shelf. Res., Vol. 25, 2111-2146.

Zhou, M. 2002. Test results of the Massachusetts Bay hydrodynamic model (Year 1994), University of Massachusetts Boston, Department of Environmental, Coastal and Ocean Sciences, ECOS 2002-2, 35 pp.

Massachusetts Water Resources Authority
Charlestown Navy Yard
100 First Avenue
Boston, MA 02129
(617) 242-6000
http://www.mwra.state.ma.us